SUSTAINABLE MANUFACTURING OF GRAPHENE-REINFORCED POLYPROPYLENE COMPOSITES BY TAILORING COMPOUND PROPERTIES AND PROCESS TECHNIQUES

by

Gülayşe ŞAHİN DÜNDAR

Submitted to the Graduate School of Engineering and Natural Sciences
in partial fulfilment of the requirements for the degree of

Doctor of Philosophy

Thesis Advisor: Assoc. Prof. Dr. Burcu SANER OKAN

SABANCI UNIVERSITY

JULY 2023

SUSTAINABLE MANUFACTURING OF GRAPHENE-REINFORCED POLYPROPYLENE COMPOSITES BY TAILORING COMPOUND PROPERTIES AND PROCESS TECHNIQUES

Approved by:

Date of Approval: July 19, 2023

ABSTRACT

SUSTAINABLE MANUFACTURING OF GRAPHENE-REINFORCED POLYPROPYLENE COMPOSITES BY TAILORING COMPOUND PROPERTIES AND PROCESS TECHNIQUES

Gülayşe ŞAHİN DÜNDAR

Doctor of Philosophy, 2023

Material Science and Nano Engineering

Thesis Advisor: Assoc. Prof. Dr. Burcu SANER OKAN

Keywords: Graphene, Nanocomposites, Thermoplastic Processing, Graphene Synthesis, Hybrid Nanocomposites, Polymer Blends, Polypropylene (PP), High-Density Polyethylene (HDPE)

Graphene, which attracts the attention of scientists, academia, and industry, is the subject of numerous scientific studies, and in light of graphene's remarkable properties, the field of polymer composites is one of its most highly anticipated applications. However, obstacles such as high cost, sustainability, processability, scaling, serial production, and interphase problems with graphene-based materials need to be optimized to adapt them into polymer compounding processes. Furthermore, according to the production type of graphene, a variety of graphene derivatives exist, such as single-layer graphene, graphene oxide (GO), multilayer GO, reduced graphene oxide (rGO), and graphene nanoplatelet (GNP), which lead to distinctive peculiarities in both graphene quality and the final product. Even though the studies of graphene/polymer composites are escalating in academia and industry, there are deficiencies in the literature on understanding their interactions through the composite constituents, which could be altered by tailoring synthesis routes, modification methods, production techniques, and formulations. Therefore, the main objective of this thesis is to facilitate the adaptation of graphene into

commodity polymer composite applications in general and in Polypropylene (PP) composites in particular, based on the circular economy and sustainability issues, by exploring and developing their mechanical, rheological, thermal, and morphological properties.

Within this framework, a variety of graphene-based materials, such as electrochemically synthesized GO, waste tire-derived and upcycled GNP, modified GNP, and GNP-coated glass fibers (GFs), were integrated into PP-based composites, blends, and hybrid composites to understand the interactions and compatibility of graphene as well as to tailor polymer processing conditions. This study demonstrated an efficient interface model to develop a scalable methodology of melt-processing of PP with the addition of 1 wt.% GO produced by an improved and eco-friendly electrochemical exfoliation, resulting in a significant enhancement in the mechanical performance of PP composites. In another part of the work, the compatibilizer effect of grafted and recycled GNP with a loading ratio of 0.1 wt.% led to the enhancement of the viscoelasticity performance of PP composites during injection molding. In addition, the interface effect was examined by adjusting the localized regions of GNP within the PP/HDPE blends using comprehensive microscopic techniques. In the last part of the work, a compounding study combined the conventional properties of glass fibers and talc with the superior properties of upcycled GNP to provide lightweight with a 10% weight reduction in the targeted compound formulations.

To conclude, several routes were discussed and offered to design and produce stronger, lighter, and novel graphene-based polymer composite materials by enhancing the compatibility and dispersion of fillers in thermoplastic composite systems and integrating them into commercial products with sustainability in mind and environmentally friendly solutions.

ÖZET

GRAFEN TAKVİYELİ POLİPROPİLEN KOMPOZİTLERİN POLİMER İŞLEME SÜREÇLERİNE VE TEKNİKLERİNE UYGUN OLARAK SÜRDÜRÜLEBİLİR ÜRETİMİ

Gülayşe ŞAHİN DÜNDAR

Doktora Tezi, 2023

Malzeme Bilimi ve Nano Mühendisliği

Tez Danışmanı: Doç. Dr. Burcu SANER OKAN

Anahtar Kelimeler: Grafen, Nanokompozitler, Termoplastik İşleme, Grafen Sentezi, Hibrit Nanokompozitler

Grafen, bilim insanları, akademisyenler ve endüstri tarafından dikkat çeken bir konudur ve birçok bilimsel çalışmanın konusu olmuştur. Grafenin olağanüstü özelliklerine dayanarak, polimer kompozitler alanında uygulamaları oldukça ilgi çekicidir. Ancak, grafen tabanlı malzemelerin yüksek maliyet, sürdürülebilirlik, işlenebilirlik, ölçeklenebilirlik, seri üretim ve arayüz sorunları gibi engelleri, polimer bileşikleme süreçlerine uyum sağlamak için optimize edilmesi gerekmektedir. Ayrıca, grafenin üretim türüne bağlı olarak tek tabaka grafen, grafen oksit (GO), çok tabakalı GO, indirgenmiş grafen oksit (rGO) ve grafen nanoparçacığı (GNP) gibi çeşitli grafen türevleri mevcuttur ve bu türevler hem grafen kalitesi hem de nihai ürün üzerinde farklı özelliklere sahiptir. Grafen/polimer kompozitlerine yönelik çalışmalar hem akademide hem de endüstride hızla artmaktadır, ancak bu kompozitlerin bileşenleri arasındaki etkileşimlerin anlaşılmasında literatürde eksiklikler bulunmakta ve bu etkileşimler, sentez yöntemlerinin, modifikasyon yöntemlerinin, üretim tekniklerinin ve formülasyonların uyarlanmasıyla değişebilmektedir. Bu tezin temel amacı, grafenin genel olarak ticari polimer kompozit uygulamalarına ve özellikle polipropilen (PP) kompozitlere adaptasyonunu, döngüsel ekonomi ve sürdürülebilirlik konularını göz önünde

bulundurarak kolaylaştırmaktır. Bu amaçla, elektrokimyasal olarak sentezlenmiş GO, atık lastik kaynaklı ve geri dönüştürülmüş GNP, modifiye GNP ve GNP ile kaplanmış cam elyaf (GFs) gibi çeşitli grafen tabanlı malzemeler, PP bazlı kompozitler, blendler ve hibrit kompozitlerde kullanılmış ve grafenin etkileşimleri ile uyumluluğunu anlamak ve polimer işleme koşullarını uyarlamak amaçlanmıştır. Bu çalışmada, geliştirilmiş ve çevre dostu bir elektrokimyasal eksfolasyon yöntemiyle üretilen %1 ağırlıkça GO eklenerek PP'nin eritme işlemesinin ölçeklenebilir bir yöntemini geliştirmek için verimli bir arayüz modeli gösterilmiş ve PP kompozitlerinin mekanik performansında önemli bir iyileşme elde edilmiştir. Çalışmanın diğer bir bölümünde, aşılanmış ve geri dönüştürülmüş GNP'nin %0,1 ağırlıkça yükleme oranıyla PP kompozitlerinin enjeksiyon kalıplama sırasındaki viskoelastikiyet performansını artıran bir uyumlaştırma etkisi incelenmiştir. Ayrıca, GNP'nin lokalize bölgelerini PP/HDPE blendlerinde kapsamlı mikroskopik tekniklerle ayarlayarak arayüz etkisi incelenmiştir. Çalışmanın son bölümünde, cam elyafı ve talkın geleneksel özelliklerini geri dönüştürülmüş GNP'nin üstün özellikleriyle birleştirerek hedeflenen bileşimlerde %10 ağırlık azaltma ile hafifleme sağlanan bir bileşim çalışması gerçekleştirilmiştir.

Sonuç olarak, döngüsel ekonomi prensiplerine uygun, sürdürülebilir ve çevre dostu çözümlerle daha güçlü, daha hafif ve yenilikçi grafen tabanlı polimer kompozit malzemelerin tasarımını ve üretimini sağlamak için farklı çözümler sunulmuştur.

Dedicated to my beloved sister…

ACKNOWLEDGEMENTS

I would like to express my sincere gratitude and appreciation to Assoc. Prof. Dr. Burcu Saner Okan, my esteemed dissertation supervisor, for her guidance, invaluable support, and insightful advice throughout the research process. Her expertise and dedication have been instrumental in shaping the direction of this work and her guidance and encouragement have been truly invaluable.

I would like to express my deep regards to my jury members Prof. Dr. Yusuf Menceloğlu, Prof. Dr. Fevzi Çakmak Cebeci, Prof. Dr. Atilla Taşdelen, and Prof. Dr. Figen Kaya for their invaluable contribution and for providing valuable insights and expertise that have been immensely valuable in enhancing the quality and rigor of this work.

I am incredibly grateful to my dear friend Dilara Çelik for being such a wonderful friend and for always being there for me. I would like to thank Nargiz Aliyeva, Kuray Dericiler, Ayşenur Sümbül Boztaş, Shaghayegh Saeidiharzand, Taha Behroozi, Büşra Çetiner, Havva Başkan Bayrak, Semih Doğan, Gizem Kurtulmuş, Gizem Arıtürk, Çiğdem Uçar, and Atakan Kocanalı for their unwavering support and encouragement throughout this journey.

I would like to express my heartfelt gratitude and appreciation to my dad Hasan Şahin, for his guidance, wisdom, and passion for chemistry. I would like to thank my mom Çiğdem Şahin, for nourishing me with delicious meals and nurturing my spirit with her love and care. I am grateful to have the best sister Zeynep Şahin, who has always been my pillar of strength. I feel so lucky to have my brother Faruk Şahin who has shown me what it means to be resilient, determined, and compassionate, and his two adorable children Alva Şahin and Elis Şahin for their infectious positivity and the smiles they bring to my face. They have been a constant source of joy and inspiration. I also would like to thank my cat, Gunther, for being more than just a pet. He was a loyal companion and a cherished member of our family.

I would like to extend a special acknowledgment and heartfelt gratitude to my husband Anıl Dündar. Throughout this journey, he has been a constant source of support,

encouragement, and motivation. His love and support have uplifted me in ways words cannot express. His presence in my life is a blessing.

I would like to thank Sabancı University, Faculty of Engineering and Natural Sciences, for providing a travel grant for the international conferences. Finally, I would like to thank the Scientific and Technological Research Council of Turkey (TUBITAK) with project numbers 118C046 and 5200117, and Arçelik A.S for supporting our research and industrial studies.

JULY Gülayşe ŞAHİN DÜNDAR

TABLE OF CONTENTS

ABBREVIATIONS

DSC : Differential Scanning Calorimetry

EDA : Ethylene diamine

FTIR : Fourier Transform Infrared

GF : Glass fiber

GNP : Graphene nanoplatelet

GO : Graphene oxide

HDPE : High-Density Polyethylene

MAPP : Maleic anhydride grafted Polypropylene

MSA : Methane sulfonic acid

PP : Polypropylene

Pt : Platinum

rGO : Reduced graphene oxide

SEM : Scanning Electron Microscopy

TEM : Transmission Electron Microscopy

TGA : Thermogravimetric Analysis

XPS : X-ray photoelectron spectroscopy

XRD : X-ray Diffraction

SYMBOLS

Å : Armstrong

Tm : Melting temperature

Tc : Crystallization temperature

Tg : Glass transition temperature

η* : Complex viscosity

E : Tensile modulus

E' : Storage modulus

E'' : Loss modulus

ΔHm : Heat of Fusion

Xc : Relative Degree of Crystallinity

wt : Weight Fraction

µm : Micrometer

nm **:** Nanometer

mm : Millimeter

cm : Centimeter

g : Gram

mg : Milligram

µg : Microgram

°C : Degree Celsius

°K : Degree Kelvin

N : Newton

s : Second

min : Minute

h : Hour

mbar : Millibar

rpm : Revolutions per Minute

mL : Millilitre

L : Liter

M : Molarity

MPa : Megapascal

V : Volt

θ : Theta

w : Angular frequency

LIST OF TABLES

LIST OF FIGURES

CHAPTER 1: State of Art

The thesis is structured into six comprehensive chapters, each shedding light on different facets of the research. In the first chapter here, we present a state-of-the-art overview, along with our motivations and research insights, laying the foundation for this groundbreaking study.

In the second chapter, studies on electrochemically produced GOs which can be synthesized quickly and easily in more environmentally friendly environments were carried out and their effects on compounding were investigated. This chapter provides a comprehensive roadmap from GO synthesis to the production of well-dispersed nanocomposites, addressing key interactions between GO and PP polymer chains. The study fills gaps in the literature by investigating the effects of oxidation and exfoliation of GO, as well as the mechanical and rheological behaviour of GO sheets within the polymer matrix. By providing a versatile and eco-friendly processing route for scalable graphene manufacturing, the research opens new horizons for the industrial application of these advanced nanocomposites. The findings from this work not only advance the field of polymer composites but also lay the foundation for future investigations into the optimization of graphene-based materials for tailored applications.

In the third chapter, functionalization and modification studies were carried out by using graphene produced from waste tires. In this way, it is aimed to increase the compatibility of graphene in polymer composites by grafting one of the commonly used and commercially available compatibilizers onto the GNP surface and to reduce the external compatibilizers that are highly used in PP processing. The chapter focuses to gain a comprehensive understanding of the interactions between widely used maleic anhydride grafted PP, and graphene by thoroughly analysing the physical and chemical interactions.

In the fourth chapter, the use of GNP as a compatibilizer in PP/PE blend systems was investigated and results showed that GNP can compatibilize PP and HDPE surfaces and enhance the mechanical properties. Despite the extensive industrial usage of polymers like PP and HDPE, there is still limited understanding of the impact of blending these polymers, particularly when introducing graphene. The literature gap pertains to the

optimization of factors such as additive selection, mixing methodology, composition, and processing conditions for successful ternary nanoblend systems. This knowledge is crucial for achieving the desired mechanical, rheological, and thermal properties. To address this issue, the incorporation of a third additive, graphene, into polymer blends has garnered significant attention as a promising approach to improve compatibility and overall performance. In response to this gap, recent research has focused on overcoming the entropy barrier between PP and HDPE using a high shear rate thermo-kinetic mixer and employing upcycled graphene through interface engineering. Comprehensive investigations encompassing morphological, mechanical, rheological, and thermal analyses have been conducted on binary and ternary nanoblend systems to elucidate the effects of graphene incorporation on polymer blends.

In the fifth chapter, a facile and practical coating technique was employed to treat glass fibers (GF) with upcycled graphene nanoplatelets (GNPs), and the coated materials (GNP-c-GF) were integrated into hybrid composites containing GNP, GF, and PP by twin screw extruder. The incorporation of GNP-c-GF into composites played a crucial role as a compatibilizer, effectively enhancing the homogeneity of the composite system and promoting a uniform dispersion within the matrix. Additionally, several investigations were conducted to address the challenges and enhance the performance of a commercially available formulation that contained a high concentration of talc additive. The study focused on reducing the reliance on inorganic additives by incorporating graphene nanoplatelets (GNP), thereby offering more sustainable solutions.

In the last chapter, the general conclusion and future aspects of the thesis were shared. Through this study, advancements are anticipated in effectively incorporating graphene into polymer composites, propelling the field toward greater sustainability and performance. By bridging the gaps in knowledge and addressing the challenges, this research sets the stage for harnessing the full potential of graphene-based materials in advancing the realm of polymer composites. With a focus on sustainable practices and optimized performance, this research contributes valuable insights to the ongoing pursuit of innovative and eco-friendly materials for a multitude of applications.

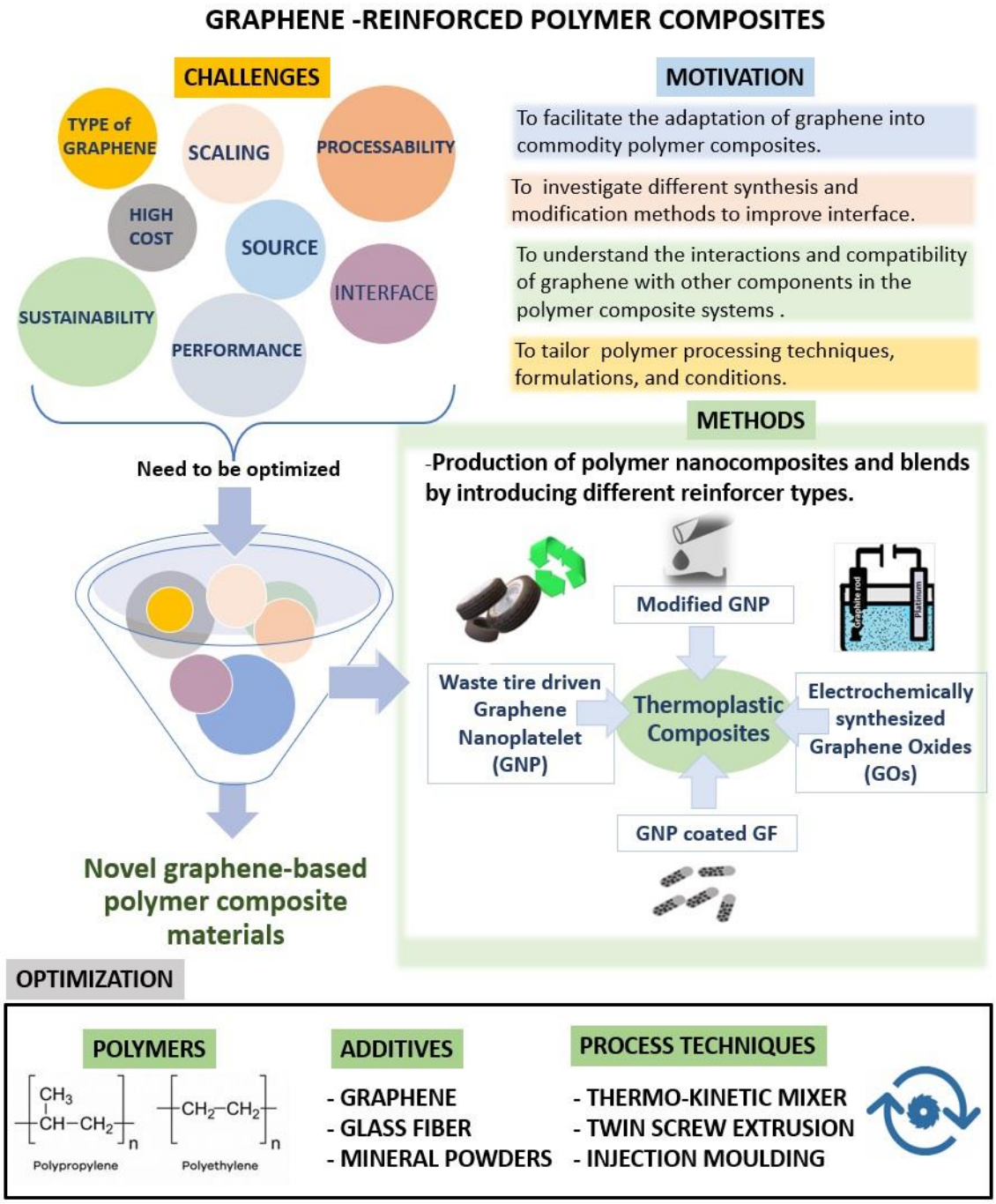

Figure 1. Summary diagram of the scope of the thesis

CHAPTER 2: Simple and scalable adaptation methodology of melt-processing of polypropylene with graphene oxide produced by an improved and eco-friendly electrochemical exfoliation

2.1. Abstract

This study developed a scalable and straightforward adaptation methodology for the melt-processing of polypropylene (PP) to provide a high degree of exfoliation of multi-layer graphene oxide (GO) by using a high-shear mixer. GO was first produced by an improved and eco-friendly electrochemical exfoliation by using an environmentally friendly aqueous methane sulfonic acid (MSA) and a sodium sulfate salt system to minimize the environmental impact. The produced GOs then were melt blended with PP and their mechanical, thermal, and morphological properties were investigated under different GO loadings to attain ideal configuration and increase interfacial interactions between polymer matrix and reinforcer. Comparisons were made by producing different PP composites using two different GO types produced in salt and acid environments. Additionally, by applying different voltages to the salt system, the effect of applied voltage on the properties of both GO material and the composites was discussed. The characterization results indicated that GO obtained in MSA solution caused a 71% increase in flexural modulus and 46% in flexural strength with the addition of 1 wt. % GO. The rheological characterization also showed that dispersion and viscosity improved with lower GO loadings compared to the neat polymer by providing cost-effective and scalable graphene manufacturing.

2.2. Introduction

Substantial effort has been made to prepare graphene-based polymer composites with all kinds of morphologies, dimensions, structures, and properties [1]. Among those polymers, polypropylene (PP) is one of the most commonly used in thermoplastic composite applications as a matrix since it possesses high heat distortion temperature, transparency, flame resistance, dimensional stability, and high impact strength [2]. Moreover, significant weight reduction can be achieved when PP is integrated into

commodity products due to its low density compared to other polyolefins. [3]. Countless studies on graphene/PP composites can be found studying their mechanical, thermal, and electrical properties [4, 5]. However, there are challenges in selecting an ideal graphene type and processing techniques to get enhanced properties from the composites. There are some attempts to provide homogenous distribution of graphene-based materials by applying different polymer processing techniques. For instance, Pingan *et al.* showed that 75% increase in yield strength and a 74% increase in Young's modulus with the use of 0.42% PP latex-coated graphene by volume via melt blending [6]. In another study, Adars *et al*. reported that using less oxygen content graphene/PP nanocomposites prepared by solution mixing method yields an increase in degradation temperatures of the composites [7]. On the other hand, Na Song *et al*. prepared hot-pressed PP/graphene composites in the presence of matrix modifiers and improved the thermal conductivity of the composites 55 times higher than that of pure PP [8]. Various contents of large-sized graphene nanoplatelets were melt blended within the PP matrix and a low percolation threshold of 2.9 vol% was achieved while less flexural and tensile strength improvement was observed [9]. Therefore, different parameters such as graphene type and processing technique directly affect the polypropylene's performance.

Despite some improvements in the final properties of the PP/graphene nanocomposites, poor dispersion and agglomeration of graphene remain a challenge [10, 11]. A direct relationship exists between obtaining enhanced composite properties and the distribution of fillers in the matrix [12]. Different methods have been applied to produce PP/graphene composites to get a high degree of dispersion. Functionalization of additive surfaces is an alternative way to modify surfaces. Mainly, the use of functionalized graphene is required to increase compatibility, thus the dispersion and distribution of graphene in the PP matrix. In a study, a well-dispersed state of filler in the PP matrix was reported by using functionalized GO with maleic anhydride-grafted PP in PP matrix [13]. In another study, Lee *et al.* improved the dispersion state of nanofillers in melt blended PP matrix by using 2 wt.% fluorinated graphene oxide and showed 31% and 15% improvement in elastic modulus and tensile strength, respectively, compared to neat PP [14]. Cardanol-functionalized GO was used to increase the compatibility of the filler with the PP matrix in the presence of p-xylene [15]. However, to facilitate industrial applications of graphene-based composites, direct use of graphene as filler was preferred [16]. Pristine graphene can be used in composites due to its high quality but the striving bottom-up

synthesis, agglomeration, and poor solubility of pristine graphene make the use challenging [17]. Therefore, graphene derivatives such as GO (graphene oxide) also have aroused enormous research interest offering a wide range of possibilities to synthesize graphene-based functional materials for various applications [18]. Using GO instead of pristine graphene in composite applications is generally characterized by good particle dispersion degree [19]. Additionally, it may provide advantages such as preventing aggregation and facilitating modification of GO. There are different methods to produce GOs, and Hummers' method is one of the most widely used ones. In a recent study, Naz *et al.* enhanced the poor creep resistance of PP by 28% with 0.5 wt. %GO prepared by the Hummers method and followed by hydrothermal reduction [20]. Although the Hummers' method is widely used for GO production, there is an explosion and toxic effects due to the strong chemicals that are used, such as sulfuric acid, phosphoric acid, and potassium permanganate. Furthermore, a couple of steps are required to have the final graphene used in the composites. As a matter of fact, not only producing good quality of graphene but also the capability of large scalable production remains a major challenge [21]. Moreover, engineering applications that take advantage of graphene's extraordinary properties require facile large-scale production of graphene. Mechanically exfoliated graphene shows high quality, however, it is not considered as a suitable method for large-scale production [22]. In the case of liquid-phase exfoliation, the solvents that are used are known to be expensive, corrosive, and usually toxic [23]. On the other hand, another method called electrochemical exfoliation of graphite produced in anodic or cathodic conditions has been considered safe, scalable [24], facile [25], and time and cost-efficient. This method allows intercalation of molecules between layers of graphene [26] in the presence of an aqueous electrolyte. To initiate the structural deformation of graphite, an electrical voltage is applied between the working (typically graphite rod or foil) and counter electrode (generally Platinum). This allows ions in the electrolyte to penetrate between graphene layers, thus resulting in intercalation or exfoliation of graphene sheets. Up to now, salts and acids have been used to produce electrochemically produced graphene oxide [27]. On the other hand, methane sulfonic acid has taken attention in terms of being a green solvent due to its high boiling point and low dangerous, volatile compounds [28]**.** However, the adaptation of this acid in graphene production is limited, and there are some unknown processes with this chemical. To the best of our knowledge, methane sulfonic acid is not used for electrochemical exfoliation to obtain GO sheets. In

the present study, the effect of salt and acid on the quality of GO was investigated to monitor controllable GO production.

Herewith, a roadmap for producing applicable, easy, and well-dispersed nanocomposites from the synthesis of GO to the production of thermoplastic composites was studied. Electrochemically produced GOs were synthesized and directly used in the production of melt-blended PP composites. To examine the effect of electrochemically produced GO by salt and acid-based systems, GO was dispersed in the PP matrix by a high shear thermo-kinetic mixer at different GO loadings. Up to now, there are several attempts for the development of high-performance graphene-reinforced thermoplastic composites in the literature but an interface model between polymer and graphene is still under investigation. This work elaborates on the interactions of GO with PP polymer chains by addressing the degree of oxidation and exfoliation of GO and the rheological behavior of GO sheets through polymer chains. In addition, there is no published work for a few gram scales of GO in the presence of environmentally friendly acid of methane sulfonic acid under the electrochemical production process. Furthermore, a comprehensive study was carried out by investigating the effect of applied voltage on the chemical and structural properties of GO sheets as well as on the mechanical and rheological properties of PP-based composites.

2.3. Materials and Methods

2.3.1. Materials

Sodium sulfate, methane sulfonic acid, and graphite rods with the length of 150 mm and a diameter of 3 mm were purchased from Sigma-Aldrich. Homo Polypropylene (homo PP, HE125MO) was supplied by BOREALIS and it has a melt flow index of (MFI) 12 g/10 min, a density of 905 kg/m3, and a melting temperature of (Tm) between 220 ^{o}C-260 ^{o}C.

2.3.2. Electrochemical exfoliation of GO by different solvent systems

Electrochemical exfoliation of graphene oxides (GOs) was carried out in two different mediums: one is in an aqueous inorganic salt solution (sodium sulfate), and the other one is in an environmentally friendly aqueous methane sulfonic acid solution which was studied for the first time in the electrochemical synthesis of GO. 0.5 M sodium sulfate and 0.5 M methane sulfonic acid electrolytes were prepared separately. The graphite rod was used as a working electrode and connected to the anode, while a platinum (Pt)

electrode was used as a counter electrode and connected to the cathode. The distance between the electrodes was kept at 2.5 cm. The applied voltages were changed according to the electrolyte type to obtain the fastest and the most stable process. These were a voltage of 20 V for sodium sulfate medium and a voltage of 8 V for methane sulfonic acid medium. Additionally, to understand the effect of the magnitude of applied voltage, the graphene in sodium sulfate medium by applying a voltage of 10 V was also tested. As soon as the graphite rod was broken, the applied voltage was turned off, and the broken graphite rod in the electrolyte was removed with tweezers. The final product was filtered, washed, and dried in a vacuum oven at 80 ^{o}C for 48 h.

The basic experimental setup can be seen in Figure 2. Graphite rod as a working electrode was connected to anode while Pt as a counter electrode connected to the cathode. By applying a bias to the systems, the graphite rod started to get thinner and exfoliated from the rod's surface into the solution. This is also the stage where oxidation takes place. The process continued until the graphite rod was peeled off sufficiently. After a certain amount of time, the rod was broken off, and the applied bias was stopped. The filtered and dried GO was then melt compounded with PP by using a high shear rate thermo-kinetic mixer followed by injection moulding.

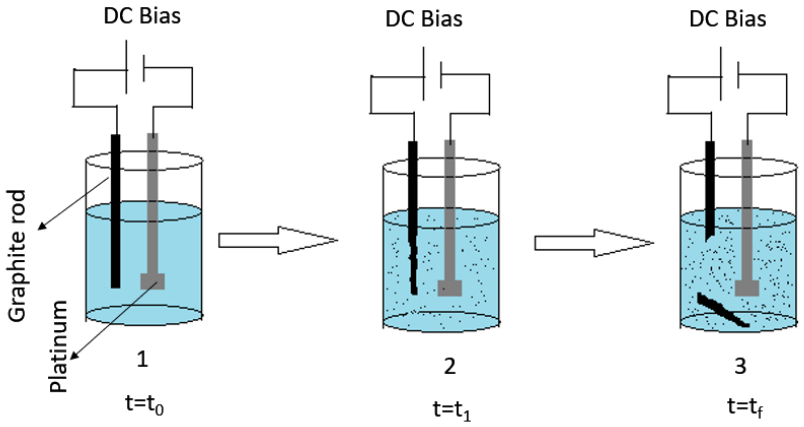

Figure 2. Representative experimental stages of electrochemical exfoliation set-up (1): at time zero (t0), (2): after a certain amount time (t1), and (3): at a time final (tf).

2.3.3. Fabrication of GO reinforced PP composites by thermokinetic mixer

Manufacturing of GO/PP composites was carried out in a melt phase, at 3500-4000 rpm and 200 ^{o}C by using a custom-made Gelimat Thermo-kinetic Mixer (Dusatec Co, USA). At this high shear rate, GO can be easily exfoliated in PP chains. Homogeneous dispersion of difficult compounding systems can be attained compared to composites produced by traditional twin-screw extrusion [29].GO contents in the PP matrix range from 0.1% to

1% in weight. GO obtained in methane sulfonic acid by 8-volt bias (GO-CH_4O_3S-8 V), GO obtained in sodium sulfate by 20-volt bias (GO-Na_2SO_4-20 V), and by 10-volt bias (GO-Na_2SO_4-10 V) were synthesized, and their effect on mechanical, thermal, and rheological behaviors on the melt blended Polypropylene nanocomposites was investigated. Table 1 summarizes the sample names and their explanations. The numbers from 0.1 to 1 at the end of the composite names indicate the GO weight content. For example, PP/GO-Na2SO4 /0.1 states that it contains 0.1 wt. % GO-Na_2SO_4 in PP.

Table 1. Process conditions for electrochemically produced GO samples

Sample Name	Electrolyte	Molarity [mol/L]	Applied Voltage [V]	Termination Time [min]
GO-Na_2SO_4-20V	The aqueous sodium sulfate salt	0.5	20	70
GO-Na_2SO_4-10V	The aqueous sodium sulfate salt	0.5	10	140
GO-CH_4O_3S-8V	Aqueous methane sulfonic acid	0.5	8	75

2.3.4. Characterization

Characteristic properties of GOs and their composites were examined by using various spectroscopic and microscopic techniques. Raman Spectroscopy was used to understand the quality of GOs. X-ray Diffraction (XRD) was performed to analyse the structural characterization of graphene materials by using a Bruker D2 PHASER Desktop diffractometer utilizing a CuKα radiation (λ=1.5406 nm). X-ray Photoelectron Spectroscopy (XPS) was used for monitoring functional groups and chemical compositions. Composite samples were fractured under liquid nitrogen and coated with a thin layer of gold to investigate the surface morphology and examined under a Leo Supra 35VP Field Emission Scanning Electron Microscope (FESEM). The mechanical tests were conducted using Instron 5982 Static Universal Test Machine (UTM) for tensile and three-point bending tests according to the ISO 527-2 and ISO 178 standards. Cross-head displacement rate for the tensile and flexural tests were 2mm/min and the span-to-depth ratio was 64mm for the flexural specimens. Specimens for tensile and flexural tests were prepared by using Xplore brand IM 12 brand micro injection moulding at 200 ^oC with 5 bar compression and 8 bar closing pressure according to the ISO 527-2 and ISO 178 standards. Rheological tests (frequency sweep) were performed in Anton-Paar MCR 702 Rheometer at 230^oC and strain of 1% in an angular frequency range of 0.01-1000 rad/s.

2.4. Results and Discussion

2.4.1. The effect of electrolyte type and applied voltage on the formation of GO in electrochemical exfoliation

Electrolyte type and applied voltage have a great influence on the electrochemical process and GOs' properties. In this method, the quality of the graphite rod, the type of solvent or salt, and voltage directly affect the characteristics of graphene and, therefore the performance of the composites. In the present study, it is aimed to investigate the effect of electrochemically produced GOs on the final properties on the thermoplastic PP/GO composites. Therefore, it is important to define GO sheets' characteristic properties by considering electrochemical process parameters. Herein, Raman spectroscopy is a powerful technique used to characterize carbon-based materials as it provides valuable information about defects and disorders in the structure [30]. Therefore, it was used to investigate the quality of GOs that are produced in different electrolytes. Figure 3(a), and Table 2 compares the structural differences of obtained GO samples. G peaks at about 1500 cm^{-1} -1600 cm^{-1} are attributed to the stretching of the C-C bonds in all graphitic materials. Broadened G peaks with significant D peaks were observed in all graphene samples. Edges, functional groups, and structural disorders caused D peaks to appear [31]. Due to the observed edge defects presented in the samples (D band) [32], it was proven that the graphitic structure was destroyed. The observed sharp 2D peak in the graphite rod (G-rod) started to disappear as oxidation takes place. Slightly observed 2D peaks at between 2500 cm^{-1} -2800 cm^{-1} in GO materials showed that partial oxidation took place. It also represents the multi-layer structure of graphene materials. Calculated defect ratios (D/G) revealed that the highest defect belongs to the GO-Na_2SO_4-10 V with a defect ratio of 1.12. Defect ratios for GO-CH_4O_3S-8 V and GO-Na_2SO_4-20 V resulted in 1.04 and 1.03, respectively. Consequently, low voltages for GO-Na_2SO_4 samples lead to higher oxidation and defects. From the XRD characterizations Figure 3(b), the pure crystalline structure of graphite was broken down, and more amorphous structures were obtained due to the intercalated structure. A sharp and high-intensity peak of raw graphite positioned at 26^o can be seen. For synthesized GO samples, broadened 002 peaks were observed near at 26^o, attributed to the reduced graphene oxide materials [33]. XRD software automatically calculates the crystalline and amorphous parts for each sample. The crystalline and amorphous part of the GO materials are presented in Table S4 (supplementary document)**.** The crystallinity of graphite rod decreased to a great extent

from approximately 84% to the range of 45%-47% after electrochemical treatment due to the existing functional groups on the GO layers. Additionally, d-spacing was calculated as 10.5 nm for all graphene materials.

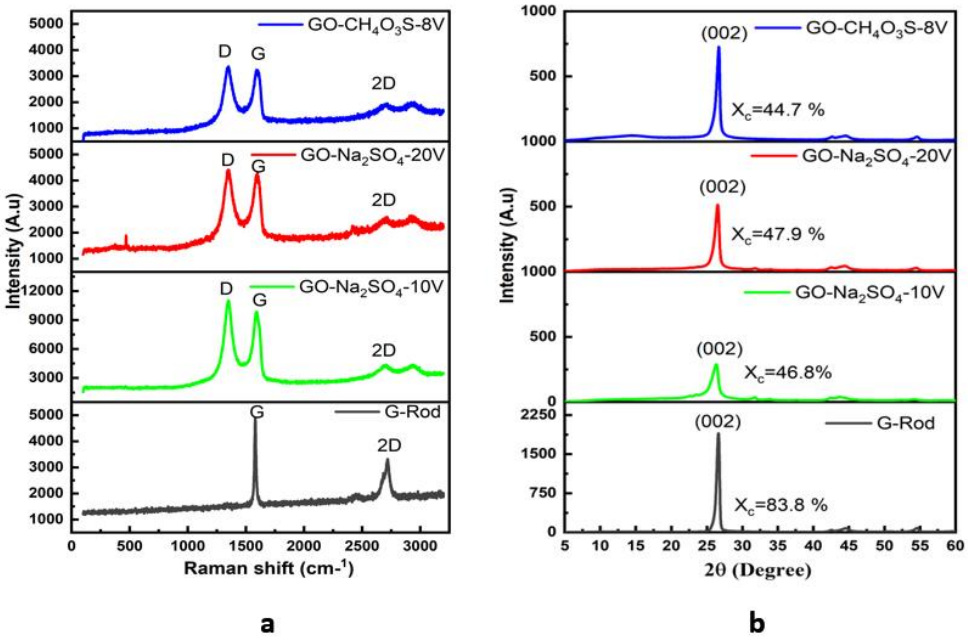

Figure 3. (a): Raman spectra, and (b): XRD patterns of GO-CH4O3S-8 V (blue), GO-Na2SO4-20 V (red), GO-Na2SO4-10 V (green), and G-rod (black)

Table 2. Raman peak intensities and ID/IG ratios of G-rod, GO-Na2SO4-10 V, GO-Na2SO4-20 V, and GO-CH4O3S-8 V.

Sample name	**D intensity (a.u)**	**G intensity (a.u)**	**2D intensity (a.u)**	**I_D/I_G**
G-Rod	-	4881	3316	-
GO-Na_2SO_4- 10V	11030	9854	4368	1.12
GO-Na_2SO_4 -20V	4410	4293	2595	1.03
GO-CH_4O_3 S-8V	3374	3229	1950	1.04

To understand the surface chemistry, X-ray photoelectron spectroscopy (XPS) was carried out to confirm the complete oxidation of graphite. Acidic environment excited the oxidation process. The highest degree of oxidation was observed in GO-CH_4O_3S-8 V with a degree of 20% oxidation, as seen in Table 3. With a pKa value of -1.16, MSA is known as a strong and non-toxic organic acid [28]. Therefore, a high degree of oxidation for GO-CH_4O_3S-8 V is understandable. GO-Na_2SO_4-10 V exhibited an oxygen content of 14.23%, while 10.93% was found for GO-Na_2SO_4-20 V. When comparing the effect of voltage on the oxidation degree of graphene in aqueous sodium sulfate (Na_2SO_4)

mediums, production by 10 V resulted in a higher degree of oxidation than 20 V. Some studies stated that high voltage facilitates a higher degree of oxidation [24]. However, here it has been observed that production by low voltage for sodium sulfate medium leads to a more stable and higher degree of oxidation. This may be because when the voltage is low, the termination of the reaction (breaking of the graphite rod) is prolonged, allowing more time for oxidation. On the contrary, increasing the voltage may have created a more dynamic medium and decreased the possibility of selective reactions. Figure 4 shows deconvoluted C1s spectra of obtained materials. Binding energies of 284.14 eV and 284.22 eV are assigned to (C=C) groups, while 284.7 eV and 284.8 eV are allocated to (C-C) groups. Epoxide groups (C-O-C) and carbonyl (C=O) groups appeared at the binding energies of 285.8/286 eV and 288/289 eV [34] respectively. Additional C-S groups can be found in GO-CH_4O_3S-8V at a binding energy of around 283.7 eV [35]. Since the intensity of the C-S peak is relatively high, there might be some physical adsorbed sulfite groups on graphene oxide surfaces. More information of C1s, O1s, and S2p can be found in the supplementary material (Table S1).

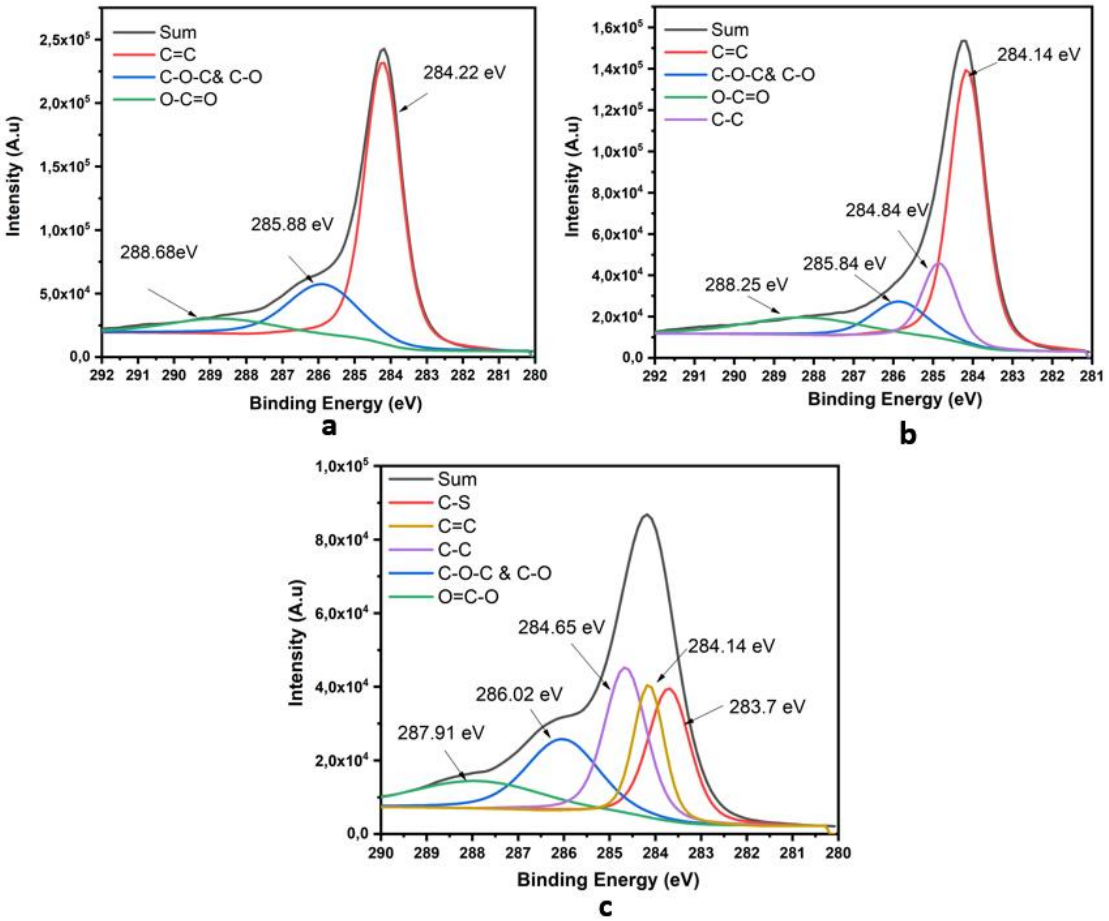

Figure 4. XPS deconvoluted C1s peaks of (a) GO-Na_2SO_4-10 V, (b) GO-Na_2SO_4-20 V, and (c) GO-CH_4O_3S-8 V

Table 3. XPS survey scan results of GO samples

Samples	C (at%)	O [at%]	Others [at%]
GO-Na_2SO_4-10V	82.55	14.23	3.22
GO-Na_2SO_4-20V	85.41	10.93	3.66
GO-CH_4O_3S-8V	75.74	20.48	3.78

The thermal stability of graphite and synthesized GO materials can be seen in Figure 5. G-rod has no observable decomposition in the range of tested temperature intervals, meaning no existing oxygen-containing functionalities. However, as oxidation took place, the thermal stability of the synthesized materials decreased. Among synthesized materials (excluding G-Rod), GO-Na_2SO_4-20 V has the highest thermal stability due to the observed delay in decomposition. It is known that groups containing oxygen functionalities decompose up to 400 ^oC. After 400 ^oC, slow decomposition of more stable oxygen functionalities can be seen [36]. Additionally, some of the weight loss between 100 ^oC and 200 ^oC can be attributed to physically adsorbed water [37]. At 790.1 ^oC, and 786 ^oC degradation of sodium sulfate was observed. The amount of sodium sulfate was 2.8 wt.% and 2.3 wt.% for the GO-Na_2SO_4-10 V and GO-Na_2SO_4-20 V respectively. This shows that the salt could not be removed entirely in GO samples produced with sodium sulfate. The effect of voltage influences the thermal stability of the GO-Na_2SO_4-20 V and GO-Na_2SO_4-10 V samples. Since the amount of oxidation is higher in low voltage production, its thermal stability is also lower. GO-CH_4O_3S-8 V showed the least thermal stability due to the production in an acidic medium. The reason for this is that GO has a higher oxidation capacity in an acidic environment and as a result, the amount of oxygen functionality increases. Oxygen functionalities facilitate degradation, resulting in less thermal stability of GOs.

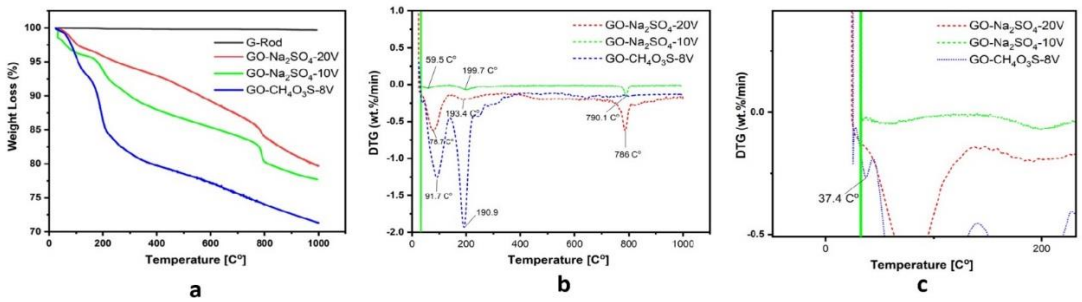

Figure 5. (a): TGA, (b): DTG, and (c): zoom DTG curves of GO-CH_4O_3S-8V (blue), GO-Na_2SO_4-20 V (red), GO-Na_2SO_4-10 V (green), and G-rod (black)

SEM images of graphite rod and GO samples produced in the media of Na_2SO_4 and CH_4O_3S are shown in Figure 6. Compared to the graphite rod in Figure 6(a), more wrinkled and layered structures are seen in Figure 6(b) and 6(c). With the introduction of oxygen groups on the graphene, it is seen that there are defects on the edges of the layers since oxidation of layers leads to the formation of crumpled structures (yellow circles). The functional groups break the delocalized π bonds in the molecular layer, weaken the van der Waals forces and form intermolecular hydrogen bonds, resulting in many defects in the planar structure of GO [38].

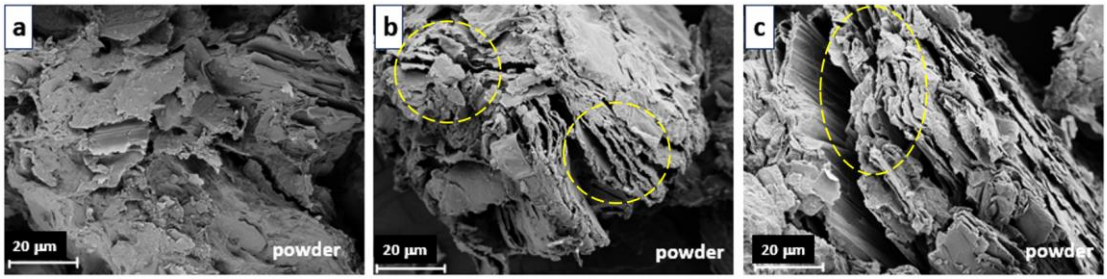

Figure 6. FE-SEM images of (a): G-rod in powder, (b): GO-Na_2SO_4 in powder, (c): GO-CH_4O_3S in powder

2.4.2. The effect of GO types and GO concentration on the mechanical behaviour of PP composites

The effect of the applied voltage during the electrochemical exfoliation of GOs on the mechanical performance of PP/GO composites was also investigated to attain an ideal GO type (the results are provided in supplementary document). Therefore, two kinds of GO, obtained by applying 10 V and 20 V in Na_2SO_4 environment, were used for PP composite manufacturing and results regarding to comparison were presented in the Table 4. It is seen that GO/ Na_2SO_4 /0.25/20V and GO/ Na_2SO_4 /0.25/10V composites have similar mechanical properties. Increases of 30% for flexural modulus and 23% and 25% for flexural strength were observed in the GO/Na_2SO_4/0.25/ 20 V and GO/Na_2SO_4/0.25/ 10 V composites for the GO samples produced with both 20 V and 10 V, respectively. A comparison of the two results reveals that although the applied voltage difference caused significant differences in the properties of the obtained GOs, it did not cause a significant difference in the final properties of the composites. Hence, this enables the use of a speed-up process by applying high voltages to the graphite for the composites applications since it provides graphene production in a shorter time. Therefore, GO-Na_2SO_4-20 V and GO-CH_4O_3S-8 V were used in the production of the composites for a faster process and their

characterizations are compared for the remaining of the manuscript. The flexural properties of the GO/PP composites are shown in Figure 7(c, d), Figure 8(a, b), and Table 4. Regarding PP/GO-Na_2SO_4 composites, with the addition of only 0.1 wt.% GO-Na_2SO_4 into the PP matrix, the flexural modulus and flexural strength of the composites increased by 25% and 24%, respectively. As graphene concentration goes up from 0.1 wt.% to 1 wt.%, slight increases in flexural modulus were observed. Flexural strength values were not much affected by the graphene concentration and stabilized by increasing 26% with the 0.5 wt.% and 1 wt.% graphene loadings.

For the PP/GO-CH_4O_3S samples, with the addition of 0.1 wt.% graphene, the flexural modulus and flexural strength of the composites increased by 37% and 26%, respectively. There was a high change in modulus and strength with the increase in GO content, resulting in a maximum increase of 71% and 46%, respectively, for the PP/CH_4O_3S/1 composites. The existence of extra-functional groups on GO produced in the MSA environment may have contributed to transmitting the load from the matrix to the reinforcer. At the same time, these functional groups may have provided a better distribution in the matrix by reducing the interactions between the GO layers. The results show that MSA is an acid that has the potential to be used in the electrochemical production of graphene and can be used as an alternative to instead of using harsh acids such as sulfuric and/or phosphoric acid in the synthesis of GO.

Tensile properties can be seen in Figure 7(a, b), Figure 8(c, d), and Table 4. The addition of only 0.1 wt.% GO increased tensile modulus of 26% for PP/GO-Na_2SO_4/0.1 and 42% for the PP/GO-CH_4O_3S/0.1 composites. After that composition, slight changes were observed for all composites. The result indicates that the addition of a small amount of nanomaterial leads to a large change compared to the pure matrix material. From Figure 7(a) and 7(b), the images shown by zooming clearly show that the yield points of the composites are considerably increased. Yield strength is a measure of the resistance of materials to deformation and is of great importance in plastic parts. After the yield point, the material changes from elastic deformation to plastic deformation and the deformation in the material is irreversible. Therefore, the improved yield strength is a proof that produced composites can still show elastic change under higher forces. The tensile strength results are slightly reduced compared to the pure PP matrix. This may be due to insufficient adhesion between matrix and reinforcer [39]. Although dispersive and distributive forces have been achieved by using the thermo-kinetic mixer, sufficient

adhesion may not be provided at some points between GO and PP. Insufficient bonding between the polymer matrix and filler might led to lower tensile strength [40]. However, if the material is not to be used in an application subject to direct tensile force, the decrease in maximum tensile strength can generally be tolerated because the yield strength is more considered since it is of great importance that plastic parts do not undergo permanent deformation under high forces. To sum up, it was observed that the mechanical properties of the materials increased significantly with the use of both types of GO and the results are promising since high increases in mechanical properties were achieved with the use of low amounts (maximum 1 wt. %) of GO. With the use of 0.1 wt. %GO, much higher results were obtained in mechanical properties compared to the findings in the literature. Ali recently gave comparisons on the mechanical properties of polymer composites containing GNP from different studies, and the mechanical values obtained in this study are higher [41].

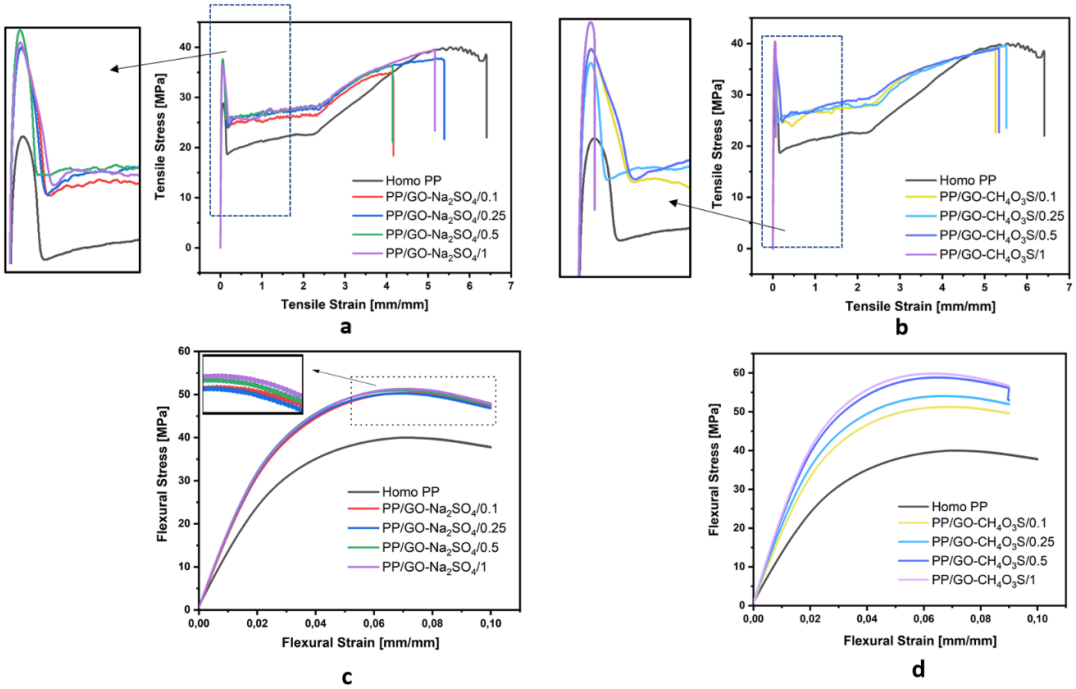

Figure 7. Tensile stress-strain curves of (a): PP/GO-Na_2SO_4 samples, (b): PP/GO-CH_4O_3S samples, and flexural stress-strain curves of (c): PP/Na_2SO_4 and (d): PP/GO-CH_4O_3S samples at different GO loadings

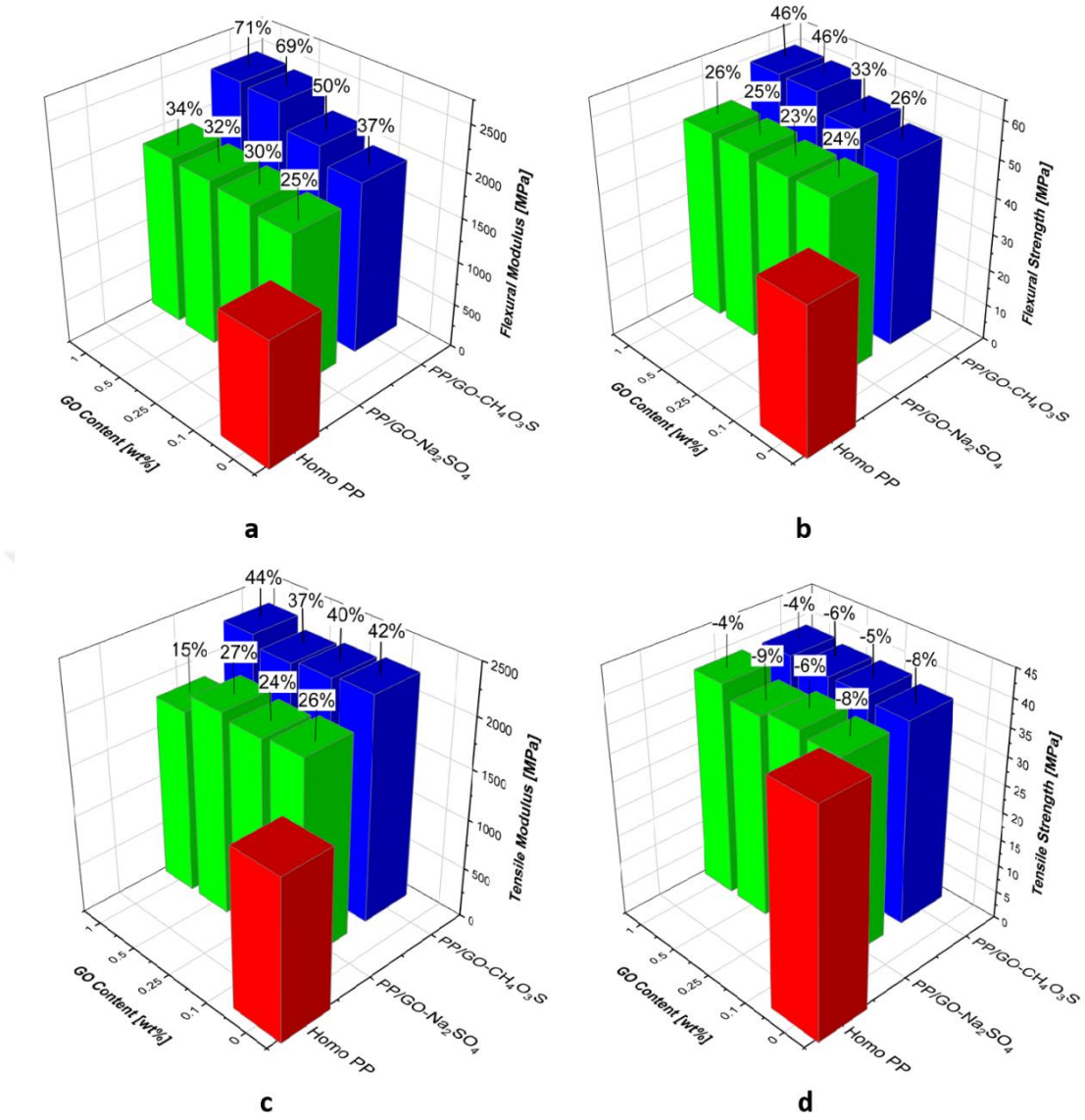

Figure 8. Effects of GO content on (a): flexural modulus, (b): flexural strength, (c): tensile modulus, and (d): tensile strength of the composites.

Table 4. Mechanical properties of PP/GO Composites

Sample Name	Flexural Modulus [MPa]	Flexural Strength [MPa]	Tensile Modulus [MPa]	Tensile Strength [MPa]
Homo PP	1424 (±42.71)	40.7 (±0.86)	1587 (±100.25)	40.3 (±0.20)
PP/GO-Na_2SO_4/0.1	1783 (±41.95)	50.4 (±0.33)	2003 (±59.45)	36.9 (±1.99)
PP/GO-Na_2SO_4/0.25	1853 (±36.78)	50.1 (±0.24)	1969 (±55.36)	37.8 (±2.67)
PP/GO-Na_2SO_4/0.5	1886 (±2.25)	51.1 (±0.18)	2018 (±92.64)	36.6 (±0.88)
PP/GO-Na_2SO_4/1	1913 (±48.43)	51.4 (±0.29)	1831 (±16.84)	38.8 (±1.91)
PP/GO-CH_4O_3S/0.1	1947 (±45.66)	51.5 (±0.53)	2249 (±125.75)	37.1 (±2.00)
PP/GO-CH_4O_3S/0.25	2130 (±62.56)	54.3 (±0.55)	2218 (±202.67)	38.1 (±1.83)
PP/GO-CH_4O_3S/0.5	2401 (±78.59)	59.4 (±0.95)	2180 (±124.29)	38.0 (±0.78)
PP/GO-CH_4O_3S/1	2429 (±65.95)	59.6 (±1.27)	2287 (±71.85)	38.6 (±1.48)
PP/GO-Na_2SO_4/0.25*	1857 (±28.82)	50.9 (±0.33)	1890 (±80.66)	37.3 (±1.63)

Produced with 10V

2.4.3. The effect of GO types on the rheological behaviour of PP composites

Rheology is an important tool for analysing the microstructure of the composites as well as the nanoparticle dispersion, polymer-graphene interactions, and flow properties which are very significant in terms of polymer processing [42]. Figure 8 shows the rheological behaviour of the produced composites. Complex viscosities of the composites as a function of angular frequency are shown in Figure 9(a, d). All materials exhibited shear thinning behaviour as viscosity increases rapidly with decreasing frequency and reaches a plateau. This behaviour is known as the shear-thinning behaviour of pseudoplastic materials and is observed mainly in polymers. As the shear rate increases, deformation forces begin to orientate the polymer chains, and the viscosity drops. At high shear rates, it is assumed that there is no chain entanglement among polymer chains, and therefore, a large drop in viscosity is observed. To interpret the nanoparticle distribution in a matrix, low-frequency values are taken as a basis since the shear forces on the polymers start to disappear in this region. In polymers with good nanoparticle distribution, the network formation of nanoparticles in the low-frequency region manifests itself as an increase in viscosity. For the PP/GO-Na_2SO_4 composites, the highest viscosity was observed with the addition of only 0.1 wt.% GO compared to neat PP. Low-frequency rheologic behaviours of PP/GO-CH_4O_3S composites were slightly affected. Although the best network formation was achieved with a composite containing 0.5 wt.% GO-CH_4O_3S, and 0.1 wt.% GO-Na_2SO_4, the viscosity was not affected much by the nanomaterial concentration. One of the explanatory reasons of slight viscosity change in the low-frequency region could be the good shear-thinning behaviour and high melt strength of pure PP itself. Since PP is highly crystalline and already showed a significant increase of viscosity in the low shear rate region, it may be compelling to uprise further. Another reason might be the insufficient amount of graphene loading. Higher concentrations might be needed to get the percolation threshold. As a result, it is possible to reach the ideal mechanical properties with low GO loadings into the PP matrix without any need to change the process parameters of PP by taking a reference of rheological behaviour.

The frequency-dependent storage modulus (G') and loss modulus (G'') of the composites are given in Figure 9(b, e). The tan δ (loss factor) values and δ (phase shift angle) are shown in Figure 9c and 9f. Slight increases in G' and G'' values were observed compared to homo PP for each composite specimen since GO particles are capable to slow down the relaxation process of linear polymer chains [19]. The loss modulus showed higher

values than the storage modulus in the low-frequency region meaning that at low frequencies, the materials exhibited liquid-like behaviour. However, as the frequency increased, the materials started to react more elastic, and the storage modulus started to increase. It is seen that the storage modulus and loss modulus values converged at the high-frequency region. Considering the loss factor and calculated phase ship angles, comments can be made about the viscoelastic behaviour of the materials. The materials exhibit viscoelastic behaviour at angles ranging from 0 to 90^{o} and when phase shift angle is 45^{o}, the viscous and elastic portions are equal. In the frequency sweep range in Figure 9(c, d), it is seen that highly liquid-like behaviour is dominant at low frequencies while this liquid-like behaviour is reduced towards the high frequencies just as homo PP. Therefore, results emphasized that PP/GO composites are also as easily processable as homo PP since there is no major change in the flow properties of PP with the addition of GO. This can be a great advantage as the flow behaviour of materials is a crucial parameter in polymer processing.

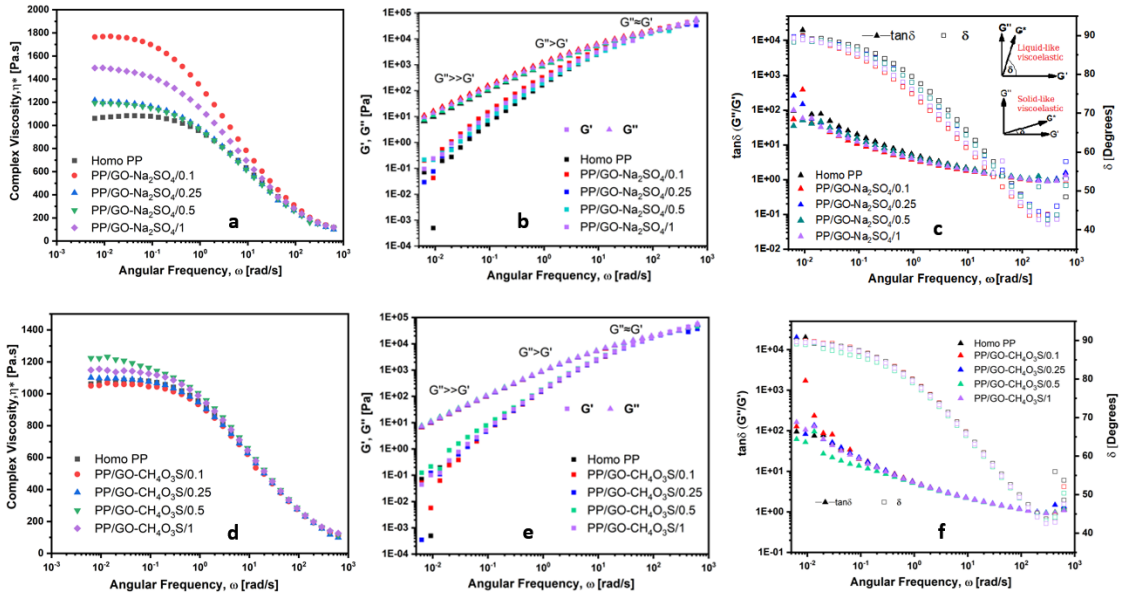

Figure 9. Complex viscosity of (a): PP/GO-Na_2SO_4, and (d): PP/GO-CH_4O_3S composites, storage and loss modulus of (b): PP/GO-Na_2SO_4, and (e): PP/GO-CH_4O_3S composites, and phase shift of (c): PP/GO-Na_2SO_4, and (f): PP/GO-CH_4O_3S composites

2.4.4. Cross-sectional analysis of GO reinforced PP composites by SEM

Freeze fractured surfaces of neat PP, PP/GO-Na_2SO_4, and PP/GO-CH_4O_3S composites with a loading of 1 wt.% were investigated by SEM and the related images are provided in Figure 10. The typical fracture surface of a ductile polymer at ambient temperature is seen [36]. There are some micro and nano voids on the PP surface (a1-a2). Also, the wide

cracks between the lamellae are shown in the black circle and appear densely in the neat polymer (a3-a4). When the fracture surface of the PP/GO-Na2SO4/1 composite is examined, a ductile fracture surface is observed again (b1). Agglomerations of graphene sheets were observed at some points and are indicated by the red circle (b2). However, compared to PP, it was observed that the gaps between the lamellae decreased and became more integrated with the matrix as indicated by the green circle (b3-b4). In the PP/GO-CH4O3S/1 composite, interface images of a more fragile material were obtained on the fracture surface (c1). The absence of agglomeration or orientation in any direction indicates that the distribution is effective. The interaction between matrix and GO-CH_4O_3S seem to be stronger because the fractured surface is even compared to PP/GO-Na_2SO_4 system [43]. No gaps are observed between the lamellae, and the matrix is much more united and has a gapless structure (c3-c4).

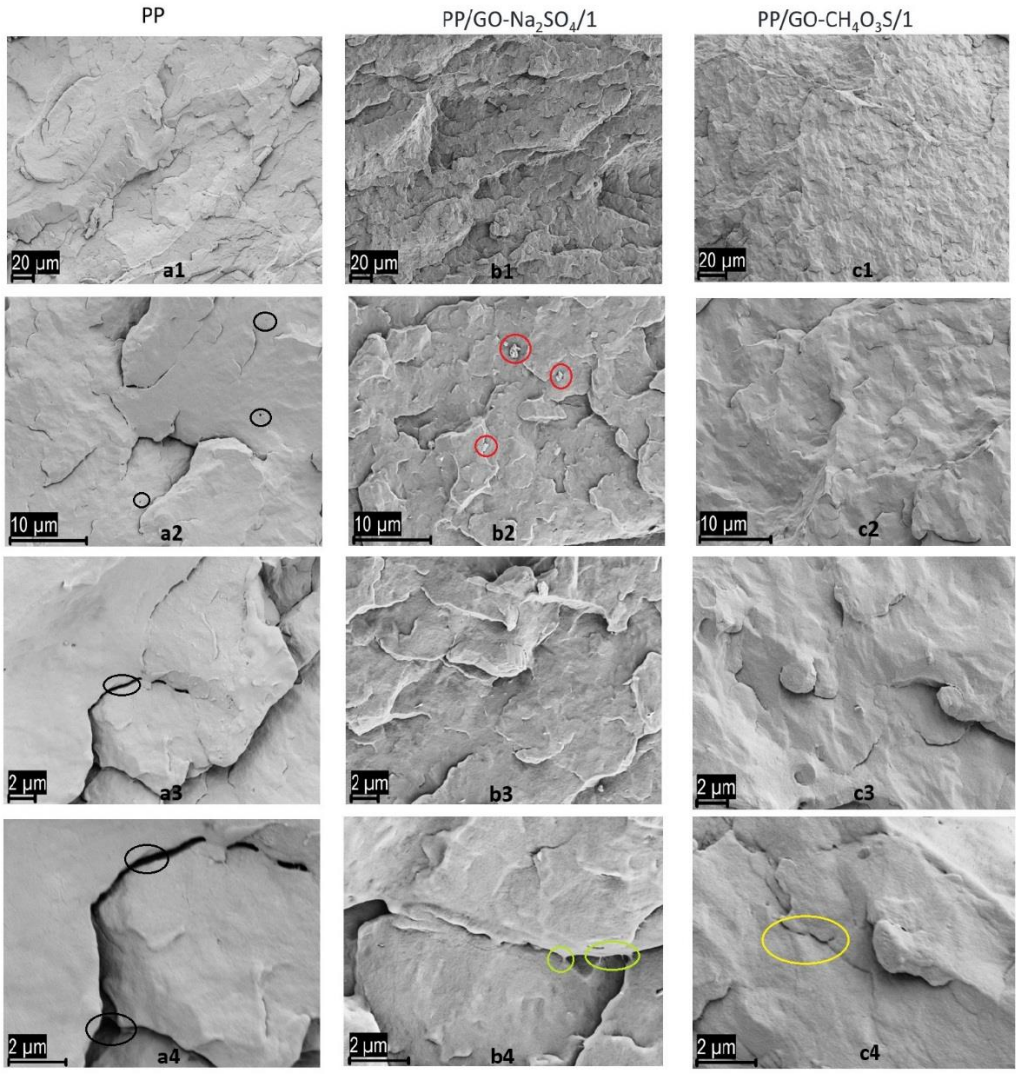

Figure 10. FE-SEM imageas of (a1-a4): Homo PP, (b1-b4): PP/GO-Na_2SO_4/1, and (c1-c4): PP/GO-CH_4O_3S/1

2.5. Conclusions

The current study achieved to disperse sheet-like GO materials through commodity plastics of PP by using a high shear mixer by providing a high degree of exfoliation compared to conventional extrusion process systems since these systems suffer from the agglomeration problem of graphene materials and suitable screw design is required to tailor feeding parameters. Simple and scalable melt-processing of PP with GO was achieved by using an improved and eco-friendly electrochemical exfoliation of GO as a reinforcement to attain high performance commodity plastics. By using the electrochemical approach, GO synthesis was successfully carried out in aqueous and environmentally friendly methane sulfonic acid for the first time. The obtained GO materials were directly used in the manufacturing of PP/GO composites. By the addition of 1 wt.% GO obtained from methane sulfonic acid solution (PP/GO-CH_4O_3S/1), the flexural modulus, flexural strength, and tensile modulus of PP composites increased by 71%, 46%, and 44%, respectively without applying any surface modification or adding any compatibilizer. Additionally, the effect of applied voltage on the quality of GOs obtained in an aqueous sodium sulfate solution in electrochemical production showed that while high voltage led to fewer oxygen groups on GO (%10.93), this situation didn't greatly influence the mechanical properties of the composites. Therefore, to obtain PP/GO composites with high mechanical properties, a faster production can be achieved by increasing the applied voltage in the electrochemical synthesis of GO since high voltage process terminated 2 times earlier than that of low voltage. Rheological results also emphasized that PP/GO composites are also as easily processable as homo PP since there is no major change in the flow properties of PP with the addition of GO. The results demonstrates that GO can be electrochemically synthesized by lowering the environmental impact by using non-toxic acids and salts. GOs, which are produced much faster by electrochemistry, can be used directly in composite productions, and have the potential to significantly increase the performance of the polymer composites. The distinct barrier in mass-scale commercialization of graphene materials might be overcome by electrochemistry and the results show that the electrochemical synthesis of GO materials is open to the development with different solvent systems and can be easily upscale to overcome the needs of composite industry.

CHAPTER 3: Functionalization and Modification of Graphene In Order to Compatibilize Various Surfaces in PP Composites

3.1. Abstract

The interface problem encountered with the graphene addition in polyolefin composites is an important issue and it is necessary to use various compatibilizers to overcome this problem. Maleic anhydride grafted Polypropylene (MAPP), which is an extensively used compatibilizer in PP composites tends to eliminate these interfacial problems by interacting physically through PP chains and allows easier stress transmission from matrix to reinforcer. However, there is a lack of understanding about how this compatibilizer works with graphene-based PP composite systems since MAPP is mostly used to harmonize hydrophilic surfaces of fillers with non-polar PP. With this study, instead of direct usage of MAPP and GNP separately, waste tire driven graphene nanoplatelets (GNP) was grafted by MAPP and the resulted material (MAPP-g-GNP) was compounded with PP by applying high shear rates at a melt phase. Effect of MAPP-g-GNP on the processability, viscoelastic response, and mechanical performance of PP composites were investigated, and high degree of interfacial enhancement was achieved by chemically combined MAPP with amphiphilic type of GNP in PP matrix. The use of MAPP-g-GNP at a loading ratio of 0.1 wt.% resulted in 38% increase in flexural modulus and 26% in flexural strength and tensile modulus compared to neat PP. The two additives used in the PP composite (2 wt.% MAPP and 0.1wt % GNP) were reduced to a single additive (PP/MAPP-g-GNP) with a 95% weight reduction in the additive content of PP. Rheological studies support that MAPP is not as successful as MAPP-g-GNP in strengthening the interface when used alone with GNP due to the lower complex viscosity and the higher crossover frequency. This study contributes to the production of high-performance PP materials with a very low amount of combined GNP and compatibilizer by integrating the circularity approach in compound development by using GNP obtained from recycled and upcycled waste tires.

3.2. Introduction

Due to its ease of processing, low density, high mechanical properties, and low cost, polypropylene (PP) is a thermoplastic polymer, which is widely used commercially, and has applications in many areas such as automotive [44], household goods, and packaging [45]. There is much focus on PP-based composites to improve their mechanical and thermal properties [46]. Using graphene derived materials seems an option and discovery and research on carbon nanofillers has been an attractive area of interest for many researchers in the field of composites [47, 48]. A great effort has been made since 2004 to explore the usages of graphene and graphene-based materials in multi-functional fields [49]. Several attempts using pristine or modified graphene have been reported for PP/Graphene nanocomposites with increased mechanical property [50]. However, the use of functionalized graphene seems to be necessary to strengthen the compatibility of graphene with PP matrix [51]. Additively, using a compatibilizer is generally favoured to overcome surface incompatibility problems. Maleic anhydride grafted polypropylene (MAPP) is a commonly used compatibilizer in PP composites with intent to effectively combine different additive systems such as glass fiber [52], minerals [53], clays [54], and other types of fibres [55, 56] with PP. Due to the low polarity of PP, it is highly difficult to disperse polar group contained reinforcers. Consequently, usage of low amount of MAPP allows formation of an organic surfactant by eliminating the disadvantage of low polymer surface energy with the presence of maleic anhydride [57]. Most of the studies indicate the direct usage of MAPP to combine the inorganic fillers such as glass fiber with PP [52]. One of the uses of MAPP has been graphene based composite materials and studies on the use of MAPP as compatibilizer in graphene-derived composites have recently been the focus of attention [58, 59]. However, MAPP, which is mostly used to harmonize polyolefins with hydrophilic surfaces such as glass fibers, is not able to show the same compatibilizer efficiency in graphene-based composite systems. Such improvements obtained with the addition of 1-2wt.% MAPP in PP/Graphene composites cannot be compassable as it is in PP/GF composites, or this is only achievable with an increase in MAPP content. Additionally, MAPP interaction with graphene changes according to the morphology of the graphene such as sheet or platelet form or according to the type of the graphene such as graphene oxide, reduced graphene oxide or functionalized graphene. Several attempts have been proposed in the literature using MAPP in PP/graphene composites either through physical or chemical attachment. In one

of the studies, 4 phr MAPP in PP/GNP composite resulted increase in tensile strength and modulus by 8% and 96% while 4 phr MAPP in PP/GO composite resulted increase in flexural strength and modulus by 24% and 28% respectively at their optimum content [59]. In another study, 2 phr GNP and 15 phr pyrene functionalized MAPP was used to enhance compatibility in PP composites produced by melt-blending assisted with solvent mixing, which resulted in increase in Young's modulus by 43% compared with that of PP [50]. There are also some attempts to graft MAPP onto graphene oxide through various amine products in order to improve GOs dispersion state in composites [13, 60, 61]. Graziano et al. used 4wt.% MAPP modified RFGO to localize the functional graphene at the interface of the of PP/PE blends [61]. In another study by converting maleic anhydride grafted PP to amino pyridine grafted PP (PP- g-Py), 94 wt.% increase in flexural modulus was obtained by using 20 wt.% GNP and 10 wt.% PP- g-Py. Despite of some improvements, in most of these studies, either the content of GNP (more than 1 wt.%) or the compatibilizer (between 2 wt.%- 15 wt.%) is too high. For scaling up graphene integrated commodity PP products, it is important to adjust the surface properties and provide high degree of graphene exfoliation by using as little additives as possible due to price performance and environmental concerns. It should be emphasized that the choice of appropriate production techniques and the utilization of each resource directly affect the final qualities of the produced graphene and graphene related materials [62]. Therefore, this study showed a way to modify sustainable and upcycled and partially oxidized graphene nanoplatelet from waste tires by using MAPP and comprehensive benchmarking study was carried out to monitor the effect of MAPP either stand alone in the matrix or direct attachment on graphene. To the best of our knowledge, there are few studies focusing on the mechanical performance of MAPP modified graphene in platelet form by addressing the interface effect of the compatibilizer in compounding process of PP with graphene. To understand the interaction of MAPP with GNP and PP, a development of interface model was designed by revealing the differences between adding MAPP separately to the process and grafting it onto GNP. For the functionalization process, GNP was initially functionalized by amino groups and then MAPP was grafted on the GNP surface. Their composites were manufactured in melt phase and comprehensive study was carried out by investigating mechanical, rheological, thermal, and morphological properties of PP composites as well as elaborating the interactions of GO with PP polymer chains by addressing the compatibilizer efficiency of commonly used MAPP. The mechanism for the interface interactions has been

elucidated and study showed that chemically modified GNP might eliminate the excessive usage of compatibilizer and reduce the total amount of required GNP while allowing superior mechanical properties.

3.3. Materials and Method

3.3.1. Materials

Homo Polypropylene (PP) with the density of 905 kg/m^3 and melt flow rate of (MFR) 12g/10 min (230 ^{o}C/2.16 kg) was supplied by Borealis, Austria. Waste tire derived Graphene Nanoplatelet having 9at% oxygen groups (GNP) was supplied by NANOGRAFEN Co., Kocaeli, Turkey (the detailed characterization of GNP was provided in supplementary document). Ethylene diamine Reagent Plus®, ≥99% (EDA), ethanol, and hydrazine hydrate were purchased from Sigma Aldrich, US.

3.3.2. GNP Surface Modification

A literature procedure was adapted and modified from the study published by *Graziana et al.* [61]. In the first step, 0.6 g of waste tire driven GNP was added to 900 mL of deionized water and sonicated for 1 h at a certain cycle and power. 6 ml of ethylene diamine (EDA) was added and stirred for 24 h at room temperature. After 24 h, 6 ml of hydrazine hydrate was added, and the temperature was increased to 95 ^{o} C, and the reaction was followed for 5 h. The product obtained by washing with a mixture of water and ethanol was subjected to vacuum filtration. In the second step, 0.4 g of MAPP was dissolved in 67 ml of toluene at 110 ^{o}C for 1 h. In parallel with this, 0.1 g of the previously synthesized functionalized reduced GNP (FRGNP) material was received, and a new dispersion was prepared by sonication process in the deionized water of 67 ml. After the MAPP/toluene solution had cooled to room temperature, the prepared FRGNP aqueous dispersion was added. The temperature was increased to 95 ^{o}C, and the reaction continued for 18 h under nitrogen atmosphere. After the reaction product cooled to room temperature, vacuum filtration was performed, and drying was carried out in a vacuum oven at 80 ^{o}C for 24 h. The product obtained at the end of these steps was coded as MAPP-g-GNP (MAPP grafted GNP). Drying was done in a vacuum oven at 80 ^{o}C for 24 h.

3.3.3. PP based Compound Production by thermo-kinetic high shear mixer

Manufacturing of all composites were carried out in a melt phase, at 3500-4000 rpm and 200ºC by using custom-made Gelimat-Thermokinetic Mixer (Dusatec Co, USA). When MAPP was added to the composite on its own, it was kept at 2% by weight, which is the general usage rate in the literature and industry. However, when grafted onto GNP, the complete additive system was kept at 0.1% by weight. Table 5 summarizes compound formulations tailored by GNP, MAPP, and modified GNP.

Table 5. The compositions of the produced specimens by thermo-kinetic mixer

		Homo PP (wt %)	**MAPP (wt %)**	**GNP (wt %)**	**MAPP-g-GNP (wt %)**
1	PP	100	-	-	-
2	PP/GNP-0.1	99.9	-	0.1	-
3	PP/MAPP/GNP-0.1	97.9	2	0.1	-
4	PP/MAPP-g-GNP-0.1	99.9	-	-	0.1

3.3.4. Characterization

Raman Spectroscopy was used to understand the quality of functionalized GNP and X-ray Diffraction (XRD) was performed to analyse the structural characterization of materials by using a Bruker D2 PHASER Desktop diffractometer utilizing with a CuKα radiation source. X-ray Photoelectron Spectroscopy (XPS) and Thermo Scientific Fourier transform infrared spectroscopy (FTIR) were used for monitoring functional groups and chemical compositions in the synthesized materials. Thermal analysis was investigated by Differential Scanning Calorimetry (DSC) 3 + 700 (Mettler Toledo, Columbus, OH, USA) under nitrogen gas with 10 °C min-1 heating rate. Synthesized materials and the freeze fractured surfaces coated with a thin layer of gold. Surface morphologies were examined under a Leo Supra 35VP Field Emission Scanning Electron Microscope (FESEM). The mechanical tests were conducted using Instron 5982 Static Universal Test Machine (UTM) for tensile and three-point bending tests according to the ISO 527-2 and ISO 178 standards. Frequency sweep and temperature sweep tests were performed in Anton-Paar MCR 702 Rheometer at 230ºC and strain of 1% in an angular frequency range of 0.01-1000 rad/s. Specimens for tensile and flexural tests were prepared by lab-scale injection moulding at 180º according to the ISO 527-2 and ISO 178 standards.

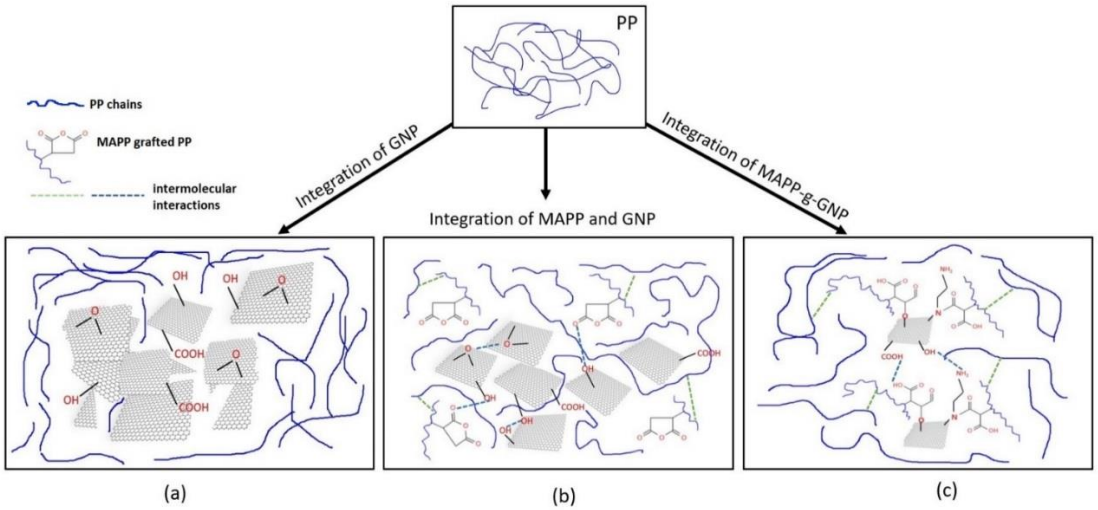

Figure 11. Possible interaction schemes in PP composites with GNP

3.4. Results & Discussion

3.4.1. The characteristics of MAPP modified GNP

MAPP is a widely used compatibilizer to provide high degree of compatibility between PP matrix and the various kind of fillers or reinforcers. To be able to illustrate the physical or chemical interactions, Figure 11 represents the possible interaction schemes upon integration of MAPP either directly to the composite or grafting it onto GNP. GNP with including 9 at. %Oxygen content which will be indicated in the forthcoming sections, shows both hydrophilic and hydrophobic interactions due to its surface oxygen entities and the strong Van der Waals interactions among GNP stacks. Therefore, in the absence of MAPP, GNP tends to agglomerate due to the incompatibility with PP matrix as demonstrated in Figure 11a. When MAPP is added at a certain amount to the composite, the oxygen functionalities of GNP may attach with the anhydride group of MAPP allowing higher degree of exfoliation as illustrated with Figure 11b. However, when MAPP is grafted onto GNP, interface is becoming stronger due to the chemical attachment of MAPP onto GNP by the help of amino functional groups of EDA. Reaction mechanism of functionalization of GNP with EDA followed by MAPP grafting is explainable as the EDA attacks the OH of the carboxyl groups at the edges of GNP and introduces NH_2 moieties meanwhile breaking the epoxy group on the main lattice of GNP so-called "cyclization-removal deoxygenation mechanism by the reconstruction of the sp^2 C=C bonds, with releasing of hydroxylamine molecules [61]. Lastly the amidation reaction took place between carboxyl groups of MAPP and the NH_2 which was also demonstrated in Figure 11c.

FTIR spectra of the GNP, FRGNP and MAPP-g-GNP are shown in Figure 12a. The newly formed peak at 1254 cm^{-1} depicts the vibrational movements of the C-N bond proving that the amination reaction was successful. Peaks at the 2957 cm^{-1} band are belong to the C-H bonds of ethylene diamine. Similar results on diamine-functionalized carbon materials have been reported in previous literature [63]. In Figure 12b, the binding of MAPP on FRGNP is shown. The disappearance of the C-N peak in FRGNP and the newly formed peak at the 1587 cm^{-1}in MAPP-g-GNP confirms the amidation linkage formed by the reaction of amine and carboxyl groups. While the broad peak observed at 3438 cm^{-1} belongs to the OH groups, the vibrational N-H bonds of the amine and amide groups, which are expected to be observed in the 3200 cm^{-1} band, coincide within the broad OH peak. [64]. Figure 12c shows the comparison of the FTIR spectra of MAPP and MAPP-g-GNP to distinguish differences between the two. The disappearance of the peak in the 1715 cm^{-1} band observed in the MAPP and the peak at 1587 cm^{-1} in MAPP-g-GNP indicates that the reaction occurs via acid groups on maleic anhydride and the formation of amide linkage. Additionally characteristic absorption peaks of MAPP at 1781 and 1715 cm^{-1} (–C=O stretching bands of maleic anhydride), 1455 cm^{-1} (asymmetric C–H bending vibration of $–CH_2$ and $–CH_3$ groups), 1375 cm^{-1} (symmetric C–H bending vibration of $–CH_2$ and $–CH_3$ groups) can be detected as the similar findings have also been reported in previous literature [65].

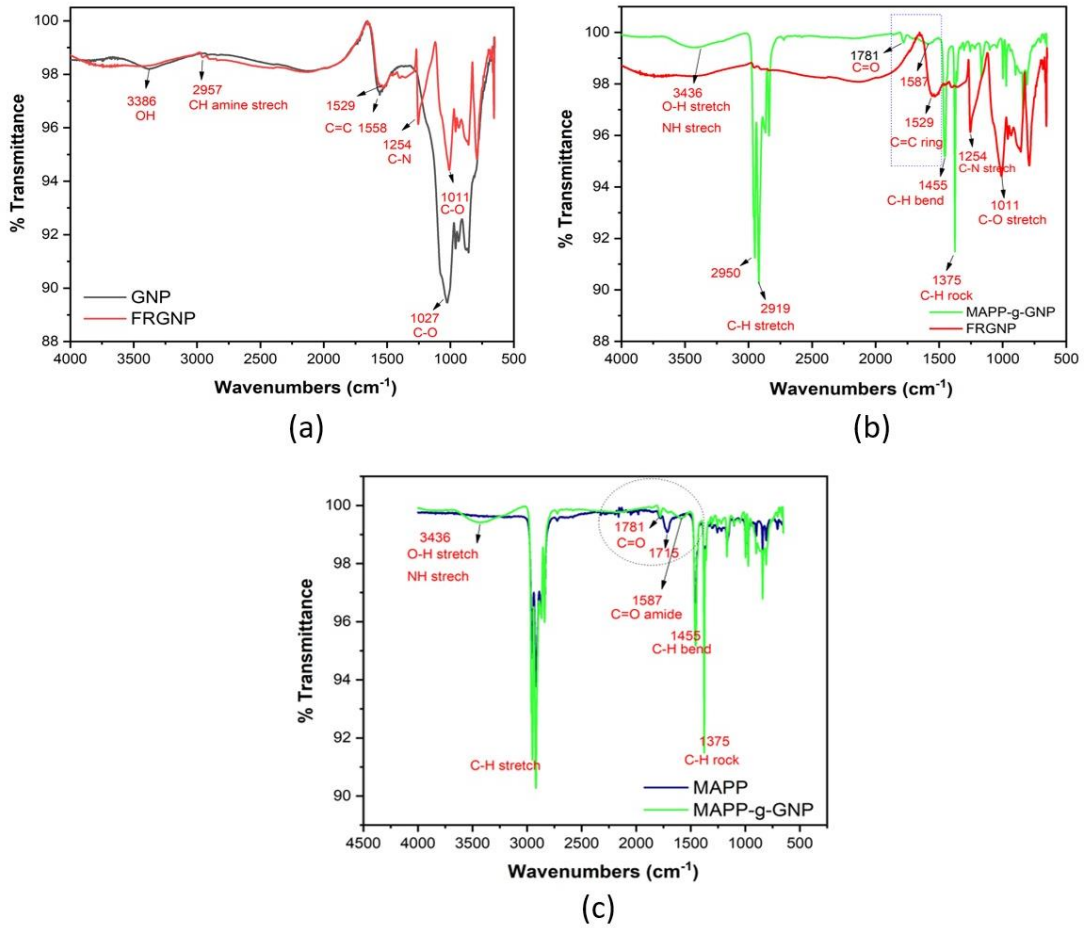

Figure 12. FTIR spectra of comparison of (a) GNP and FRGNP, (b) MAPP-g-GNP and FRGNP, and (c) MAPP and MAPP-g-GNP

Another characterization method used for the analysis of functional groups formed on the surface of FRGNP and MAPP-g-GNP is X-ray photoelectron spectroscopy. The analysis results obtained from X-ray photoelectron spectroscopy of GNP, FRGNP and MAPP-g-GNP are shown in Figure 13 and Table 6. According to the results, while nitrogen content is 1.87% in modified GNP, this ratio is 0.88% in MAPP-g-GNP. In the C1s spectra seen in Figure 13a and 13b, the binding energy of the carbon-nitrogen atom is detected at 285.08 eV. In Figure 13c, N1s spectrum of FRGNP at 400.58 eV corresponds the C-NH_2 bonds [66]. In Figure 13d, the binding energy of the amide bond is seen at 399.28 eV. According to the results, it is possible to conclude that amine groups are attached on GNP and that both amine and amide groups are attached on MAPP-g-GNP. In this case, it is seen that the modification studies were carried out successfully.

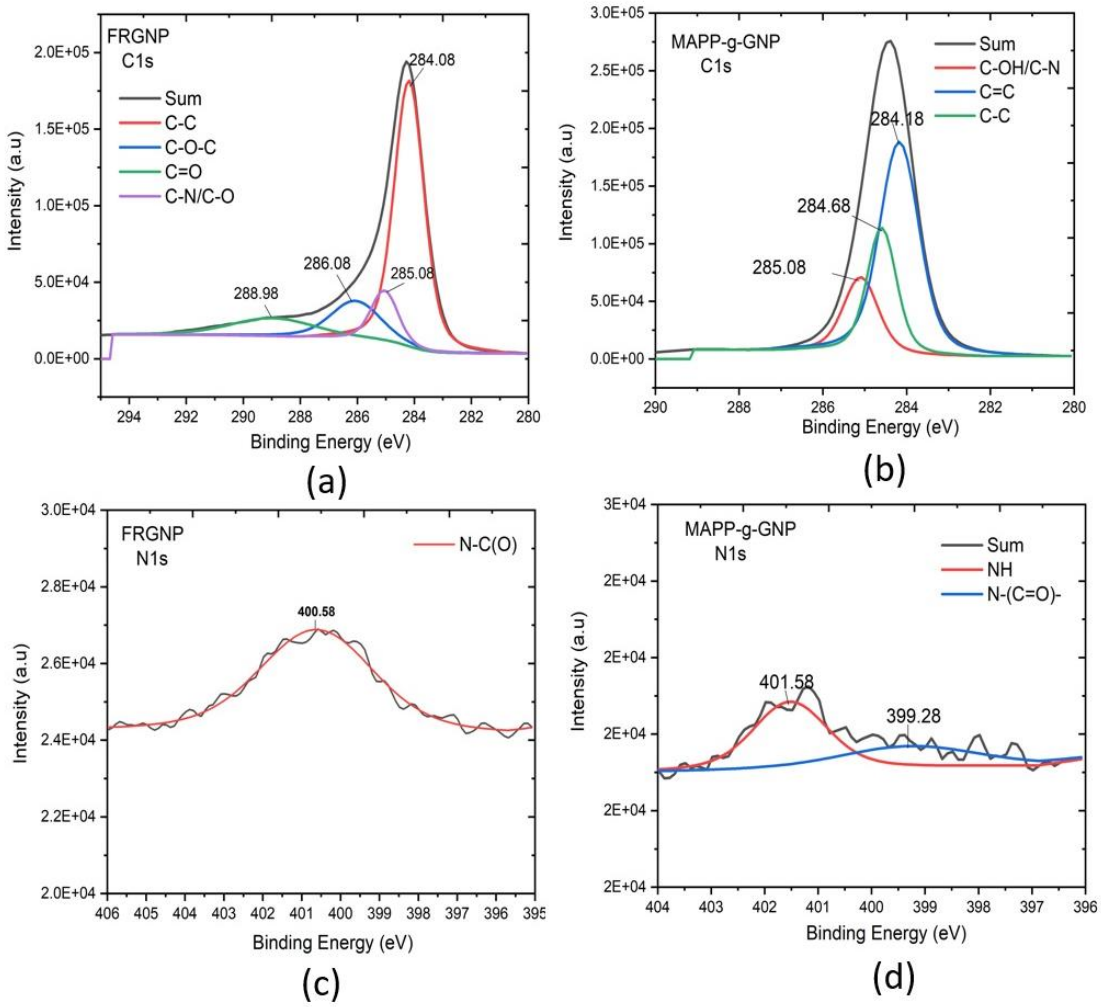

Figure 13. XPS deconvoluted C1s peaks of (a) FRGNP, (b) MAPP-g-GNP, and N1s peaks of (c) FRGNP, (d) MAPP-g-GNP

Table 6. XPS survey scan results of GNP and its functionalized samples

Sample Name	C (at%)	O (at%)	N (at%)	Others (at%)
GNP	87.39	9.13	-	3.47
FRGNP	82.34	11.56	1.87	4.22
MAPP-g-GNP	93.96	4.48	0.88	0.68

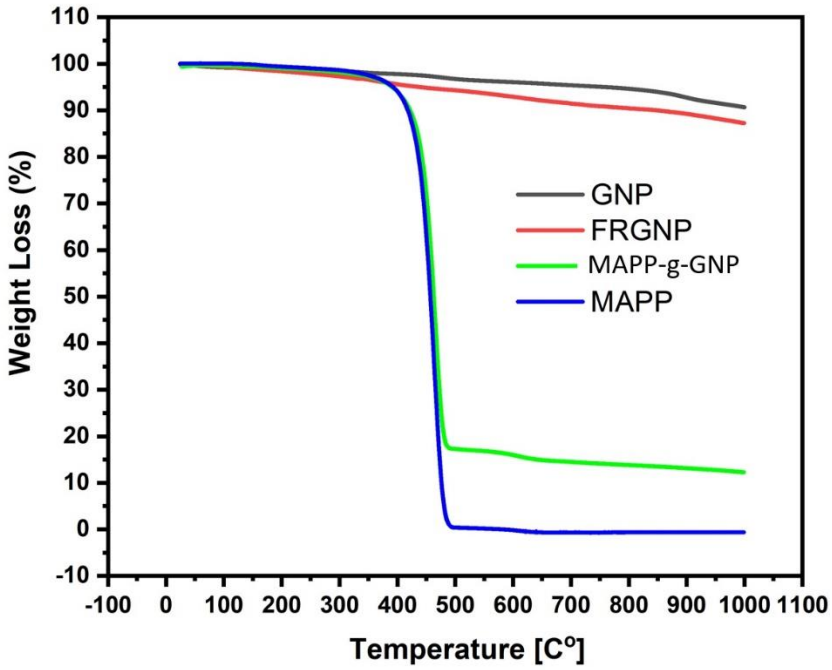

Figure 14. TGA curves of GNP, FRGNP, MAPP, and MAPP-g-GNP

The graph of the TGA test performed in the nitrogen atmosphere of the synthesized graphene-based materials is shown in Figure 14. While the residual weight of GNP calculated as 90%, the residual weight in FRGNP is found to be 87%. In this case, the 3% difference in residual weight is due to the amine functionalization on the GNP and the amine content is 3 wt.%. Residual weight of MAPP was 0%, while it is 12 wt.% in MAPP-g-GNP indicating that the modification with GNP on MAPP is successful and around 12% in weight.

SEM images of untreated GNP and MAPP-g-GNP at different magnifications presented in Figure 15. As seen in Figure 15a, the untreated GNP is in the form of platelet and layered structure. In Figure 15b-d, GNP platelets are densely visible on the surface of MAPP. Some of the GNPs on the MAPP are also indicated by yellow arrows. GNPs seen locally at the ends of the polymer layers and a little inward from the ends prove that GNP is strongly attached to MAPP. Further characterization regarding to GNP modification can be found in the supplementary document.

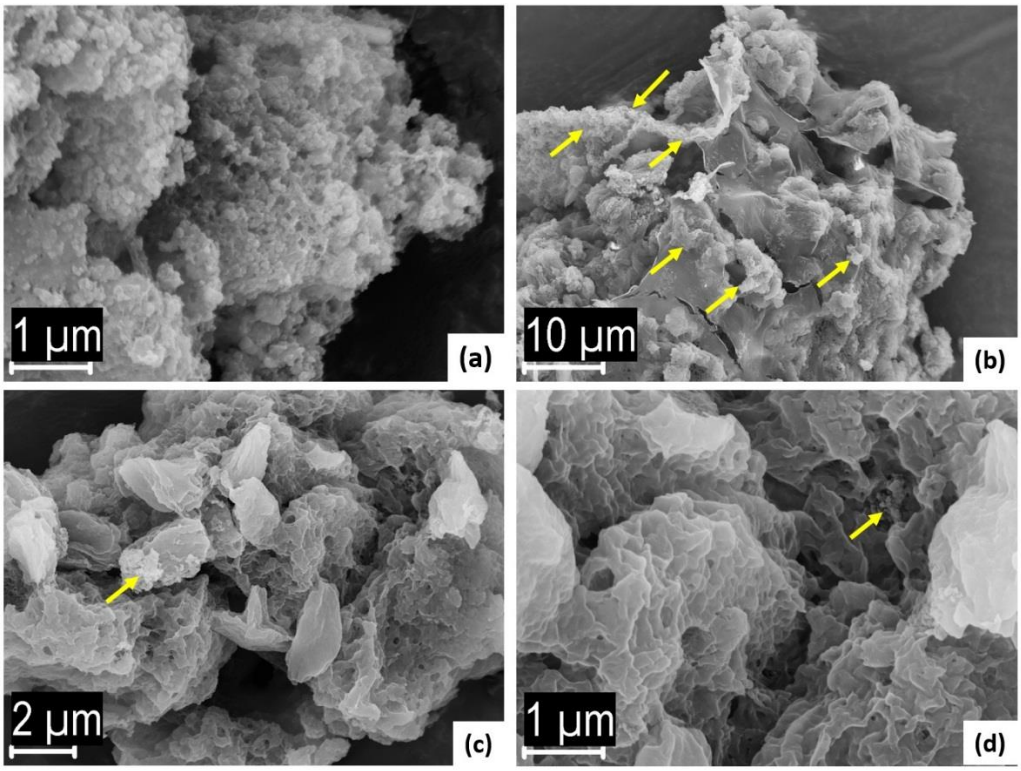

Figure 15. SEM images of (a), (b) GNP and (c), (d) MAPP-g-GNP at different magnifications

3.4.2. Mechanical performance of PP composites reinforced by MAPP-g-GNP

Incorporation of graphene into polymer matrices will significantly enhance the mechanical properties which depend on several factors such as processing conditions, type of graphene, aspect ratio and loading content of graphene [67]. In-Situ polymerization, melt mixing, and solution mixing are the main composite production techniques and here melt mixing method was used for all composite manufacturing and the disadvantage of poor dispersity of melt mixing was overcome by using a high shear thermokinetic mixer instead of commercial twin screw extruder [68]. By keeping the GNP ratio to a minimum, mechanical performance of the composites was investigated in terms of tensile and flexural tests. Stress-strain curves are presented in Figure S2 (supplementary document). As shown in Table 1, MAPP-g-GNP was used as an additive in the PP/MAPP-g-GNP composite at an only 0.1 wt.% while the other composites include much more additive and GNP content. Table 7 and Figure 16 summarize the obtained results and positive increases in mechanical properties occurred with the addition of both MAPP and MAPP-g-GNP due to the increased interfacial interactions between polymer and GNP. MAPP, which acts as a bridge for stress transfer between the matrix and graphene improved the mechanical stability of the composites. PP/MAPP-g-

GNP achieved 38% and 26% improvements in flexural modulus and flexural strength, respectively, while an increase of 26% and 7% was observed in the tensile modulus and the tensile strength. The modified graphene, MAPP-g-GNP, has been successful in improving the interface. Although the mechanical increases of PP/MAPP/GNP-0.1 and PP/MAPP-g-GNP-0.1 seem to be approximate, it should be noted that while the ratio of MAPP compatibilizer in the PP/MAPP/GNP-0.1 sample is 2% and the GNP content is 0.1%, the total compatibilizer and GNP in the PP/MAPP-g-GNP is only 0.1% in total. Nominately, while the total additives used in the PP/MAPP/GNP-0.1 composition are 2.1% (2% MAPP + 0.1% graphene), the total additive content is only 0.1% in the PP/MAPP-g-GNP sample. Functionalized GNP with MAPP is much more effective improving mechanical properties than that of separate integration of MAPP and GNP. Additionally, obtained results are much more promising since in most of the studies in PP/GNP composites, the GNP content is between 1 wt.% to 10 wt.% as reviewed by Lee et al [69].

Table 7. Summary of mechanical properties of GNP and functionalized GNP reinforced PP composites

Sample Name	Flexural Modulus (MPa)	Flexural Strength (MPa)	Tensile Modulus (MPa)	Tensile Strength (MPa)	Elongation at Break (mm)
PP	1263 (± 35.6)	38.3 (±0.4)	1556 (± 87.8)	38.9 (± 1.7)	540 (± 38.3)
PP/GNP-0.1%	1546 (± 7.05)	43.8 (± 0.3)	1659 (± 46.0)	40.5 (± 0.4)	610 (± 14.8)
PP/MAPP/GNP-0.1%	1690 (± 34.6)	48.1(± 0.3)	1947 (± 27.3)	39.0 (± 0.4)	550 (± 48.0)
PP/MAPP-g-GNP-0.1%	1737 (± 30.6)	48.2(± 3.0)	1963 (± 27.2)	41.5 (± 2.6)	533 (± 5.8)

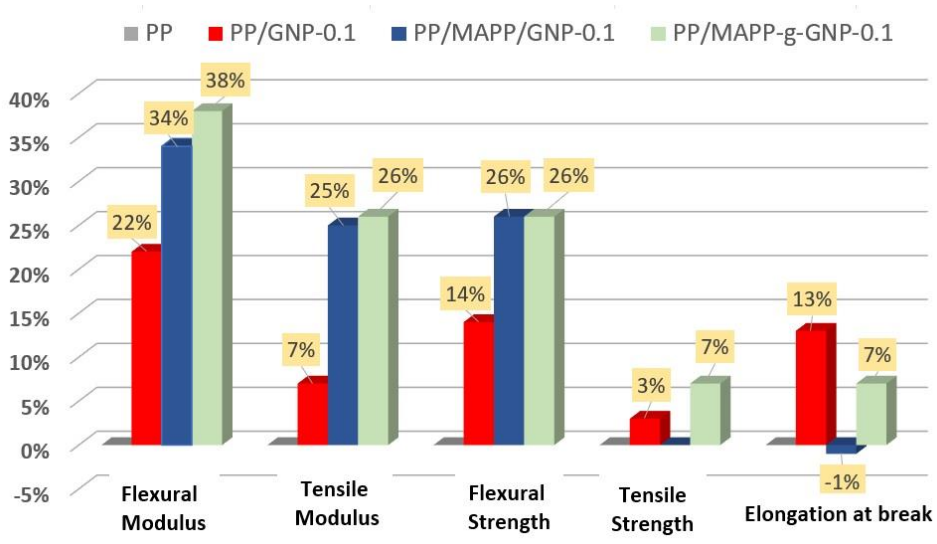

Figure 16. Mechanical improvements of GNP and functionalized GNP reinforced homoPP composites compared to unfilled homoPP

3.4.3. Rheological behaviour of PP composites reinforced by MAPP-g-GNP

The mechanical properties of polymer nanocomposites are directly related to the dispersion state of the particles and polymer-particle interactions, and therefore it is very important to be able to measure the size and degree of dispersion of the particles embedded in the polymeric matrix [19]. Complex viscosity, storage modulus, loss modulus, and crossover frequency of composites are presented in Figure 17. Adding GNP lowered the complex viscosity compared to Neat PP and additional MAPP lowered the viscosity further due to the lubricant effect of GNP and MAPP together. However, in PP/MAPP-g-GNP-0.1 composite, viscosity improved since the dispersion quality of GNPs much better by modifying GNP surface with MAPP. The polymer melt shows fluidity at low frequencies and the loss modulus is higher than the storage modulus. When the frequency is high enough, the material starts to behave more elastically, and the elastic modulus intersects with the storage modulus. The point of this overlap is called the crossover frequency and gives important information about the relaxation times of the materials. A shift to lower values in the crossover frequency indicates that the relaxation time of the polymer is increased [70]. PP/GNP composites pushed forward the crossover frequency compared to Neat PP meaning that composite remains viscous at longer shear range interval. The reason for this crossover occurring at high frequencies is that the polymer chains do not have enough time to respond to this stress [71]. Viscous portion of PP/GNP-0.1 and PP/MAPP/GNP-0.1 composites lead to increase in energy dissipated as heat due to the improved rearrangement ability of deformed polymer segments with GNP and MAPP incorporation. In PP/MAPP-g-GNP-0.1 composite, the crossover frequency decreased to 158 rad/s, lower than that of neat PP, which means elastic behaveour starts to dominate at a lower frequency. The transition to viscous behaviour shifted to a lower frequency because the stress required to break the microstructure of the material with the developing interface began to be less than the material strength, so the storage time of this energy increased, and the storage modulus improved.

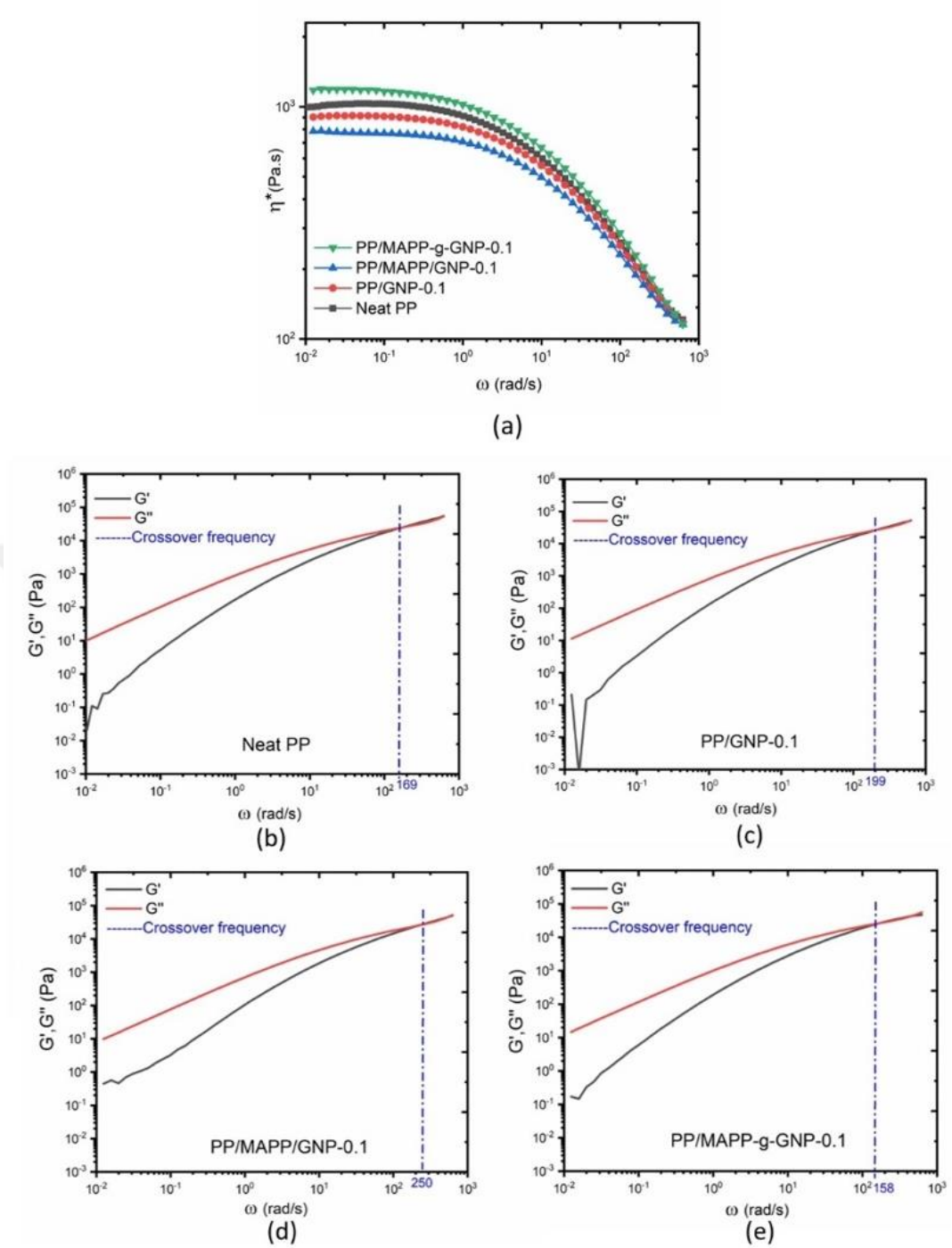

Figure 17. (a) Complex viscosities of the composites, and storage modulus, loss modulus and crossover frequencies of (b) Neat PP, (c) PP/GNP-0.1, (d) PP/MAPP/GNP-0.1, (e) PP/MAPP-g-GNP-0.1

Figure 18 shows the complex viscosity, storage modulus and, loss modulus values of the composites as a function of temperature. As the temperature decreased, the viscosity of the materials increased because the chain movements were restricted with the decreasing temperature. However, in PP/MAPP-g-GNP-0.1 composite, a greater resistance developed at around 135 °C compared to other composites as a result of improved molecular interactions along with the improved melt strength of the composite. Another

reason for this such elevation might arise from chemically attached MAPP onto GNP since it affects the mobility of GNP layers as these MAPP molecules create a heavy load on these very light GNP layers which leading steric hindrance and limited movement of the GNP concurrently resulted in restricted polymer matrix.

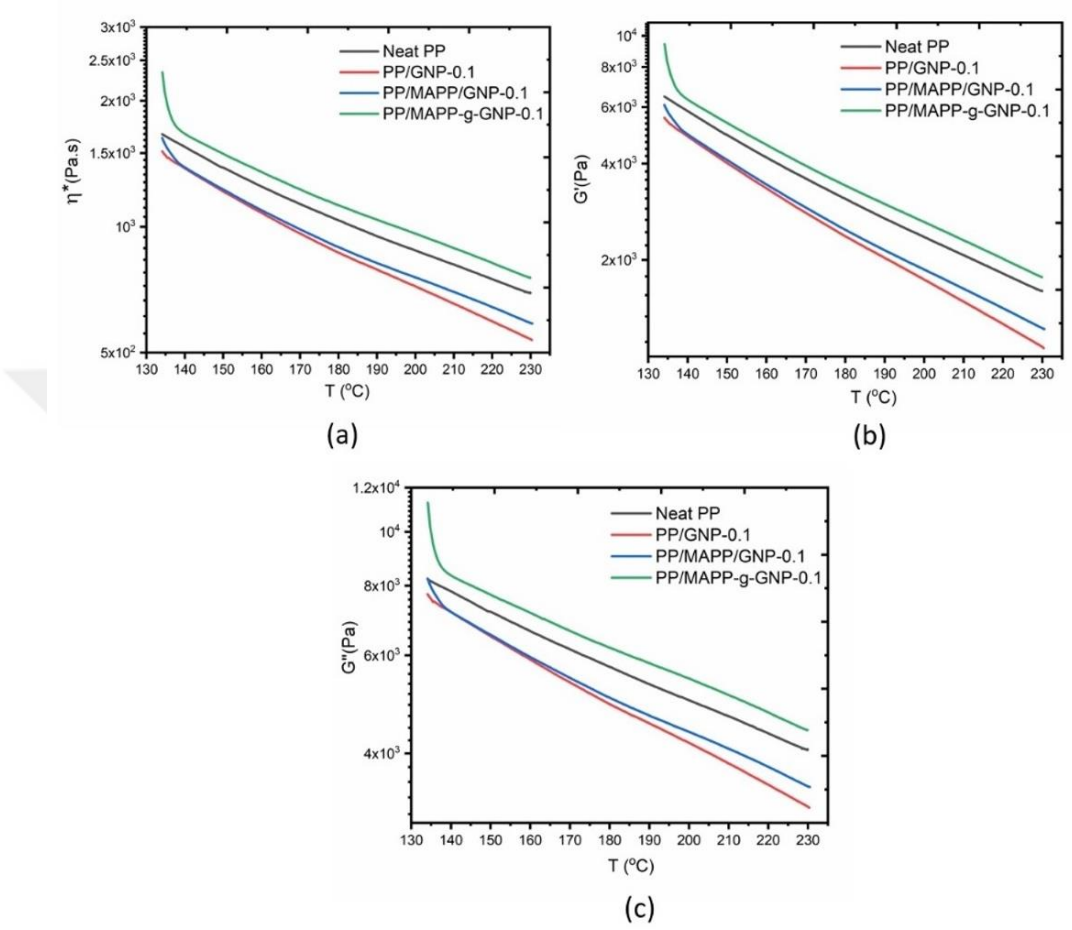

Figure 18. (a) Complex viscosity, (b) storage modulus, and (c) loss modulus of the composites as a function of temperature

3.4.4. Thermal characteristics of MAPP-g-GNP reinforced PP composites

DSC is a practical analysis tool for finding the melt and crystallization behaviour of polymeric materials. In this study both the melting temperatures (Tm) and crystallisation (Tc) temperatures were evaluated by using DSC and the extracted results are reported in Figure 19 and Table 8. The nucleating effect of GNP accelerating crystallization is revealed since the crystallization temperatures of all composites shifted to higher temperatures compared to neat PP and that is consistent with the studies in the literature in PP/GNP composites. Addition of GNP raised the Tc by 9^{o}C because of the GNP acting as nucleating agent [72]. As a result of the high Van der Waals interactions between the GNPs, this may automatically contribute to the crystallization of the polymer chains as

well. Since the GNPs are located between the polymer chains, the intense interaction of the GNPs with their own platelets can facilitate heterogeneous crystallization by making it easier for the chains to converge. PP/GNP-0.1 and PP/MAPP-g-GNP-0.1 exhibit similar behaviour in terms of % Xc and Tm. Even though they both showed 50% crystallinity, their individual crystalline peaks indicate that the crystal behaviour of matrix has changed. The crystalline arrangement is more uniform in PP/MAPP-g-GNP-0.1 due to the narrower and sharper melting peak compared to others. This proves that more equal crystal sizes are formed for PP/MAPP-g-GNP-0.1. On the other hand, PP/MAPP/GNP-0.1 showed lower crystallinity (Xc = 44%) and enthalpy values than PP and the other composites. The energy required to form crystals and to melt those crystals reduced with the addition of high amount of MAPP in the matrix since MAPP acts as lubricant and make it harder for polymer chains to cluster in cooling run resulting lower crystallization enthalpy. Following this, it is easier to melt those crystals with lower energy due to the same reason. However, Tc may still be located at higher temperatures due to the existence of GNP.

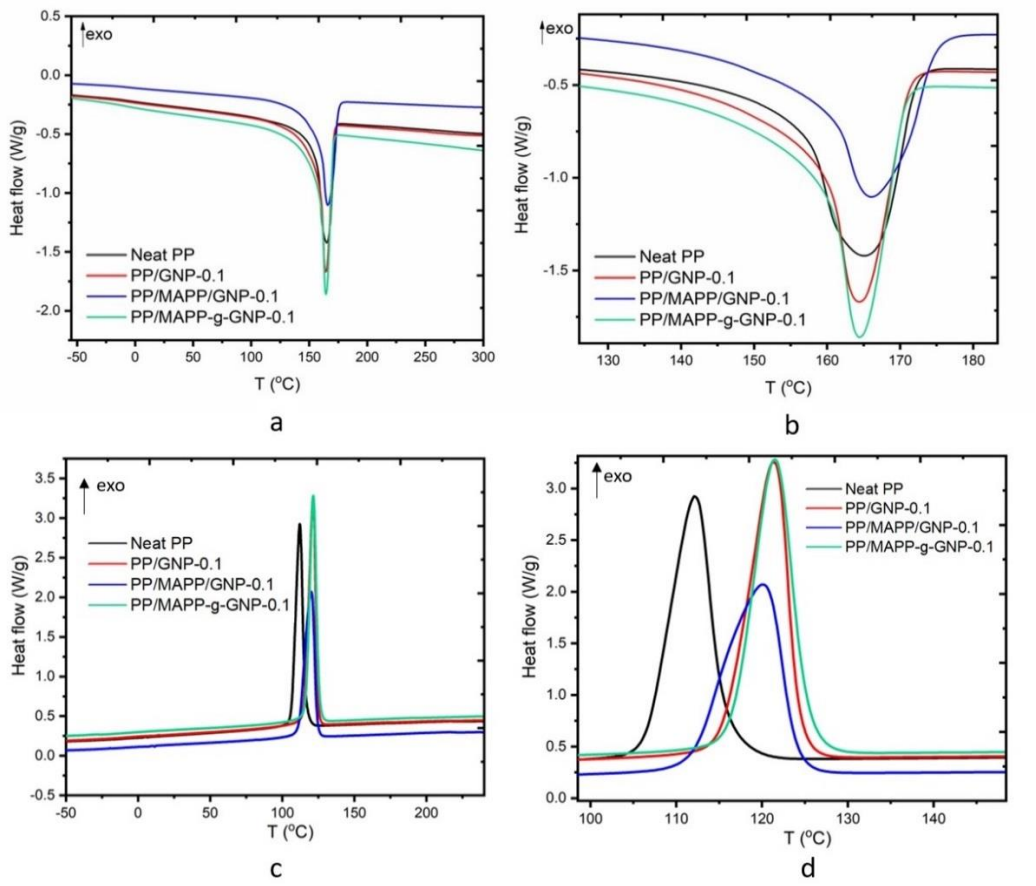

Figure 19. DSC curves: (a) Second heating run, (b) zoom second heating, (c) cooling run, and (d) zoom cooling run of PP based specimens

Table 8. Summary of thermal properties of neat PP and its GNP reinforced composites obtained from DSC characterization.

Sample	Crystallinity	Second heating run		Cooling run	
	X_c (%)	ΔH_m (j/g)	T_m (^oC)	ΔH_c (j/g)	T_c (^oC)
PP	46	96	165	94	112
PP/GNP-0.1	50	104	164	100	121
PP/MAPP/GNP-0.1	44	91	166	89	120
PP/MAPP-g-GNP/0.1	50	105	164	102	122

Thermal stability of the composites in the nitrogen atmosphere were presented in Figure 20. Depolymerization, random chains scission, and side-group elimination are the three main reactions during non-oxidative thermal degradation of polymers and random chain scission is a typical degradation mechanism for polyolefins by means of randomly created free radicals along the main polymer chains resulted in the fragmentation of polymer chains into smaller molecules [73]. With the addition of MAPP-g-GNP, the polymer began to degrade earlier compared to other materials, and polymers' thermal stability decreased. Neat PP and PP/GNP-.01 showed almost the same stability probably due to the non-dispersed agglomerates of nanoplatelets, very low amount of GNP, and the absence of products that may initiate the start degradation. Studies containing high amount of GNP (more than 1wt.%) in PP resulted in improved thermal stability [39]. Mechanism associated with these improved thermal stability has been linked to GNP acting as barrier for the movement of the volatile gases formed during degradation and are trapped within the composite and cannot escape [74]. However, in this study, the GNP content is 0.1 wt.% and therefore the thermal stability didn't change as much. On the other hand, with the presence of MAPP-g-GNP, intra molecular hydrogen abstraction may take place leading to the formation of adjacent hydroperoxides along the polymer chain that are less stable than isolated hydroperoxides and lead to an increased rate of initiation due to the functionalization steps of GNP and possibly remain residuals.

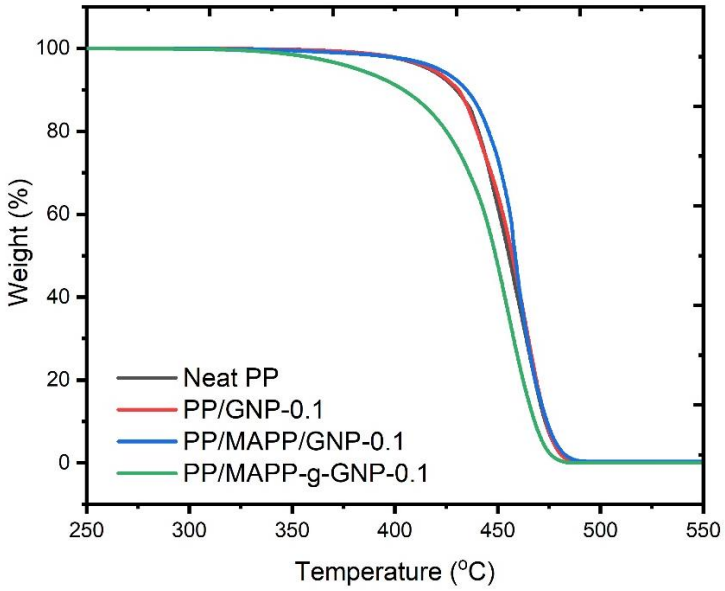

Figure 20. TGA curves of neat PP, GNP and its functionalized PP composites

3.4.5. Cross-sectional analysis of GNP and functionalized PP based composites

Surface morphologies in the fractured area provide an understanding of the dispersion behaviour of graphene in the matrix [75]. SEM analyses were performed to examine the morphology of the fracture surfaces of Neat PP and composites. When Figure 21a is examined, images of a typical ductile surface of neat PP are observed. However, the cracks indicated by the red arrow on the fracture surface indicate that there is no obstacle to prevent the progression of the crack after it has formed. With the addition of GNP into PP, the matrix became more unified, and the crystalline fragments increased, as seen in Figure 21b. GNP prolonged the crack propagation path in the composite as this possibility reported in the literature [76]. Although it is thought that the interface will improve with the addition of 2 wt.% MAPP in Figure 21c, some voids have occurred in the matrix and indicated by blue arrows. This shows that the air trapped inside cannot completely escape from the matrix. Finally, with the addition of MAPP-g-GNP, crack bridges, indicated by yellow arrows, were formed as the interface became stronger. The elongation (yellow arrows) that occur on the fracture surfaces due to the resistance of the material while breaking indicates that the matrix has changed from a brittle structure to a tougher structure.

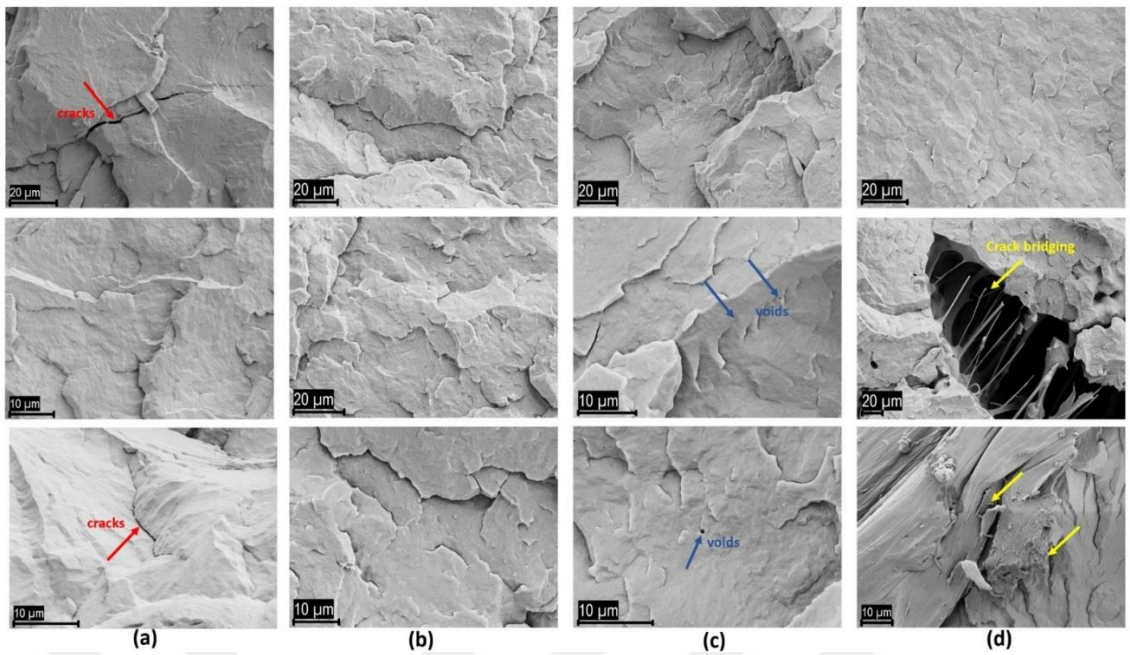

Figure 21. SEM images of column (a)PP, (b) PP/GNP-0.1, (c) PP/MAPP/GNP-0.1, and (d) PP/MAPP-g-GNP-0.1 composites at different magnifications

3.5. Conclusions

Current study achieved to graft MAPP onto upcycled GNP (MAPP-g-GNP) and disperse 0.1 wt.% MAPP-g-GNP in PP matrix by using a high shear rate thermo-kinetic mixer. MAPP was successfully grafted onto the surface of waste tire driven GNP and a single additive system (MAPP-g-GNP) was produced instead of using two additives separately (MAPP and GNP) in PP matrix. By keeping the required amount of MAPP and GNP to a minimum, the composite properties were maximized in terms of flexural and tensile behaviours as well as their viscoelastic behaviour. The use of MAPP-g-GNP at a rate of 0.1 wt.% resulted in 38% increase in flexural modulus and 26% in flexural strength and tensile modulus compared to Neat PP. Rheological investigation proved that MAPP-g-GNP strengthened the interface and improved the particle dispersion as well as strengthening the melt strength of neat PP. The mechanism for the interface interactions has been elucidated and study showed that chemically modified GNP might eliminate the excessive usage of compatibilizer and reduce the total amount of required GNP while allowing superior mechanical properties.

While the present study focused on a 0.1 wt.% loading ratio of MAPP-g-GNP, it would be valuable to explore the mechanical properties and dispersion behavior at higher filler concentrations. Assessing the performance of the composite at elevated GNP loadings would provide insights into the potential for achieving enhanced properties while

maintaining good dispersion and avoiding excessive aggregation. Expanding the investigation to other polyolefin matrices can broaden the potential applications of the MAPP-g-GNP composite system. Assessing the compatibility and performance of MAPP-g-GNP with different polyolefins, such as polyethylene (PE), could provide valuable insights into the broader applicability of the compatibilizer-grafted GNP approach. Further optimization of the compounding process parameters, such as melt temperature, shear rate, and mixing time, could potentially enhance the dispersion and interfacial adhesion between MAPP-g-GNP and the PP matrix. Systematic investigations into the effects of these processing parameters on the mechanical properties and morphological characteristics would provide valuable insights for industrial-scale production.

CHAPTER 4: Selective Localization of Upcycled Graphene in PP/PE Nanoblend Composites

4.1. Abstract

Polymer blending is a widely utilized technique that offers significant advantages in terms of cost-effectiveness and the development of materials with diverse properties. However, achieving compatibility between polymers remains a challenge due to their non-negligible entropy, particularly in the case of immiscible polymers like PP and HDPE. Incorporating a third additive into polymer blends, known as ternary nanoblend systems, has emerged as a promising approach to enhance compatibility and overall performance. However, the success of such systems heavily depends on optimizing factors such as additive selection, mixing methodology, composition, and processing conditions. Despite the extensive industrial usage of polymers like PP and HDPE, there is still limited understanding regarding the impact of blending these polymers, especially when graphene is introduced. This study addresses these challenges by overcoming the entropy barrier between PP and HDPE using a high shear rate thermo-kinetic mixer and employing upcycled graphene through interface engineering. Comprehensive investigations encompassing morphological, mechanical, rheological, and thermal analyses were conducted on binary and ternary nano blend systems. The results demonstrate that by carefully selecting the polymer weight fraction and utilizing a minimal GNP content, GNP can be localized at the blend interface, leading to remarkable mechanical performance with the optimized manufacturing technique. Incorporating 0.1 wt.% GNP resulted in a significant 38% increase in tensile modulus, while flexural modulus and flexural strength saw respective increments of 39% and 22% compared to neat PP. Further enhancements were observed with higher GNP contents. This study presents a compelling low-cost blend formulation suitable for industrial applications by replacing expensive PP with a more economical PP/HDPE blend that is potential for achieving improved mechanical performance through adaptable processing techniques.

4.2. Introduction

The production of polymer blends is a commonly employed technique to enhance the performance of polymers and considered to be economically advantageous [77]. The economic advantages of polymer blends arise from the ability to leverage the favourable properties of two existing materials through mixing, rather than resorting to the synthesis of new materials. However, in practice, the problem of the incompatibility of polymer blends is often encountered [78]. Most polymers are immiscible and they do not mix homogeneously with each other due to their inherent and unfavourably low mixing entropy [79]. Polypropylene (PP) and Polyethylene (PE) are one of these immiscible polymers as commodity plastics and there are a few attempts to improve the compatibility of PE and PP, typically by adding a third component [61]. Graziano et al. used 2 wt.% of reduced graphene oxide (RGO) in PE/PP blends resulting in finer droplet-matrix morphology [80]. In another study, they dispersed a functional graphene at the interface of PE/PP blend and improved the thermo-mechanical properties of the nanocomposites [81]. There are studies showing that polymer droplet diameters get smaller, especially if the localization of nanoparticles at the interface of two polymers can be achieved [82, 84]. Studies are showing that nanoparticles can enhance the compatibility of polymer blends by reducing the surface tension [85]. Recently, graphene and derivatives have been used to improve compatibility of different polymer blend systems [12, 45, 86]. Bera et.al used RGO for compatibilization of poly (vinylidene fluoride) (PVDF) and thermoplastic polyurethane (TPU) blend resulting finer distributed holes [87]. In another study, thermally reduced graphene oxide (TRG) was selectively localized at the interface of PP and PE blend by tailoring processing sequences [88].

Another parameter that effects the compatibility of polymer blends is the kinetic and process-related parameters since the temperature, shear force, screw design and speed also play a significant role in achieving a homogeneous distribution [89]. Therefore, a blend morphology can be tailored by choosing right manufacturing techniques and equipment. In a study, GNPs localization at the interface of a polymer blend was controlled by melt-compounding sequences, mixing times and shear rates [83]. The conventional production method in melt blending of polymers is twin-screw extrusion [90]. It involves the melting of polymers along with additives by exceeding their melting temperature using twin rotating screws with co-rotating or counter-rotating designs tailored to desired characteristics. On the other hand, another production method, known

as thermo-kinetic mixer, can offer advantages such as improved dispersion of fillers at high shear rates (3500-4500 rpm) and shorter production cycles (30 seconds), leading to better dispersion and distribution compared to conventional extrusion [91] and other type of internal mixers [92]. The thermo-kinetic mixer, especially, facilitates the easier exfoliation of nanofillers between polymer chains and prevents agglomeration issues encountered during polymer processing [51]. Therefore, morphology investigation on polymer blends by using a thermo-kinetic mixer can be effective in exploring blend compatibility, as the majority of previous polymer blend studies have primarily focused on twin-screw extrusion processes when melt compounding is under focus [89, 93, 96].

Herein, PP/HDPE binary blends and PP/HDPE/GNP ternary nanoblends were produced by using a high shear rate thermo-kinetic mixer and their mechanical, rheological, and morphological analysis were conducted to investigate compatibilization of the blend system. Results showed that by choosing the right manufacturing technique and the optimum GNP loading, GNP can be localized at the interface of the binary blends and improve the blend performance in terms of mechanical properties. Additionally, PP/HDPE blend matrix can be an alternative matrix to solely PP since the synergistic effect of this blend showed a higher mechanical property compared to neat PP and HDPE. Together with, the addition of GNP at a 0.1 wt.% resulted 38% increase in tensile modulus, while 39% and 22% increase in flexural modulus and flexural strength was achieved, respectively. Further enhancement was achieved by increasing GNP content to 1 wt.%. Therefore, this study provided a low-cost blend formulation for industrial applications by changing the matrix composition from more expensive PP to a cheaper blend of PP/HDPE by improving the mechanical behaviour via an adaptable processing technique.

4.3. Materials and Methods

4.3.1. Materials

Homo Polypropylene (PP) with the density of 905 kg/m^3 and melt flow rate of (MFR) 12 g / 10 min (230 ^{o}C / 2.16 kg) was supplied by Borealis, Austria. High density Polyethylene with the density of 965 kg/m^3 and melt flow rate of (MFR) 5.5 g / 10 min (190 ^{o}C / 2.16 kg) was supplied by Petkim. Waste tire derived Graphene Nanoplatelet containing 9 at.% oxygen groups (GNP) was supplied by NANOGRAFEN Co., Kocaeli, Turkey and the detailed characterization of GNP can be found in supporting information.

4.3.2. Polymer Blending

Manufacturing of all blends and nanoblends were carried out in a melt phase, at 3500-4000 rpm and 200 ºC by using custom-made Gelimat-Thermokinetic Mixer (Dusatec Co, USA).

4.3.3. Characterization

Specimens for tensile and flexural tests were prepared by lab-scale injection moulding at 180o according to the ISO 527-2 and ISO 178 standards. The mechanical tests were conducted using Instron 5982 Static Universal Test Machine (UTM) for tensile and three-point bending tests according to the ISO 527-2 and ISO 178 standards. Dynamic Mechanical Analyzer (DMA) (Mettler Toledo, Columbus, OH, USA) was used to investigate viscoelasticity of composites via a single cantilever bending from -20 ℃ to 100 ℃ with 1 Hz frequency and 3 Kmin-1 heating rate. Thermal analysis was investigated by Differential Scanning Calorimetry (DSC) 3 + 700 (Mettler Toledo, Columbus, OH, USA) under nitrogen gas with 10 ℃ min-1 heating rate. Frequency sweep tests were performed in Anton-Paar MCR 702 Rheometer at 230 oC and strain of 1% in an angular frequency range of 1–1000 rad/s. Freeze fractured surfaces were examined under a Leo Supra 35 VP Field Emission Scanning Electron Microscope (FESEM) by coating of cross-sections with a thin layer of gold. Optical microscope images were taken by using CLEMEX Image Analyzer System. Transmission Electron Microscopy (TEM) was conducted to examine the distribution of GNP in ternary nanoblends at varying loading levels, ranging from the lowest to the highest.

4.4. Results and Discussion

4.4.1. Mechanical Behavior of Binary Blends and Ternary Nanoblends

Polymer blends were produced by adding HDPE to PP at varying ratios of 20 wt.%, 25 wt.%, 50%, 75%, and 80% by thermos-kinetic mixer. The mechanical results of the PP/HDPE polymer blends are shown in Figure 21. Additionally, Table 9 and Table 10 illustrate the improvements compared to Neat PP. When examining the flexural modulus values, all blend formulations showed higher results compared to neat PP. In particular, the PP+HDPE 75/25 blend exhibited the highest result at 1669 MPa, representing a 26% increase compared to neat PP. Similarly, the same formulation showed the highest flexural strength with 45 MPa. The tensile modulus also exhibited the highest value at 1830 MPa, indicating a 25% increase compared to neat PP. The tensile strength value was 33.3 MPa, falling between the values of the two neat polymers. These enhanced

characteristics reveal the two blends' synergistic interaction when combined with a thermo-kinetic mixer. This circumstance gave rise to the concept that the matrix for commercial productions might be a PP/HDPE blend rather than solely PP.

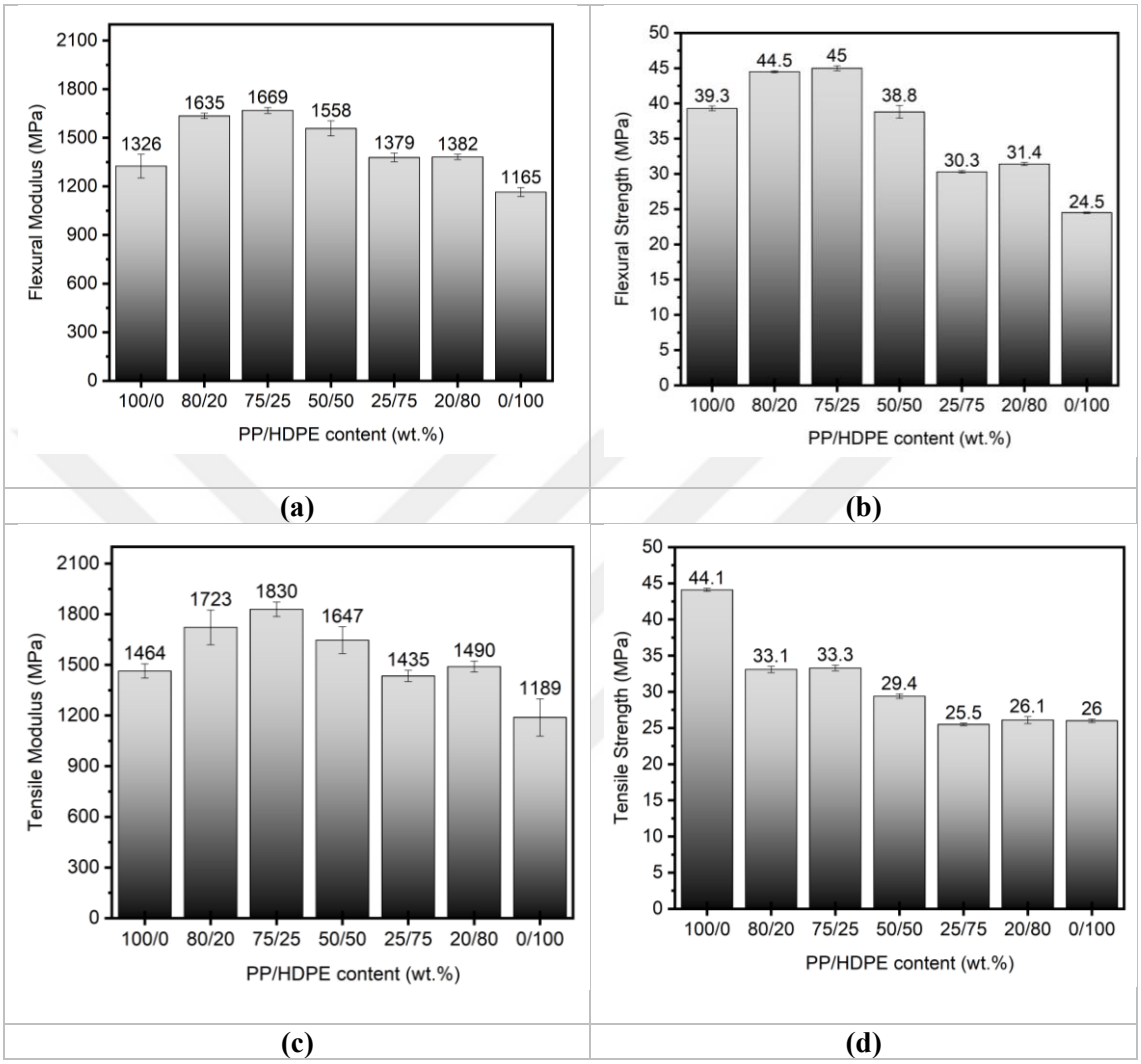

Figure 22. (a) Flexural modulus, (b) flexural strength, (c) tensile modulus, and (d) tensile strength of binary polymer blends

Table 9. Flexural properties of the blend nanocomposites and improvements (%) compared to neat PP

Sample Name	Flexural Modulus [MPa]	Flexural Modulus Improvement (%)	Flexural Strength [MPa]	Flexural Strength Improvement (%)
Neat PP	1326	-	39.3	-
PP+HDPE 80/20	1635	23	44.5	13
PP+HDPE 75/25	1669	26	45.0	15
PP+HDPE 50/50	1558	17	38.8	-1
PP+HDPE 25/75	1379	4	30.3	-23
PP+HDPE 20/80	1382	4	31.4	-20
Neat HDPE	1165	-	24.5	-

Table 10. Tensile Properties of the blend nanocomposites and improvements (%) compared to neat PP

Sample Name	Tensile Modulus [MPa]	Tensile Modulus Improvement (%)	Tensile Strength [MPa]	Tensile Strength Improvement (%)
Neat PP	1464	**-**	44.1	**-**
PP+HDPE 80/20	1723	18	33.1	-25%
PP+HDPE 75/25	1830	25	33.3	-24%
PP+HDPE 50/50	1647	13	29.4	-33%
PP+HDPE 25/75	1435	-2	25.5	-42%
PP+HDPE 20/80	1490	2	26.1	-41%
Neat HDPE	1189	**-**	26.0	**-**

In this context, nano-composite experiments were conducted by adding GNP into matrices produced with 75% PP and 25% HDPE to observe the interactions of these polymer blends with GNP. The results of the mechanical properties by adding GNP into the PP+HDPE 75/25 blend are shown in Figure B. Additionally, Table 11 presents the overall mechanical comparison and improvement of nanoblends compared to PP+HDPE 75/25 and neat PP. When 0.1% GNP was added to the compositions of the blends with reference to PP/HDPE-25, a 10% increase in flexural modulus and an 11% increase in tensile modulus were observed. The flexural strength and tensile strength also showed increases of 6% and 5%, respectively. However, it can be observed that as the GNP ratio increases, the improvements in mechanical properties become less significant and reach a plateau at certain points.

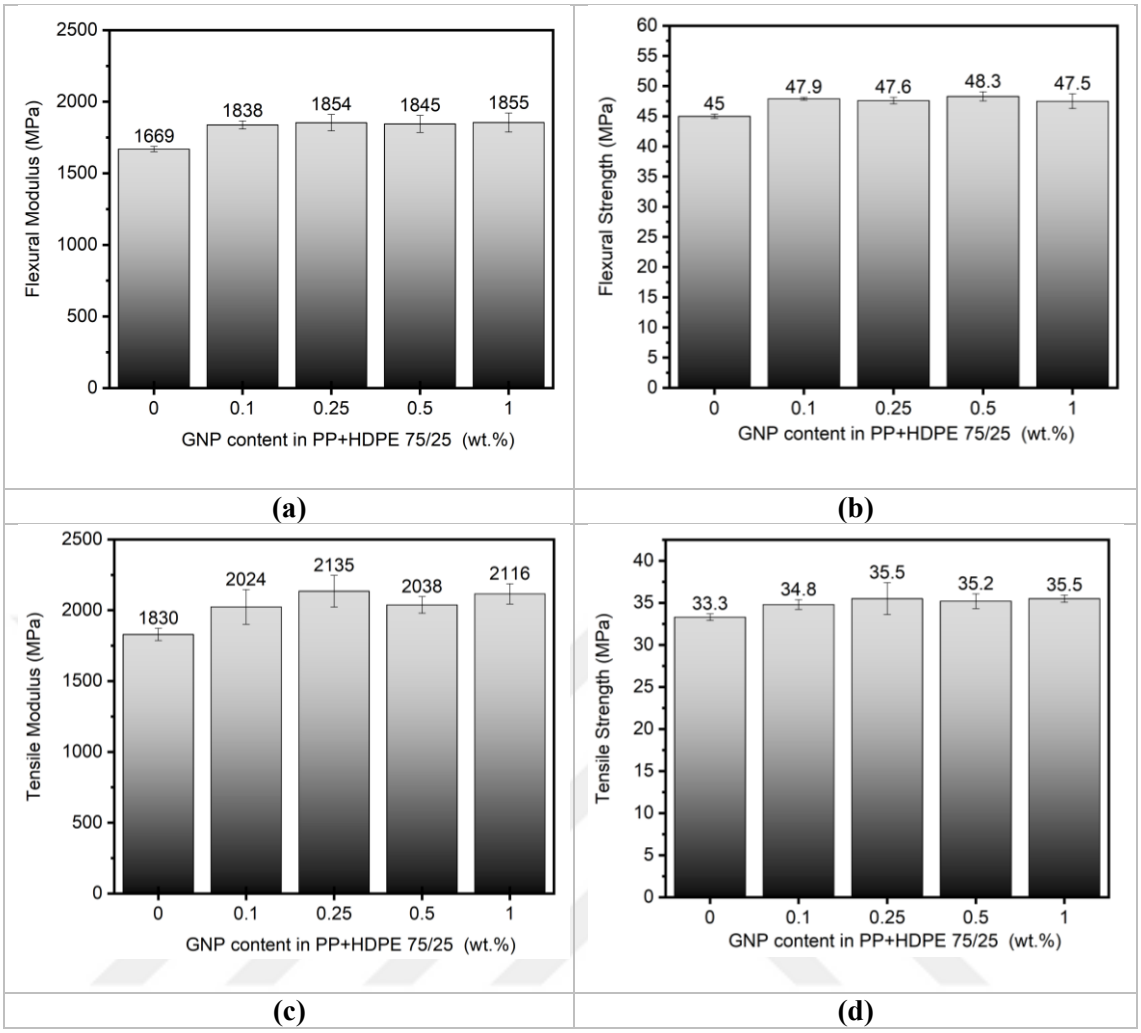

Figure 23. (a) Flexural modulus, (b) flexural strength, (c) tensile modulus, and (d) tensile strength of ternary nanoblends

Table 11. Overall mechanical comparison and improvement of ternary nanoblends compared to PP+HDPE 75/25 and Neat PP

Sample Name	Tensile Modulus [MPa]	Improvement compared to PP+HDPE 75/25 (%)	Improvement compared to Neat PP (%)
PP+HDPE 75/25 GNP-0.1	2024	11	38
PP+HDPE 75/25 GNP-0.25	2135	17	46
PP+HDPE 75/25 GNP-0.5	2038	11	39
PP+HDPE 75/25 GNP-1	2116	16	45
Sample Name	**Tensile Strength [MPa]**	**Improvement compared to PP+HDPE 75/25 (%)**	**Improvement compared to Neat PP (%)**
PP+HDPE 75/25 GNP-0.1	34.8	5	-21
PP+HDPE 75/25 GNP-0.25	35.5	7	-20
PP+HDPE 75/25 GNP-0.5	35.2	6	-20
PP+HDPE 75/25 GNP-1	35.5	7	-20

Table 11 (cont.). Overall mechanical comparison and improvement of ternary nanoblends compared to PP+HDPE 75/25 and Neat PP

Sample Name	Flexural Modulus [MPa]	Improvement compared to PP+HDPE 75/25 (%)	Improvement compared to Neat PP (%)
PP+HDPE 75/25 GNP-0.1	1838	10	39
PP+HDPE 75/25 GNP-0.25	1854	11	40
PP+HDPE 75/25 GNP-0.5	1845	11	39
PP+HDPE 75/25 GNP-1	1855	11	40
Sample Name	**Flexural Strength [MPa]**	**Improvement compared to PP+HDPE 75/25 (%)**	**Improvement compared to Neat PP (%)**
PP+HDPE 75/25 GNP-0.1	47.9	6	22
PP+HDPE 75/25 GNP-0.25	47.6	6	21
PP+HDPE 75/25 GNP-0.5	48.3	7	23
PP+HDPE 75/25 GNP-1	47.5	6	21

4.4.2. Viscoelastic Behaviour of Binary Blends and Ternary Nanoblends by DMA

Storage modulus (E') represents the elastic energy stored by the material and it signalizes the solid-like behaviour of materials. In compliance with Figure 22a, PP has the highest storage modulus compared to HDPE and its HDPE including binary polymer blends. PP storage modulus is excelsior compared to HDPE almost 1.7 times due to the methyl ($-CH_3$) group in PP structure which provides comparatively good mechanical properties. Addition of HDPE at 20 wt.% in PP matrix slightly decreased the storage modulus and 25 wt.% decreased further which is understandable by virtue of PP is still predominance as a matrix. Storage modulus of PP+HDPE 50/50 fell into between PP and HDPE due to the equal proportionality. Figure 22d shows the storage modulus of GNP included ternary polymer nanoblends by taking a reference of PP + HDPE 75/25. The storage modulus of the nanoblends reached the same level with all the GNP addition rates and became independent of the GNP concentration. This shows that with the addition of GNP, the solid-like behaviour increased compared to PP+ HDPE 75/25. By using 0.1 wt.% GNP, similar elastic properties as 1 wt.% GNP can be exhibited and there is no need to use higher ratios. Energy dissipation as heat or lost can be examined by loss modulus (E'') and viscous response of the material can be attained. In line with the Figure 22a explanation, HDPE showed highest loss modulus due to the easier chain deformation compared to PP and its addition to PP increased the loss modulus of the binary blends. PP peaks showed its β crystal peaks at around 4-5 ^{o}C and HDPE showed around 39 ^{o}C. PP+HDPE 50/50 showed a single peak at around 30 ^{o}C and their liquid-like response concurrently occur at the same temperature interval. HDPE amount exceeding 50 wt.% approached to HDPE due to its predominance at a matrix. In Figure 22e, loss modulus

changes as a function of GNP loading and temperature is given. PP+ HDPE 75/25 was compared with its GNP included ones and liquid-like behaviour underwent a change unlike their solid-like behaviour. 1wt.% GNP included nanoblend decreased the loss modulus at a temperature interval of -20 ^{o}C and 80 ^{o}C which means that stiff GNPs restricted the chain movement in PP + HDPE 75/25 but more dominantly in PP, based on the lowered peak at 4 ^{o}C which belongs to PP phase. A slight shift in maximum peak position of HDPE phase of PP+ HDPE 75/25 + GNP-1 was observed with almost no change in its value. 0.1 wt.% GNP included nanoblend has the highest loss modulus peak where it changes when it comes to HDPE phase. Tan delta values represents the viscous to elastic response (E''/E') of viscoelastic materials and the curves after 15 ^{o}C in Figure 22c also coherent with the storage modulus curves in Figure 22a. Correspondingly, with the addition of GNP in the blends, tan delta values are also converging mostly in HDPE phase when comparing Figure 22c with Figure 22d. Hereby, it is proper to say that GNP is more dominant in affecting the HDPE phase over PP in the produced nanoblends and/or prefers to locate mostly in the HDPE phase compared to the PP phase.

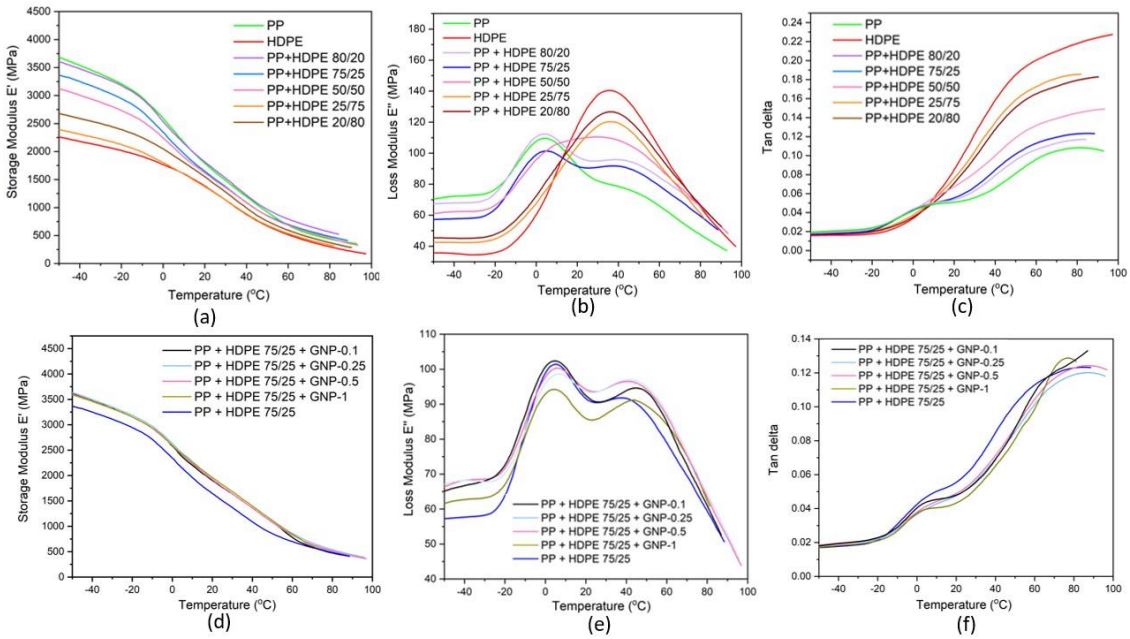

Figure 24. Results obtained from DMA (a),(c) storage modulus, (b),(c) loss modulus, (d),(e), tan delta of binary blends and ternary nanoblends.

4.4.3. Rheological Behaviour of Binary Blends and Ternary Nanoblends

The rheological investigation of ternary blends is presented in Figure 24. A sudden increase in complex viscosity was observed with the addition of a small amount of 0.1 wt.% GNP to the PP+HDPE 75/25 blend, as shown in Figure 24a. This sudden increase indicates good

nanoparticle interaction and network formation within the nanoparticles. When the ratio is increased to 0.25 wt.% GNP, the viscosity slightly decreases, possibly due to the beginning of GNP agglomeration. Further increases in viscosity was observed with the addition of 0.5 wt.% GNP and 1 wt.% GNP, indicating a restriction in the matrix's mobility possibly due to the addition of rigid GNPs in higher proportions. The storage modulus and loss modulus values also exhibit a similar pattern of increase. Modified Cole-Cole (Han Plot) can be used to analyse percolation network formation concentration and a rapid increase in the slope can be attributed to the formation of nanoparticle network [97]. All GNP concentrations showed a similar deviation from the master curve of PP+ HDPE 75/25 which demonstrates that their ability to improve rheological behaviour of the matrix is similar. The absence of a drastic slope change among the ternary nanoblends might arise from the low content of GNP regarding on the studies showed that higher GNP ratios above 2 wt.% GNP is needed to reach percolation [77]. Here, below percolation threshold, it is possible to enrich mechanical performance of nanocomposites.

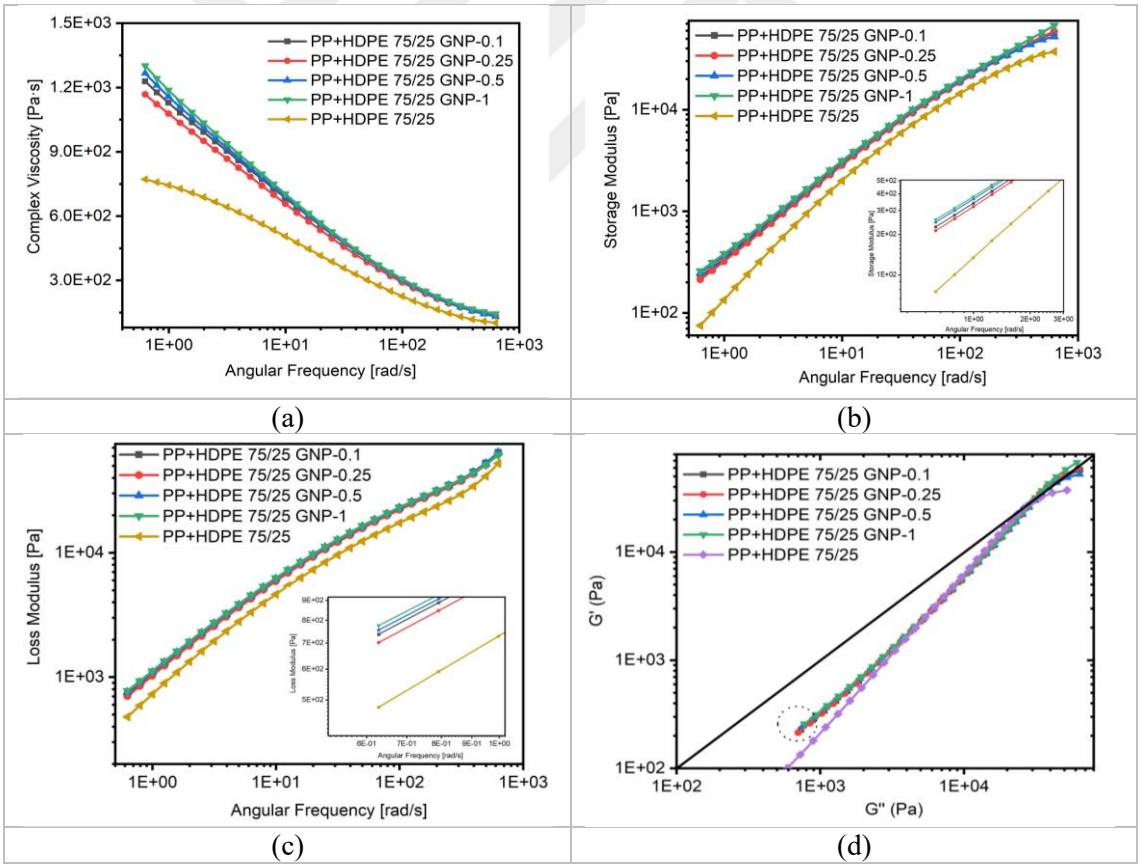

Figure 25. (a) complex viscosity, (b) storage modulus, (c) loss modulus, (d) modified cole-cole pilot of ternary nanoblends.

4.4.4. Thermal Behaviour of Binary Blends and Ternary Nanoblends by DSC

The thermal behaviour of binary and ternary polymer blends was investigated using differential scanning calorimetry (DSC), revealing valuable insights into phase transitions, melting temperatures (Tm), and crystallinity characteristics. The resulting DSC thermograms, as shown in Figure 26, provided a comprehensive understanding of the blends' thermal properties and complementary information regarding temperature, enthalpy, and crystallinity for cooling and second heating stages is summarized in Table 12. Upon examining the binary polymer blends depicted in Figure 4a, it was observed that HDPE exhibited a Tm of 137 °C, while PP displayed a Tm of 169.1 °C. Notably, an increase in the HDPE proportion led to an augmented HDPE melting peak, accompanied by a decrease in the PP peak. Additionally, the incorporation of HDPE caused a reduction of approximately 3 °C in the Tm of PP. Notably, when the HDPE proportion reached 80%, the Tm of PP experienced a further decrease of 4 °C. This downward shift in Tm can be attributed to the occurrence of phase separation between PP and HDPE, thereby influencing the overall melting behaviour. In conjunction with the Tm shift, the inclusion of HDPE in the blends resulted in a discernible reduction in the crystallinity of PP. Crystallinity calculations were conducted using the heat of fusion values of 287 J/g for 100% crystalline HDPE and 207 J/g for PP [98]. The addition of HDPE contributed to a decrease in PP crystallinity ranging from 20% to 75% by weight. This decline in crystallinity signifies a corresponding decrease in the relative proportion of crystalline regions, ultimately leading to a shift towards lower temperatures. Analysis of the crystallization temperatures (Tc) revealed that binary blends exhibited higher Tc values compared to pure PP, indicating alterations in the crystallization behaviour induced by the presence of HDPE. Furthermore, in the ternary blends, specifically the PP+HDPE 75/25 compositions, the incorporation of graphene nanoplatelets (GNP) demonstrated an increase in Tc values compared to PP+HDPE 75/25. This observation suggests that GNP may function as a nucleating agent, promoting the formation of smaller and more numerous crystalline structures within the blend. Previous studies have reported the ability of GNP to enhance the Tc of polymers [4]. For the 0.5wt.% GNP and 1 wt.% GNP compositions, the crystallization peak started to split as shown by black arrows in Figure 4d, meaning that more phase separation occurred due to the incorporation of GNP in both PP and HDPE.

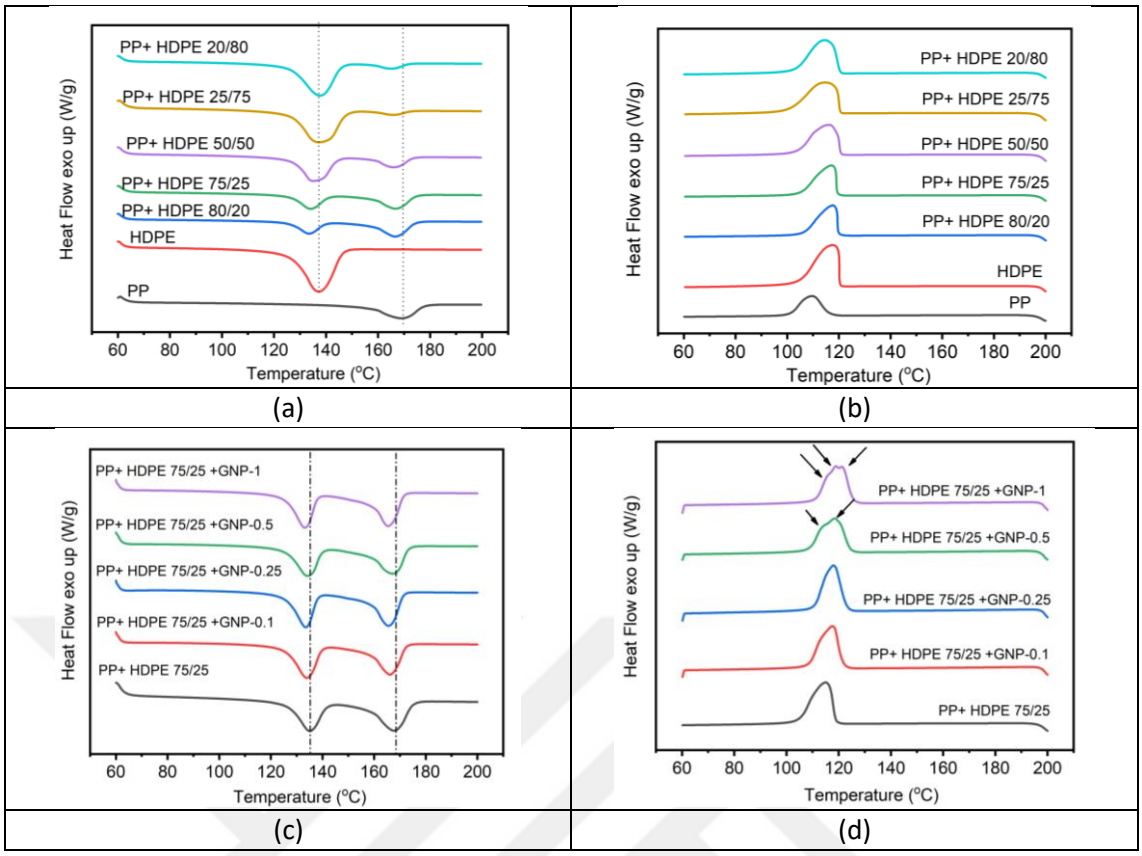

Figure 26. (a) second heating, and (b) cooling run of binary blends; (c)second heating and (d) cooling run of ternary nanoblends.

Table 12. Melting and crystallization behaviour of binary and ternary nanoblends.

	Cooling		2nd Heating				Crystallinity	
	T_c (°C)	ΔH_c (j/g)	T_m of PP (°C)	T_m of HDPE (°C)	ΔH_m of (PP) (j/g)	ΔH_m of (HDPE) (j/g)	Xc of PP (%)	Xc of HDPE (%)
PP	111.2	90.6	169.1	-	90.2	-	43.57	-
PP + HDPE 80/20	117.7	124.9	166.5	133.4	74.7	48.7	36.09	16.9
PP + HDPE 75/25	117.2	131.7	166.7	134.0	70.3	60.1	33.96	20.9
PP + HDPE 50/50	116.1	165.9	166.1	135.1	44.5	114.9	21.50	40.0
PP + HDPE 25/75	114.7	197.7	165.9	137.2	15.6	175.6	7.54	61.18
PP + HDPE 20/80	114.5	181.1	164.9	137.8	19.6	154.6	9.47	53.87
HDPE	117.5	214.3	-	137.0	-	126.9	-	44.22
PP + HDPE 75/25+ GNP-0.1	118.0	124.4	166.0	133.8	53.5	49.2	25.85	17.14
PP + HDPE 75/25+GNP-0.25	118.3	125.3	165.3	133.4	58.4	45.8	28.21	15.96
PP + HDPE 75/25+GNP-0.5	118.8	123.0	167.2	134.0	54.3	42.6	26.23	14.84
PP + HDPE 75/25+ GNP-1	119.3	125.3	165.3	133.0	58.s5	45.3	28.26	15.78

4.4.5. Morphology Investigation of Binary Blends and Ternary Nanoblends by Microscopic Techniques

Figure 27 presents semi-polarized optical microscope images of neat PP and neat HDPE Polypropylene rapidly formed spherulite, showed trap nucleation and formed crystals (a1-a4). PP has a relatively high crystallization rate that lead to form of spherulite. Additionally, Isotactic PP, which has a high degree of regularity in the arrangement of

polymer chains, tends to form well-defined spherulites. Neat HDPE showed smaller crystallization (b1-b4). Optic microscope images of the binary blends are shown in Figure 28. The large spheres seen in all figures present PP spheres considering the structures they form in Figure 27. While PP continues to form its own morphology with non-uniform sphere shapes in HDPE, it starts to form more uniform spheres with the addition of GNP, as seen in Figure 29. At the same time, the number of these formed spheres is relatively decreasing. Interestingly, these spheres did not appear at the 0.25 wt.% GNP addition. With the addition of 1 wt.% GNP, GNP increased the nucleation rate very quickly and leopard patterned morphologies began to form in certain regions due to the agglomeration.

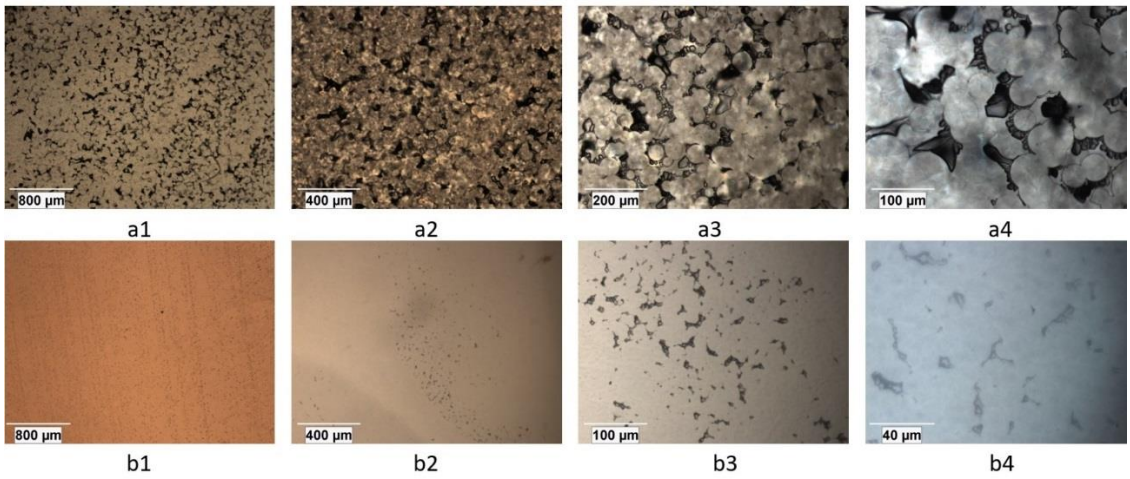

Figure 27. Semi polarized optic microscopy images of neat PP (a1-a4) and neat HDPE (b1-b4) at different magnifications.

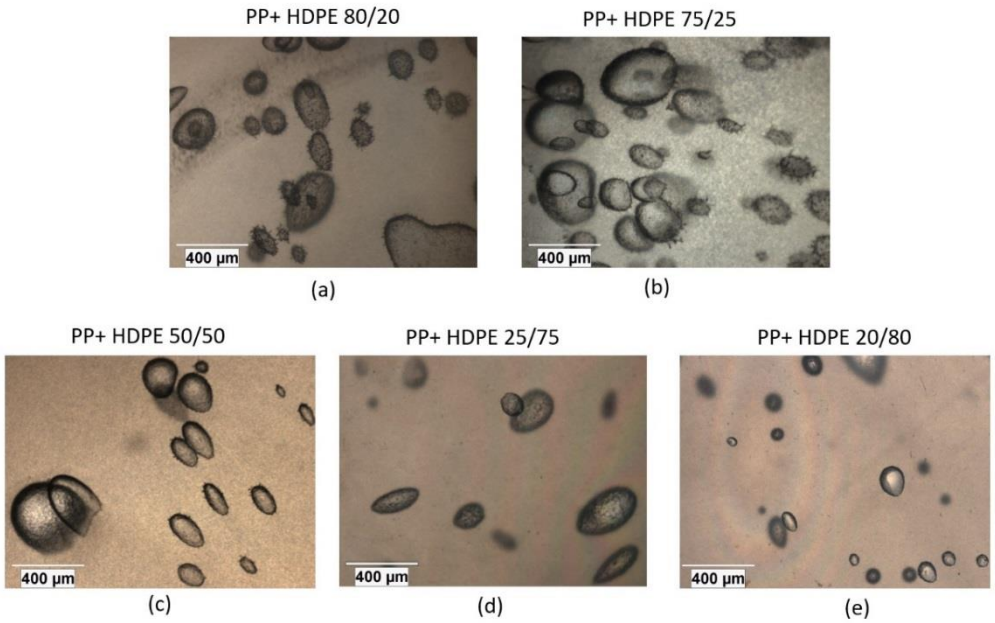

Figure 28. Semi polarized optic microscopy images of binary blends

Optic microscope images of the binary blends are shown in Figure 28. The large spheres seen in all images in Figure 28 present PP spheres considering the structures they form in Figure 27. While PP continues to form its own morphology with non-uniform sphere shapes as in Figure 28, it starts to form more uniform spheres with the addition of 0.1 wt.% GNP, as seen in Figure 29(a1). The circularity of the spheres is remarkably uniform, and there are distinct crystallization patterns observed on the outer regions of these spheres, primarily due to the localized presence of the black graphene nanoplatelets (GNP). Interestingly, these spheres did not appear at the 0.25 wt.% GNP addition. At this loading rate of GNP, it might be reached to the optimum content of GNP for reducing the PP sphere formation. Upon adding 0.5 wt.% GNP, these spheres reappeared but with reduced quantities and diameters compared to 0.1 wt.% GNP. With the addition of 1 wt.% GNP, GNP increased the nucleation rate very quickly and leopard patterned morphologies began to form in certain regions as shown in Figure 29(d1-d4). The GNPs initiate the crystallization of polymer phases from various points throughout the matrix. As the GNP content increases, closer magnifications reveal that the matrix droplets also decrease in size.

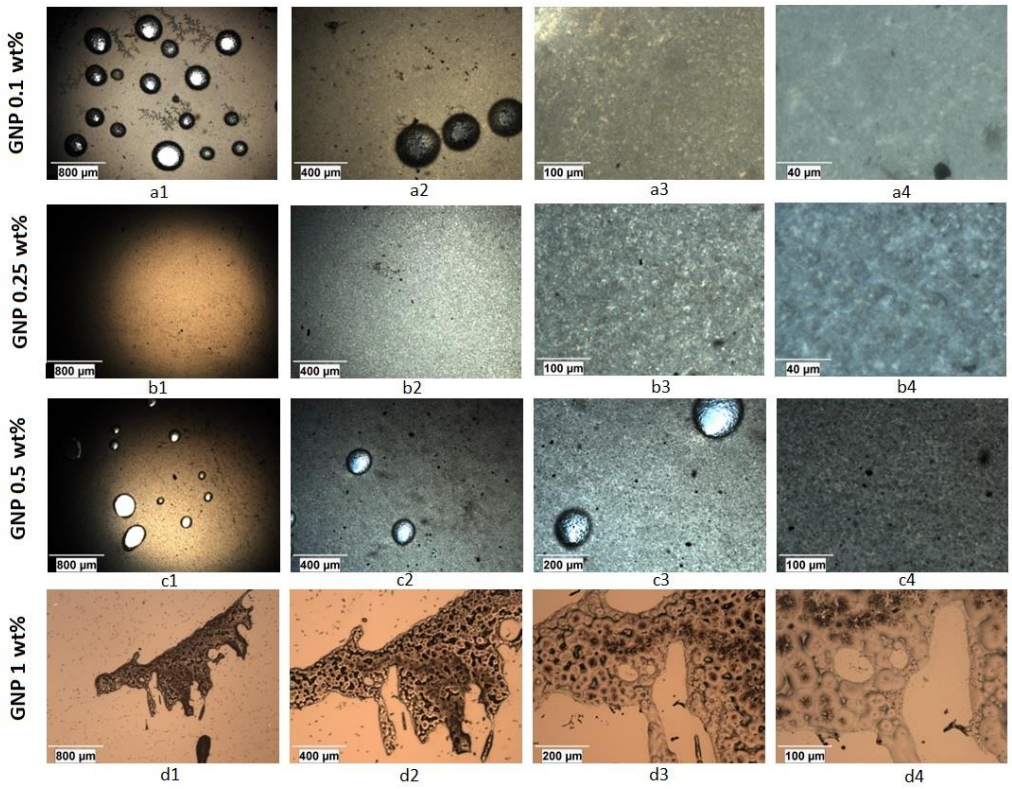

Figure 29. Semi polarized optic microscopy images of GNP included polymer blends. The polymer blend ratios of PP/HDPE is 75/25 and GNP concentrations amount varies between 0.1-1 wt.%.

Figure 30 presents the cross-sectional analyses of neat polymers and their binary and ternary blends to investigate the microstructure. In Figure 30a, the crystalline structures formed by PP are clearly observed. Figure 30b reveals the presence of a ductile morphology specific to HDPE. Upon examining the PP+HDPE 75/25 blend (Figure 30c), it can be observed that HDPE protrudes from the matrix in the form of tendrils, possibly indicating interface incompatibility. Notably, voids can be observed in the regions highlighted by red arrows, which are likely a consequence of such interface mismatch. In a 50/50 blend ratio, both PP and HDPE are equally distributed in the matrix, and due to their inherent incompatibility, PP initiates crystallization within its own domains, thus exhibiting its distinct phases. With an increased HDPE content of 75%, HDPE becomes the major phase, manifesting its dominance and leading to a fracture behaviour reminiscent of neat HDPE, displaying a more flexible nature. Figure 30f showcases the sample of PP+HDPE 75/25+GNP-0.1, where 0.1 wt.% GNP is added. Notably, compared to Figure 30c, the void structures are no longer observed, and the crystalline structure of the PP phase reappears. This observation suggests that GNP contributes to localized PP crystallization at the blend interface and within the PP matrix, indicating its potential role in enhancing crystalline characteristics.

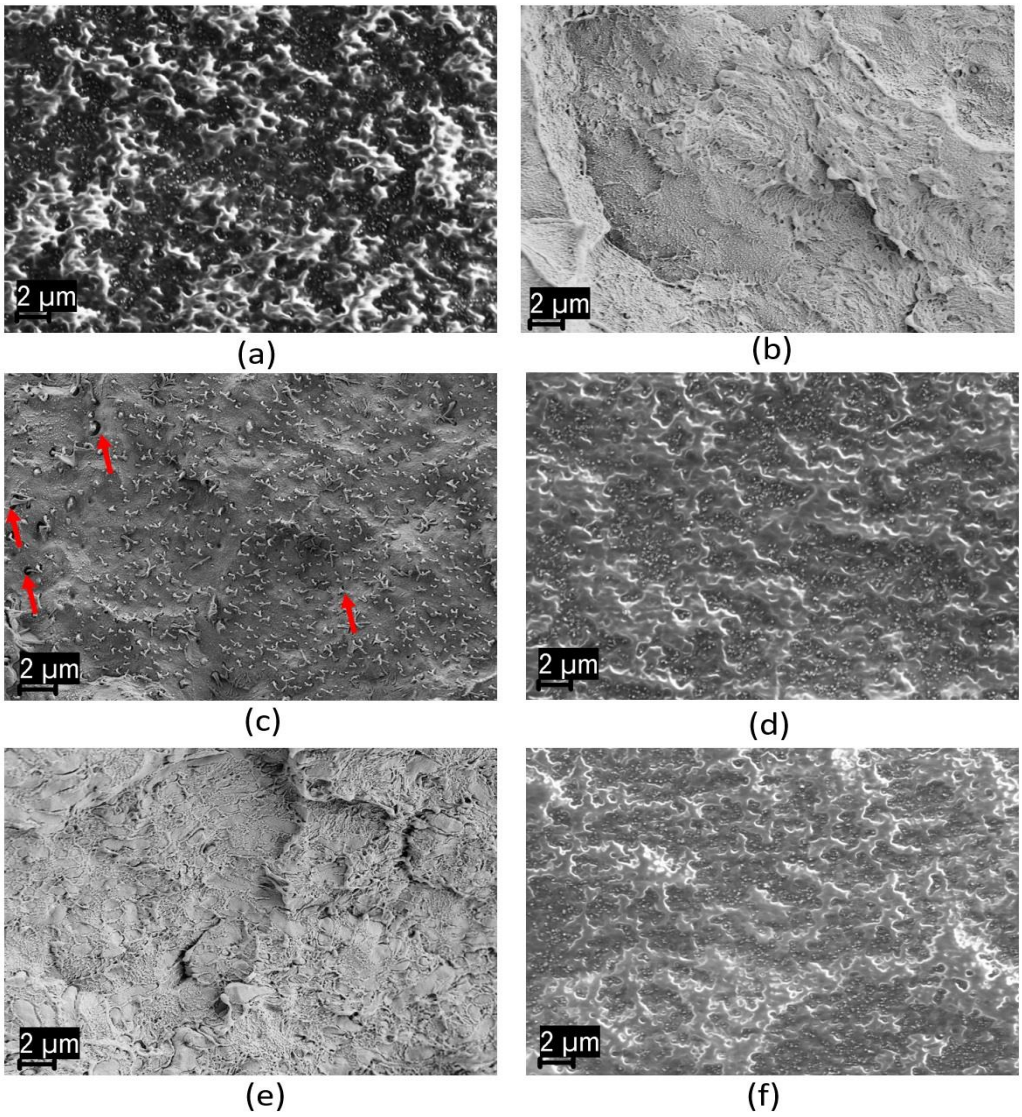

Figure 30. Cross-sectional analysis of (a) PP, (b) HDPE, (c) PP+HDPE 75/25, (d) PP+HDPE 50/50, (e) PP+HDPE 25/75, and (f) PP+HDPE 75/25 +GNP-0.1 by SEM under 3kV at 10k magnification.

The TEM micrographs of PP+HDPE 75/25+ GNP-0.1 and PP+HDPE 75/25+ GNP-1 ternary nanoblends are depicted in Figure 31. The presence of dispersed HDPE droplets surrounded by the PP matrix can be seen in Figure 31a. The GNP, represented by black dots indicated by arrows, is observed precisely at the interface between the PP and HDPE phases in Figure 31(a) and in closer view in Figure 31b and 31c. Conversely, when examining the blend with a 1 wt.% GNP content, a higher concentration of GNP particles infiltrating the interphases becomes evident. A closer view in Figure 31e reveals significant agglomeration forming clusters with a size of approximately 75 nm and resulting in a visually darker image due to GNP overlap. Consequently, successful localization of 0.1 wt.% GNP at the PP+HDPE 75/25 interface was observed, while higher GNP ratios led to undesirable agglomeration.

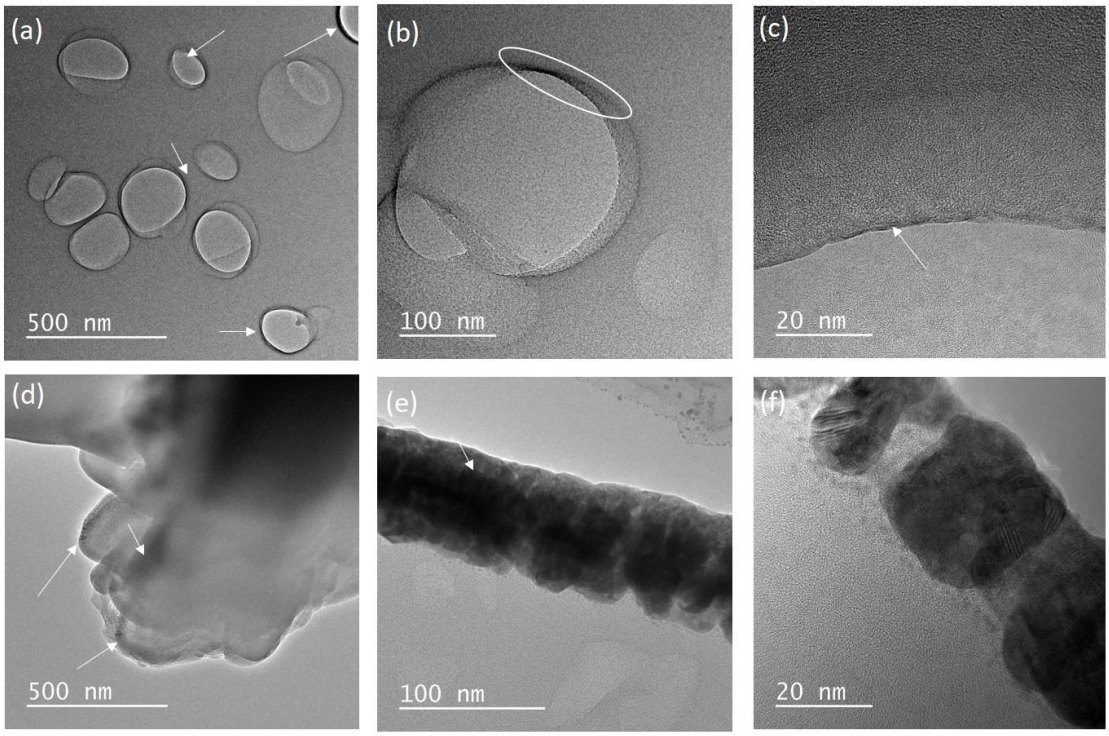

Figure 31. TEM images of (a)-(c) PP+HDPE 75/25+ GNP-0.1, (d)-(f) PP+HDPE 75/25+ GNP-1 ternary nanoblends.

4.5. Conclusion

Current study achieved to provide a cost-effective blend formulation by utilizing a PP/HDPE matrix and improving its mechanical behaviour through the incorporation of GNP via an adaptable processing technique. By utilizing a high shear rate thermo-kinetic mixer and incorporating upcycled graphene nanoplatelets (GNP) through interface engineering, the researchers successfully addressed the entropy barrier between PP and HDPE. The results demonstrated that careful selection of polymer weight fraction and optimized GNP loading facilitated the localization of GNP at the blend interface, leading to notable improvements in mechanical performance. The addition of 0.1 wt.% GNP resulted in a significant 38% increase in tensile modulus, along with 39% and 22% increases in flexural modulus and flexural strength, respectively. Rheological analysis indicated that the inclusion of GNP in the nanoblends enhanced the complex viscosity, storage modulus, and loss modulus, indicating the formation of a nanoparticle network at low GNP contents. Morphological studies confirmed the successful localization of GNP at the blend interface, leading to improved crystallization patterns and reduced void structures.

The successful incorporation of upcycled graphene nanoplatelets (GNP) in PP/HDPE blend systems through a high shear rate thermo-kinetic mixer opens promising avenues for future research and applications. Investigating the influence of different processing parameters, mixing techniques, and GNP modifications on the blend morphology and properties can provide valuable insights for tailoring materials with specific characteristics. The industrial scalability of the developed blend formulation and processing technique assess their feasibility for large-scale production. This could involve evaluating the economic viability, processing efficiency, and scalability of the thermo-kinetic mixer in comparison to conventional extrusion methods.

CHAPTER 5: Production and Optimization Studies of Graphene/GF/PP and Graphene/Talc/ PP Hybrid Composites

5.1. Production and Optimization Studies of Graphene/GF/PP Hybrid Composites

5.1.1. Abstract

The high usage ratio and elevated density of glass fibers (GFs), often surpassing twice that of polymers, can contribute to undesired increments in the overall density of polymeric materials. One potential solution is the incorporation of graphene as a secondary additive, offering lower specific gravity and exceptional mechanical properties. Under this light, waste tire-derived graphene nanoplates (GNP) were optimized for coating onto GFs by considering factors such as surface treatment of the fiber, dispersion quality of GNP, and coating technique. The resulting GNP-coated GF (GNP-c-GF) was initially incorporated into pure polypropylene (PP) at low weight percentages (0.1-1 wt.%), and 31% increase in the tensile modulus was achieved compared to neat PP. Subsequently, 1 wt.% GNP-c-GF was utilized as a compatibilizer in PP/GF/GNP composites to enhance the compatibility between GNP and GF. By strategically incorporating GNP and GNP-c-GF at a lower GF ratio, the detrimental impact on the tensile modulus of 30% GF filled PP was effectively mitigated, leading to a remarkable enhancement to an impressive value of 5658 MPa. The successful integration of GNP and GNP-c-GF exemplifies their promising potential as additives for achieving superior mechanical properties in composite materials while concurrently promoting the utilization of recycled content.

5.1.2. Introduction

Extensive research has been conducted by numerous scholars exploring the utilization of polymer composites incorporating both natural and synthetic fibers [2]. Within polymer/fiber composites, glass fiber is the most preferred reinforcement material despite its limitations [99, 100]. Glass fiber reinforced polypropylene (PP) composites are extensively employed across various applications owing to their superior mechanical and thermal characteristics, as well as their relatively cost-effective nature in comparison to alternative fiber types such as carbon and aramid [101]. But in most cases, high loadings

of glass fibers ranging from 30 to 50 weight percent are required to achieve the desired performances from the material which leads to yield unfavorable effects such as undesirable increase in specific gravity, brittleness, reduced processability, and diminished melt flow characteristics [102, 103].

Hybrid composites have gained significant popularity in diverse engineering applications due to their ability to showcase novel physical properties and functionalities [104]. There has been a tendecy to produce graphene based hybrid composites [105] to tackle encountered problems in the material or when multi-functionality is expected such as higher mechanical and thermal properties, cost reduction and lightness simultaneously. The remarkable mechanical, electronic, thermal, and magnetic properties of graphene have made it a highly sought-after subject of research in recent times [41]. In recent investigations, considerable attention has been given to the development of glass fiber/graphene/ polypropylene (PP) composites, with the objective of augmenting the mechanical [106], thermal, and electrical attributes of these materials through the integration of graphene within glass fiber-reinforced PP matrices. D.G. Papageorgiou et al. investigated the thermal stability and flame retardancy characteristics of polypropylene (PP) nanocomposites incorporating graphene nanoplatelets (GNPs), glass fibers (GFs), or a hybrid combination of both fillers, revealing a 57 °C increase in the thermal decomposition temperature of the hybrid composite (PP-GF16-GNP20) compared to neat PP and individual filler compositions. In another study, F. Ghorbani et al. prepared hybrid nanocomposites with PP, GF, and exfoliated xGnP, showing improved fiber-matrix adhesion. The inclusion of 1 wt.% and 2 wt.% graphene in samples containing 10 wt.% glass fibers increased Young's modulus by 16% and 21%, respectively [106]. While glass fiber/graphene/polypropylene (PP) composites offer various advantages, there are also some drawbacks and challenges associated with their development and application. Ensuring strong interfacial adhesion between the glass fibers, graphene, and the PP matrix is crucial for optimal composite performance. However, the presence of certain constraints such as the absence of reactive functional groups on the fiber surface and poor wettability adds complexity to the task [107]. Additional steps such as functionalization, mixing, and processing are required to ensure proper dispersion and interfacial bonding. To achieve better dispersion and interfacial bonding between graphene, glass fibers, and the PP matrix, researchers have explored various surface modification techniques [108]. Surface functionalization of graphene and glass fibers can enhance their compatibility with the PP matrix, leading to improved interfacial adhesion and overall composite performance. While

the research on glass fiber/graphene/PP composites has shown promising results, the transition from laboratory-scale experiments to industrial-scale production can present challenges since graphene is still relatively expensive compared to other reinforcing materials and therefore the high cost of graphene can limit its widespread use in industrial applications, especially in large-scale production. Scaling up the production process while maintaining the desired properties and cost-effectiveness requires further optimization and process engineering. The introduction of graphene derivatives onto the fiber surface in recent years has proven to be an effective method for improving the interfacial properties of composites, resulting in increased specific surface area and stronger chemical bonding between the fiber and the matrix [109]. Researchers and engineers in the field of composite materials have been exploring various coating techniques and formulations to successfully incorporate graphene onto glass fibers for improved performance in a range of applications [110]. While coating GNPs onto glass fiber may require careful consideration and optimization, it is an achievable process with the potential to enhance the properties of the resulting composite. Generally graphene oxide (GO) have been used to coat glass fibers by sytnhesizing from graphite with the Hummers' method which includes several steps with a variety of chemicals [110, 111]. These extra processing steps can increase the production cost and complicate the scaling-up of manufacturing processes. However, in today's culture, there is a tremendous need for materials that are lightweight, strong, and inexpensive [112]. These challenges are being actively addressed by researchers and industry professionals, and ongoing studies aim to overcome these drawbacks and improve the performance and practicality of glass fiber/graphene/PP composites.

Herein, a facile and practical coating technique was employed to treat glass fibers (GF) with upcycled graphene nanoplatelets (GNPs) derived from waste tires. The GNPs were utilized without any modifications, and a dip coating optimization study was conducted by dispersing them in water at various concentrations. The resulting GNP-coated glass fibers (GNP-c-GF) were subsequently incorporated into pure polypropylene (PP) and PP/GF/GNP composites to comprehensively evaluate their mechanical, morphological, and flow properties. The interfacial compatibility between graphene nanoplatelets (GNPs), glass fibers (GF), and the matrix (PP) was greatly improved by incorporating a small quantity of 1% GNP and 1% GNP-c-GF into the composites with varying glass fiber contents (15%, 20%, 25%, and 30%). Notably, the addition of only 1% GNP-c-GF in pure polypropylene (PP) exhibited a remarkable 31% increase in the tensile modulus

compared to neat PP. Moreover, the incorporation of GNP-c-GF into composites containing both glass fibers (GF) and graphene nanoplatelets (GNPs) played a crucial role as a compatibilizer, effectively enhancing the homogeneity of the composite system and promoting a uniform dispersion within the matrix. This strategy facilitated the attainment of enhanced performance by utilizing a compatibilizer comprised of the inherent constituents of the composite, thereby circumventing the need for the incorporation of a separate structural element.

5.1.3. Experimental

5.1.3.1. Materials

E type glass fibers coated with a silane-based sizing with a strand length of 4mm supplied from Johns Manville. Homo Polypropylene with a density of 905 kg/m^3 intended for injection moulding supplied from BOREALIS. Sulfuric acid with a purity of 99% and (30 wt.%) hydrogen peroxide were purchased from Sigma Aldrich. Graphane nanoplatelets (GNP) were supplied from NANOGRAFEN Co., Kocaeli, Turkey. The detailed characterization regarding to upcycled GNP can be found in our previous study [91].

5.1.3.2. Glass Fiber Surface Treatment

In order to remove organic coating from the surface and resize the GF, piranha solution has been used in literature [113]. Here, a safer piranha solution was used to desize and hydroxylate GF surface with the ratio for H_2SO_4/H_2O_2 was (6:1) by volume. 10 g of GF was taken into an empty beaker and certain amount of H_2SO_4 was added to it. Afterwards, H_2O_2 was added very slowly, and the reaction took place for 30 min. After cooling solution was filtered, washed, and dried and coated as hydroxylated glass fiber (h-GF).

5.1.3.3. Coating GNP onto GF

GNP/water dispersions were prepared in 4 different concentrations and 1h probe sonication was performed. Afterwards, 10 g of previously synthesized h-GF was dipped into these dispersions and kept for 1h for coating. Graphene coated glass fibers washed and dried with a mixture of water/ ethanol and were coded as GNP-c-GF.

5.1.3.4. Compounding and injection molding of polymer composites

All composites were produced by a using COPERION ZSK26 MC[18] twin screw extruder. GNP and GNP-c-GF were premixed with the PP granules and fed into the main feeder. Glass fiber were fed with the side feeding. Test samples were produced by injection molding according to ISO 527 and ISO 178 standards.

5.1.3.5. Characterization and Testing

The functional groups of the glass fiber and GNP-coated samples were analysed using Thermo Scientific Fourier transform infrared spectroscopy (FTIR), while X-ray Photoelectron Spectroscopy (XPS) was employed to monitor their functional groups and chemical compositions. Structural characterization of the coating materials was performed using a Bruker D2 PHASER Desktop diffractometer with CuKα radiation (λ=1.5406 nm) for X-ray diffraction (XRD). To examine the surface morphology, the composite samples were fractured under liquid nitrogen, coated with a thin layer of gold, and observed under a Leo Supra 35VP Field Emission Scanning Electron Microscope (FESEM). Mechanical tests were conducted using an Instron 5982 Static Universal Test Machine (UTM) following the ISO 527-2 and ISO 178 standards for tensile and three-point bending tests.

5.1.4. Results & Discussion

5.1.4.1. Structural and Morphological Analysis of GF Hydroxylation and GNP Coating

The process of coating graphene nanoplatelets (GNPs) onto glass fiber involves several steps and considerations. While it is feasible to coat GNPs onto glass fiber, the ease of the coating process can depend on various factors. The surface of the glass fiber should be appropriately prepared to ensure good adhesion and bonding between the fiber and the GNP coating. Surface treatments, such as cleaning, activation, or functionalization, may be necessary to enhance the bonding between the GNP and the fiber surface. In this context, 6:1 ratio of H_2SO_4 and H_2O_2 was used for cleaning and hydroxylation of the glass fiber surface. H_2O_2 was added dropwise very slowly on the GFs immersed in H_2SO_4. The experimental stages of the process are depicted in the Figure 32. As the reaction continued, a layer began to form in the beaker as shown in the Figure 32a as ‘h’, and the thickness of this layer increased over time. This layer corresponds to the transformation

of the oxidized and hydroxylated organic surface. After this step, the GFs have the appropriate surface chemistry to be coated with GNP.

There are various techniques available for coating GNPs onto glass fiber, including dip coating [114], spray coating [115], electrophoretic deposition [116], and resin infusion methods [117]. The choice of coating technique depends on factors such as the desired thickness, uniformity, and scalability of the coating. Each technique has its own set of advantages, challenges, and process parameters that need to be carefully considered. Dip coating offers several advantages as a technique for coating graphene nanoplatelets (GNPs) onto glass fiber. It is a relatively simple and cost-effective coating technique. It involves immersing the glass fiber into a GNP dispersion or solution and withdrawing it at a controlled speed. It offers control over coating thickness, ensuring consistency, and enabling conformal coating. The simplicity and scalability of dip coating make it suitable for both laboratory-scale and industrial-scale applications. It is a versatile technique compatible with various types of GNPs and matrix materials. Dip coating also accommodates complex geometries, allowing for uniform coating on intricate surfaces. Dip coating can be applied to glass fibers of various shapes and complex geometries. Whether it is a continuous fiber, fabric, or three-dimensional structure, dip coating can uniformly coat the entire surface, including crevices and intricate features. This compatibility with complex geometries makes dip coating suitable for a wide range of glass fiber-based composite applications. In this study, dip coating was applied to coat GNP on glass fiber due to the advantages mentioned. GNP was dispersed in water as shown in Figure 30c, and then h-GFs were immersed in this dispersion for half an hour. In the meantime, the colour of the glass fiber surfaces turned black and was washed with a mixture of water and alcohol after the process. The colour retention of the glass fibres after several washes indicates good stability of the coating. Achieving a well-controlled and consistent GNP coating on glass fibre requires optimization of process parameters such as GNP concentration, coating time, drying conditions. The optimization process may involve iterative experimentation and characterization to determine the ideal conditions for achieving the desired GNP coating thickness and uniformity. GNPs tend to agglomerate, which can hinder their effective coating onto the glass fiber surface. Therefore, achieving a stable and homogeneous GNP dispersion is crucial for successful coating. For this, the effectiveness of the coating was measured by preparing separate GNP dispersions at 4 different concentrations. GNP/water dispersions were prepared by

adding 2.5 g, 1.25 g, 0.5 g and 0.25 g GNP in 1000ml water, respectively. The amount of dispersed GNP was added to the end of the sample codes. For example, GNP-c-GF (2.5) refers to hydroxylated GF coated by dispersing 2.5 g of GNP in 1000 ml of water.

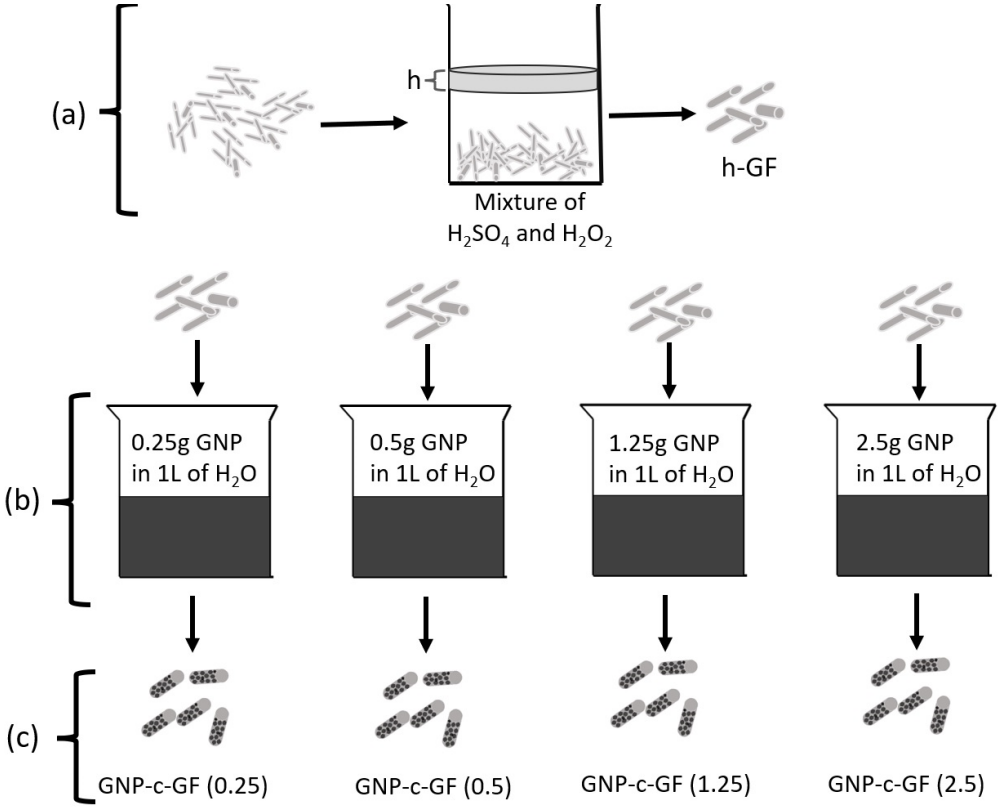

Figure 32. Experimental scheme of (a) desizing and hydroxylation of GF, (b) dip coating of GF with GNP at varying concentrations, and (c) coated samples.

SEM images in Figure 33 depict the contrasting characteristics of untreated and treated glass fibers (GF). In the untreated sample, the fibers exhibit interconnectivity with a discernible surface coating. However, following the hydroxylation process, the fibers become disconnected, leading to a smoother surface texture and increased separation between individual fibers. Consequently, the modified glass fiber surface becomes amenable to the deposition of graphene nanoplatelets (GNP).

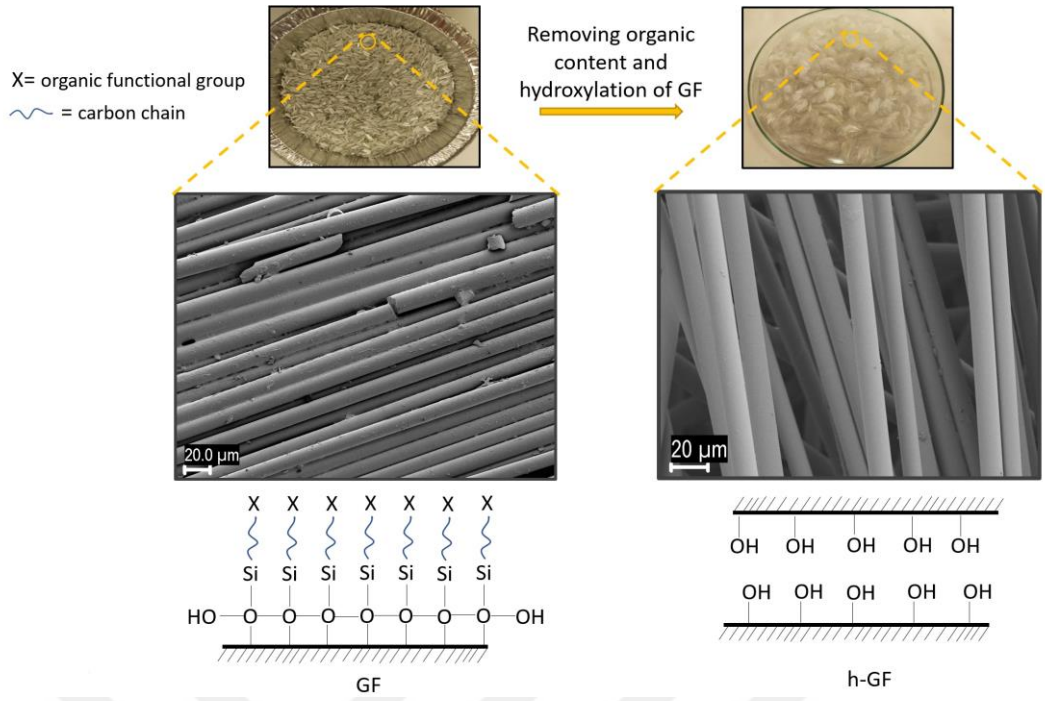

Figure 33. Related SEM images and chemical compositions belong to GF and h-GF.

The SEM images depicted in Figure 33 exhibit glass fibers that have been coated with various concentrations of GNP, captured at different magnifications. Initially, it can be inferred that the adhesion of GNPs to the fibers is robust across all concentrations. However, the extent of adhesion and the propensity for agglomerate formation exhibit notable variations. When the punctuated GNPs are classified based on the concentration of the immersion solution, the images corresponding to GNP-c-GF (0.25) are designated as a1-a3, GNP-c-GF (0.5) as b1-b3, GNP-c-GF (1.25) as c1-c3, and GNP-c-GF (2.5) as d1-d3 in Figure 34. Upon close examination of the sample with the highest GNP-c-GF concentration (2.5) (d1-d3), substantial agglomeration is observed. The GNP layers densely conglomerate in regions marked by blue arrows, resulting in an uneven distribution on the fibers. Further scrutiny of areas demarcated by yellow lines reveals denser clusters, indicating a higher concentration of the immersion solution. Although a reduction in agglomeration is apparent when the concentration is halved, clusters persist, and the distribution of GNPs on the fiber remains non-homogeneous. Upon halving the concentration of the immersion solution even further (b1-b3), the prominence of increased agglomerates diminishes, giving rise to a more homogeneous distribution. Remarkably, the formed agglomerates exhibit closer proximity to one another, with a relatively consistent interparticle distance. Notably, in columns c and d, agglomerations exceeding 1 micrometer are absent due to the merging of clusters. Upon further examination of the concentration that has been halved, an increase in particle distance

becomes evident. The gap between each GNP particle is approximately 2 micrometres, raising doubts regarding the adequacy of GNP adhesion to the fiber. In this case, GNPs were not coated on the glass fibers but appeared to be interspersed throughout the structure.

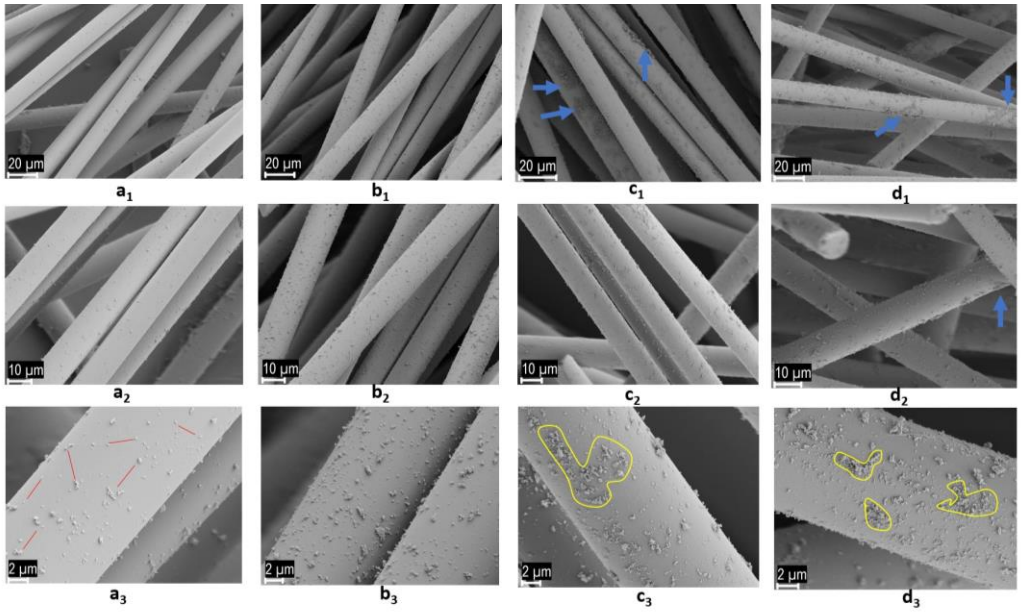

Figure 34. SEM images of (a_1-a_3) GNP-c-GF (0.25), (b_1-b_3) GNP-c-GF (0.5), (c_1-c_3) GNP-c-GF (1.25), (d_1-d_3) GNP-c-GF (2.5) at different magnifications.

Figure 35 and Table 13 illustrate the particle area distribution obtained by calculating particle sizes using Image J software over a uniform area of the coatings. The accompanying table presents the total number of particles and their distribution within specific size ranges. Increasing the concentration of GNPs results in a rise in the proportion of particles below 0.01 µm from 55% to 81%. However, to attain a uniform distribution of particles, it is crucial to take into account a wide range of particle sizes. Notably, GNP-c-GF (0.25) and GNP-c-GF (0.5) exhibit the highest proportions of particles, accounting for 28% and 27%, respectively, within the 0.01-0.05 µm range. It is worth noting that GNP-c-GF (0.25) shows no agglomerates exceeding 0.5 µm, but as mentioned earlier, the inter-particle distance is relatively large. On the other hand, GNP-c-GF (0.5) demonstrates a more homogenous particle distribution as it contains fewer particles exceeding 0.5 µm and a higher number of particles within the 0.01-0.05 µm range compared to other samples. Considering its similar characteristics to GNP-c-GF (0.5) and to avoid excessive GNP usage, GNP-c-GF (1.25) is not selected for incorporation into the composites. Notably, GNP-c-GF (2.5) exhibits visible agglomeration intensity with a significant clustering of particles above 0.5 µm.

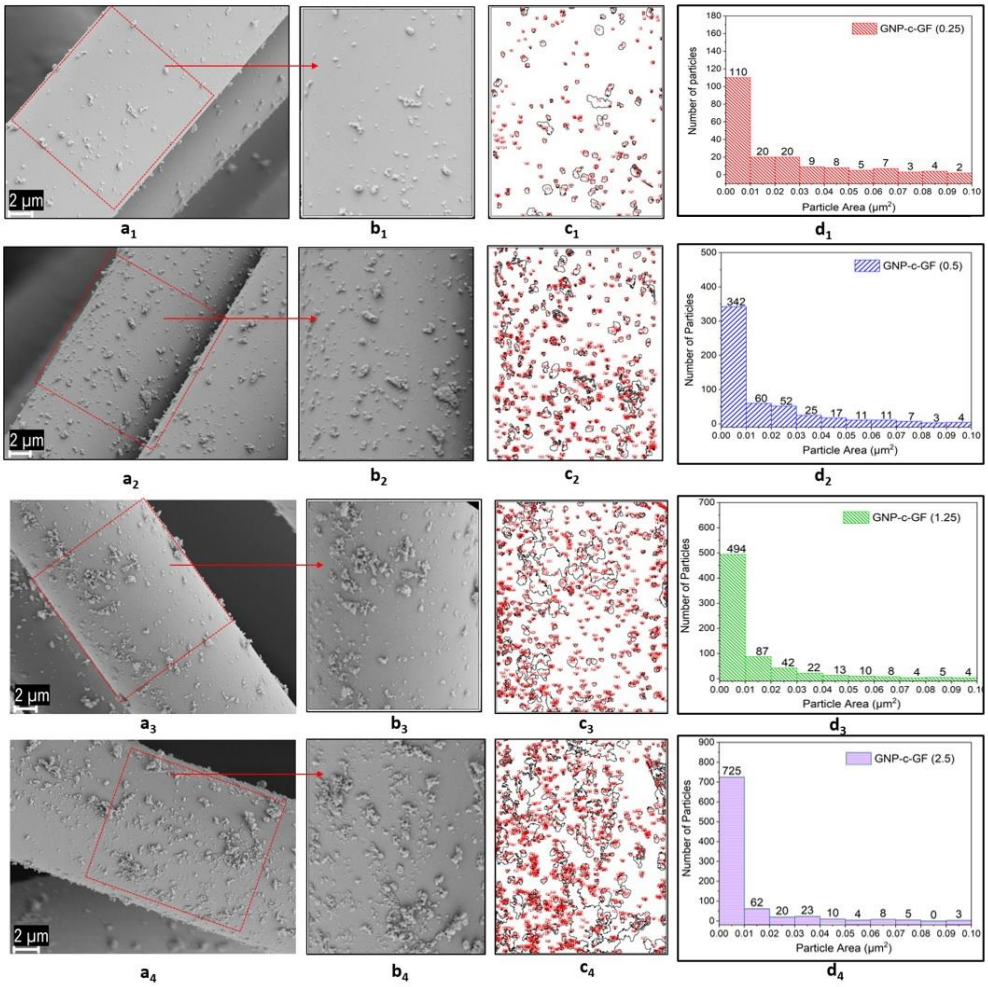

Figure 35. (a_1-a_4), and (b_1-b_4) SEM images and (c_1-c_4), (d_1-d_4) particle distrubution of GNP-c-GF (0.25), GNP-c-GF (0.5), GNP-c-GF (1.25), and GNP-c-GF (2.5).

Table 13. Number of particles in GNP-c-GF coatings and their distrubution (%) in blue.

Sample Name	Total number of particles	Under 0.01µm	Between 0.01 µm - 0.05µm	Between 0.05 µm -0.1 µm	Between 0.1 µm -0.5 µm	Above 0.5µm
GNP-c-GF (0.25)	202	110 (55)	57 (28)	21 (11)	14 (7)	-
GNP-c-GF (0.5)	563	342 (61)	154 (27)	36 (6)	29 (5)	2 (0.4)
GNP-c-GF (1.25)	725	494 (68)	164 (23)	31 (4)	30 (4)	6 (0.8)
GNP-c-GF (2.5)	897	725 (81)	114 (13)	20 (2)	31 (3)	7 (0.8)

FTIR spectroscopy is a commonly employed analytical method that investigates the interaction between infrared radiation and a specimen. It operates on the fundamental concept that distinct chemical substances absorb and emit unique frequencies of infrared light. This characteristic enables the identification and analysis of a sample's composition by studying its infrared absorption patterns. Figure 36 displays the FTIR spectra of GF,

h-GF, and GNP-coated h-GF. Upon examination of the GF spectrum indicated by the black line, stretching vibrations of the C-H groups are observed in the range of 2918 cm^{-1} to 2953 cm^{-1} [20]. This indicates the presence of sizing and an organic coating on the purchased GF. After the performed hydroxylation process, these organic groups are removed, and as shown by the green line, the CH peaks in this region are no longer present on the h-GF. Additionally, the peak observed at 3400 cm^{-1} corresponds to the hydroxyl groups [118]. This indicates the successful removal of organic groups on the GF surface through the hydroxylation process. The peaks observed at 877-948 cm^{-1} correspond to Si-O-Si bonds, which are commonly found in silicon-based materials [119]. When examining the GNP-c-GF coatings at different GNP immersion concentrations, it can be observed that the peak at 3400 cm^{-1} disappears.

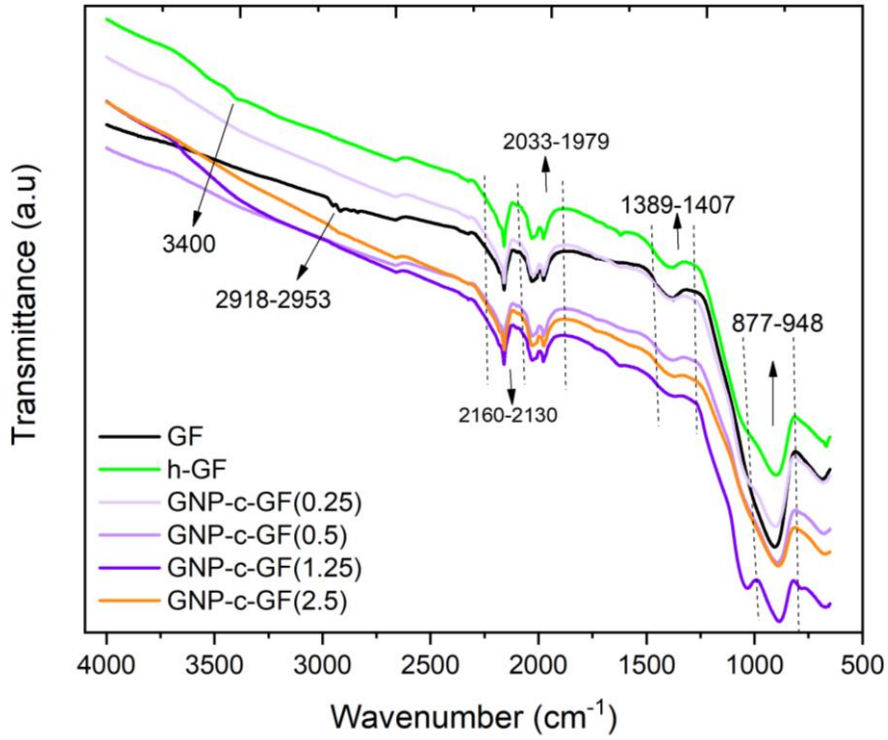

Figure 36. FTIR spectra of GF, h-Gf, and GNP-c- GF samples

X-ray Photoelectron Spectroscopy (XPS), also known as Electron Spectroscopy for Chemical Analysis (ESCA), is a powerful analytical technique used to investigate the chemical composition, bonding states, and electronic structure of materials by bombarding the sample surface with x-rays and detecting the reflected electrons [120]. XPS plays a crucial role in understanding chemical bonds since it provides information about the elemental composition of a material's surface [121]. By analysing the binding energies of core-level electrons, XPS can identify the types and relative abundances of

elements present and is a surface-sensitive technique, meaning it probes the outermost layers of a material (typically a few nanometres). This capability is advantageous for studying surface chemistry and surface modifications, as the surface plays a crucial role in many chemical processes. By investigating the chemical bonds at the material's surface, XPS can provide insights into surface reactions, adsorption phenomena, and interfacial interactions. Table of X-ray survey spectra and related deconvoluted peaks are presented in Table 14, Figure 37 and Figure 38. XPS survey data demonstrates an approximately 20% reduction in atomic C content after post-hydroxylation of GF due to the elimination of organic groups. Conversely, oxygen content exhibits an increase from approximately 19% to around 33% after hydroxylation. Following hydroxylation, the Si concentration increases to 17.84%, indicating improved signal collection from the GF surface as a result of the removal of the sizing procedure. As XPS measurements probe a specific depth, coating-related peaks become prominent. In-depth examination of GNP-c-GF samples illustrates an elevated carbon content ranging from 32.73% to 43.83% with increasing immersion concentration, suggesting the formation of a thicker and more abundant GNP layer. Additionally, the oxygen content diminishes from 42.7% to 35.45%, while the Si content slightly decreases due to the denser GNP layer formation. Figures 37a and 37b present the deconvoluted peaks of C1s for GF and h-GF, respectively. The peak detected at 284.5 eV corresponds to the C-C and C-H bonds [104], exhibiting reduced intensity in Figure 37b, representing h-GF. Conversely, the absence of a peak at 283.4 eV on h-GF, attributed to the C-Si bond from the sizing agent, indicates successful removal of the sizing agent. Likewise, Figures 37c and 37d depict the deconvoluted peaks of Si2p for GF and h-GF, respectively. In Figure 37c, the presence of Si-O-Si bonds, the fundamental constituents of glass fibers, is observed at 102.0 eV and Si-O-C bond observed at 102.7 eV [122]. Furthermore, Figure 37d displays the emergence of Si-OH groups at 102.9 eV after hydroxylation. In Figure 38, C1s spectra of GNP-c-GF samples were presented. C-C peaks in green reveals an incremental intensity from GNP-c-GF (0.25) to GNP-c-GF (2.5), indicating enhanced GNP attachment onto h-GF. The same pattern for C-O bond (blue) also observable. The red line that represents C-Si bond disappeared for GNP-c-GF (2.5) due to the high aglomeration and clustered of GNP particles on the surface.

Table 14. XPS survey scan results of GF, h-GF, and GNP-c-GF samples.

Sample Name	C (Atomic%)	O (Atomic%)	Si (Atomic%)	Others (Atomic%)	Included other elements
GF	69.68	19.62	6.57	4.13	Al, N, F
h-GF	49.08	33.07	17.84	0.01	Al, Ca, N
GNP-c-GF (0.25)	32.73	42.70	22.39	2.18	Al, S, N
GNP-c-GF (0.5)	36.73	38.16	20.65	4.46	Al, Ca, N
GNP-c-GF (1.25)	40.92	38.19	18.66	2.23	Al
GNP-c-GF (2.5)	43.83	35.45	18.39	2.33	Al, N

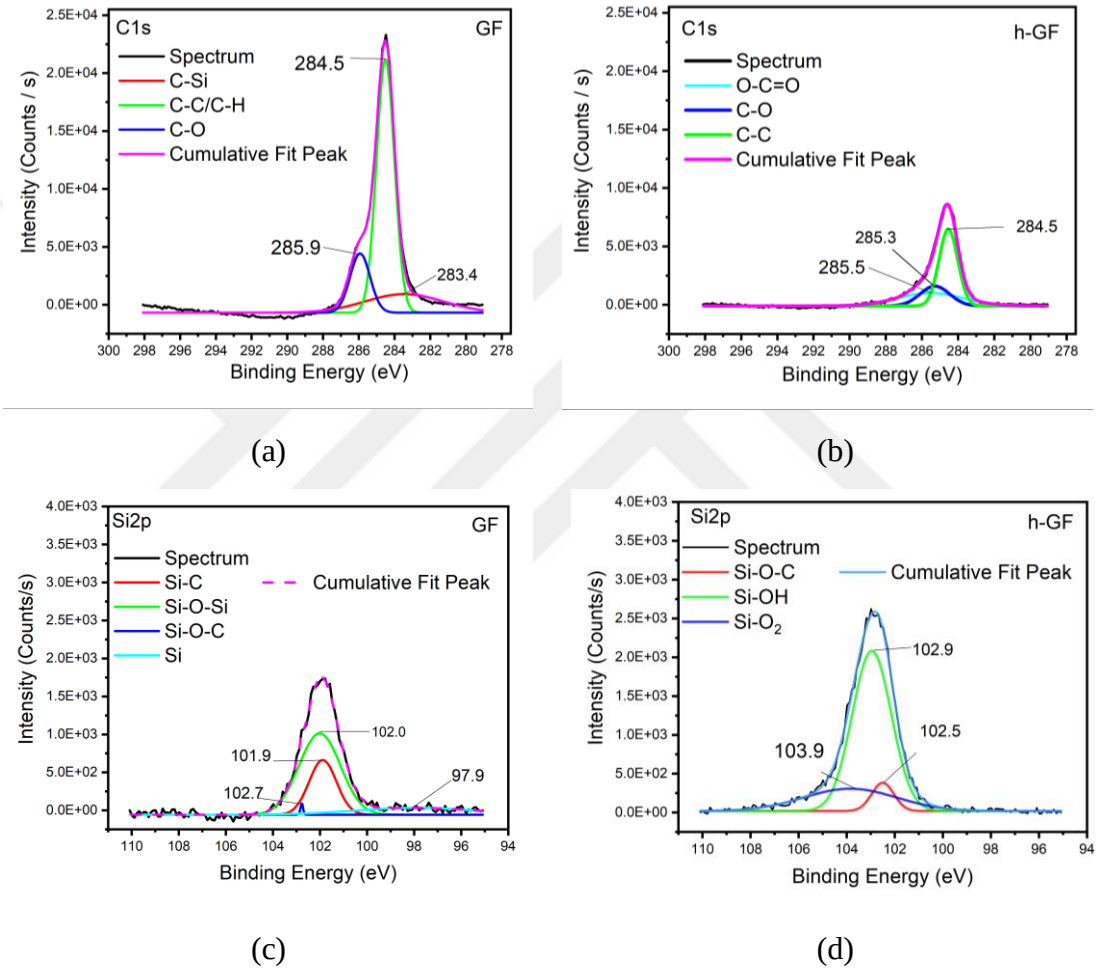

Figure 37. Deconvulated C1s of (a) GF and (b) h-GF, and deconvulated Si2p of (c) GF and (d) h-GF

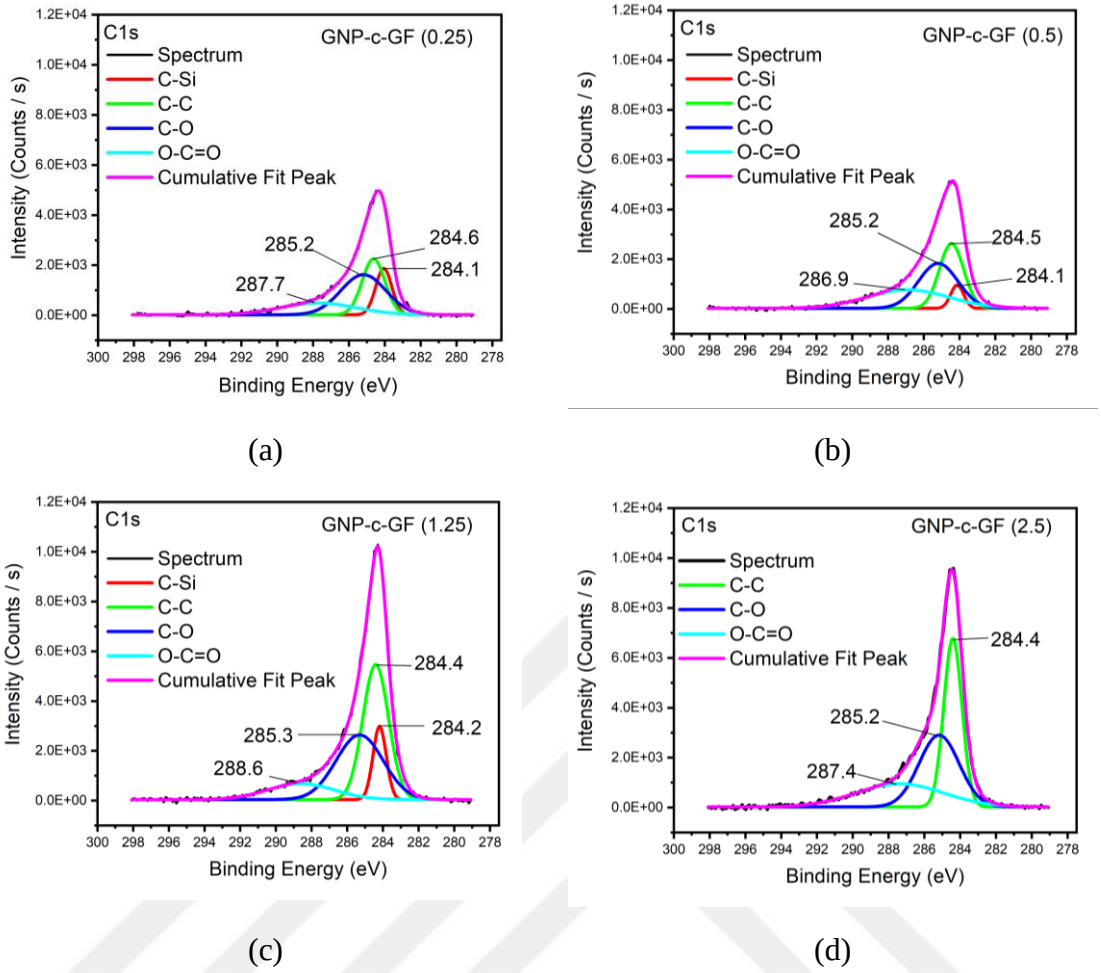

Figure 38. Deconvoluted C1s of (a) GNP-c-GF (0.25), (b) GNP-c-GF (0.5), (c) GNP-c-GF (1.25), and (d) GNP-c-GF (2.5), respectively.

Thermogravimetric analysis (TGA) is a valuable technique employed to quantify the coating content in diverse materials [123]. In the context of coatings, TGA allows for the determination of the percentage of coating within a composite material. Figure 39a depicts the residual weight of GNP, GF, h-GF, and GNP-c-GF samples and Figure 39b shows the GNP content on each coating sample. After coating on h-GF in GNP-c-GF (0.25), its residual weight increased from 98.18 to 98.40. In this case, it can be said that the difference of 0.22 is due to the GNP coating. However, since 94.64% of pristine GNP remains intact up to the same temperature, this value of 0.22 is 94.64% of GNP by weight. The GNP content obtained as a result of the calculation made in this approach and is shown in Figure 39b for each coating. As can be seen, the least GNP content was found in the GNP-c-GF (0.25) medium, while the highest GNP content was obtained in the GNP-c-GF (0.5) medium. With the further increase of the dipping concentration after this point, the adhesion rate of GNP on h-GF did not increase and much higher agglomeration was obtained with less GNP content. This proves that the GNP concentration of the

dipped dispersion and the ratio of GNP attached to the h-GF are not directly proportional and there should be an optimum concentration of GNP/water.

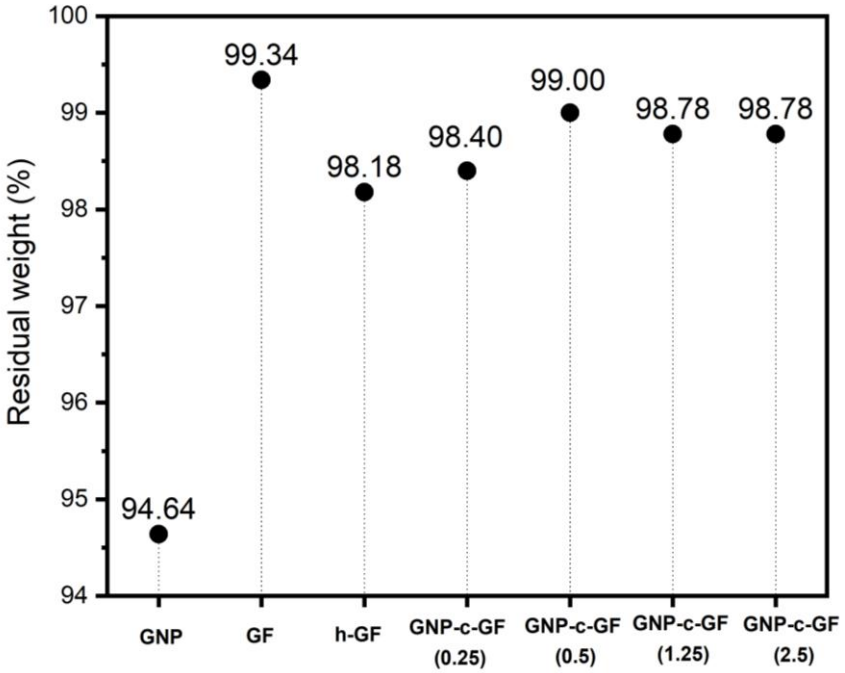

(a)

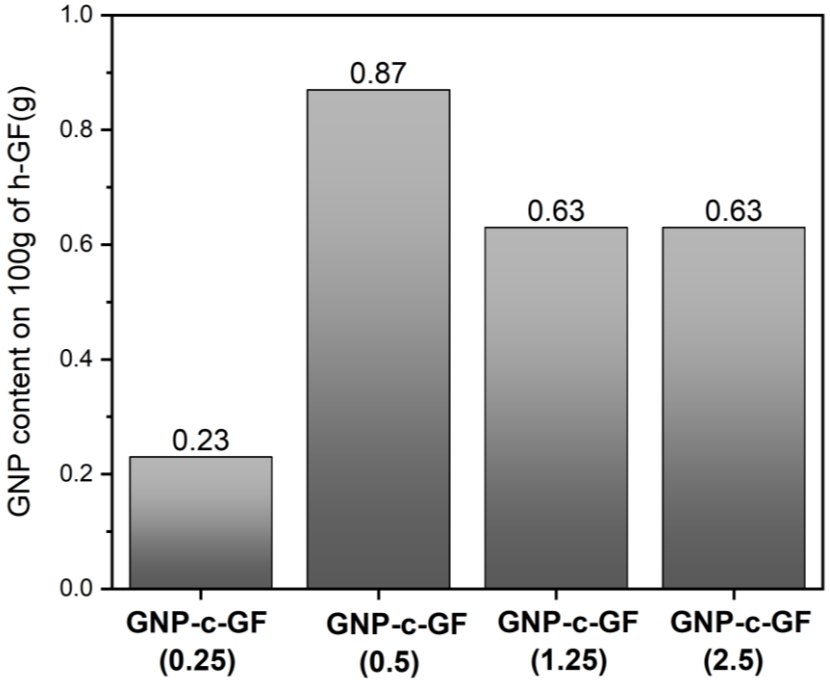

(b)

Figure 39. (a) Residual weight of GNP, GF, h-GF, and GNP-c-GF materials, (b) GNP content on GNP-c-GF samples according to TGA

X-ray diffraction (XRD) can be used to analyze graphene-coated glass fibers to gain insights into the structural properties of the material. Figure 40 displays the XRD patterns of GF, h-GF, and GNP-c-GF materials and the XRD pattern of GNP with the (001) and (002) planes can be found in supporting information Figure S2. The GF sample exhibited a high and broad peak at 2Θ= 27.3, indicating its amorphous structure [124]. After hydroxylation (h-GF), the appearance of new peaks, indicated by black arrows, can be attributed to the etched surface due to the removal of surface organic groups and the attachment of new molecules. After coating with GNP, those peaks dissappeared due to the existence of GNP on the surface for GNP-c-GF samples. The peak at 2Θ=27.3 slightly shifted to lower degrees for GNP-c-GF materials and the 002 peak of GNP [30] merged with the peak at 2Θ= 27.3 in GF, resulting in broader and more intense peaks. This observation provides evidence for the successful coating of GNP onto the h-GF surface. On the other hand, the same peak at around 2Θ= 27.3 in GNP-c-GF (2.5) exhibited a distinctive behaviour compared to other coatings, with a decrease in both peak width and intensity while the peak at 2Θ =10.3 became more noticeable. This pattern of GNP-c-GF (2.5) can be attributed to excessive GNP agglomeration which creates surface heterogeneity on the fiber.

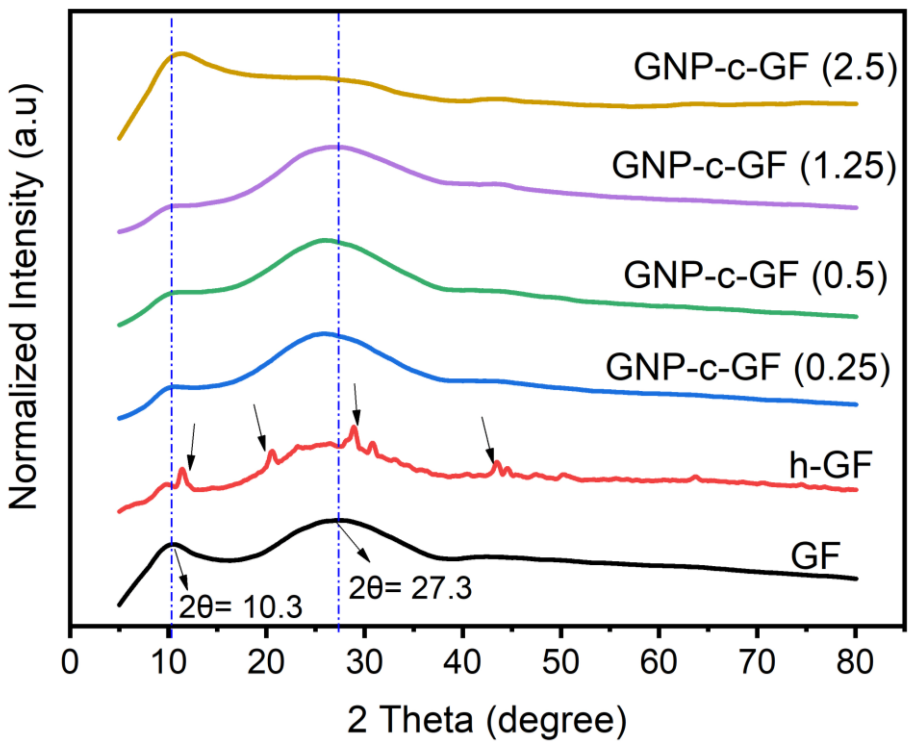

Figure 40. XRD patterns of the GF, h-GF, and GNP-c-GF materials

5.1.4.2. Effect of GNP-c-GF on the Mechanical Performance of PP composites

The evaluation of flexural and tensile properties plays a critical role in assessing the mechanical behaviour and performance of composites. These properties offer valuable insights into how the material responds to bending and tensile forces, which are commonly encountered in real-world applications. By measuring these properties, we can determine the composite's capacity to withstand applied forces, resist deformation, and maintain its structural integrity. Such measurements enable us to compare and select appropriate composite materials that meet the performance requirements of specific engineering applications. The influence of GNP-c-GF on the mechanical properties of polypropylene (PP) was investigated through tensile and flexural testing and various weight percentages (0.1-15%) of GNP-c-GF were incorporated into the PP matrix and shown in Figure 41. The findings demonstrated that even a minimal addition of GNP-c-GF at 0.1% by weight resulted in a notable enhancement of the tensile modulus. Specifically, there was a substantial 31% increase in the tensile modulus compared to neat PP when 1 wt.% of GNP-c-GF was introduced. A higher tensile modulus implies that the composite material is less prone to elongation and deformation under applied tensile loads. This increased stiffness contributes to improved structural integrity, reducing the risk of deformation or failure under load. While the flexural modulus values experienced a lesser degree of impact compared to the tensile modulus values, the inclusion of 1 wt.% GNP-c-GF exhibited a significant enhancement in flexural strength. This resulted in a remarkable 15% increase, reaching a value of 45 MPa. The primary disparity in the results between the tensile modulus and flexural modulus can be attributed to the elongated shape of the fibers and their heightened resistance when oriented in the tensile direction.

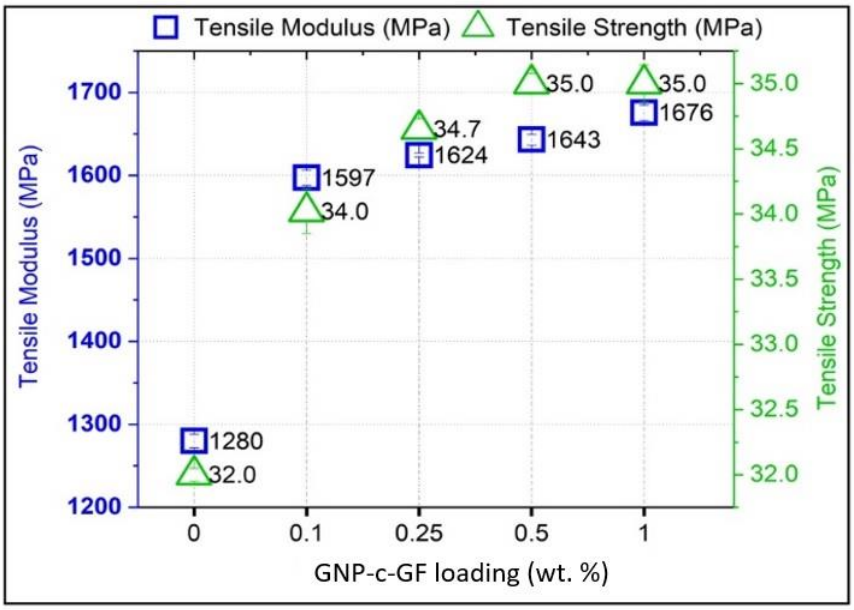

(a)

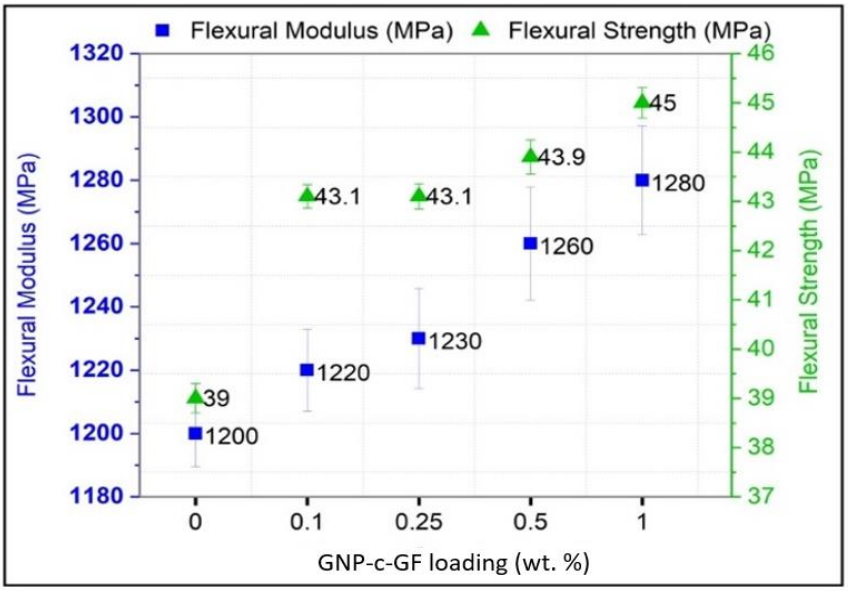

(b)

Figure 41. (a) Tensile and (b) flexural properties of PP/GNP-c-GF composites

Tensile properties are particularly important for applications where the material needs to withstand pulling or stretching forces, such as in structural components or load-bearing applications and therefore glass fiber reinforced composites are perfect match for this kind of applications. The interaction between the fibers and the matrix material is critical for achieving high tensile properties. Figure 42 presents a comparative evaluation of the tensile and flexural properties of composites with varying compositions. The composites with different glass fiber (GF) contents, namely 15%, 20%, 25%, and 30%, are denoted by the colors blue, gray, green, and black, respectively. The solid-filled columns represent

composites reinforced solely with GF, the striped and solid-filled columns represent composites incorporating both GF and graphene nanoplatelets (GNP), and the checkered and solid-filled columns represent composites consisting of GF, GNP, and GNP-c-GF. Initially focusing on the tensile modulus of the GF/PP composites, the glass fiber content was incrementally increased from 15% to 30% in the polypropylene (PP) matrix, resulting in the expected enhancements starting from 3527 MPa to 5512 MPa which can be attributed to the high aspect ratio and stiffness of the glass fibers. Furthermore, the introduction of 1 wt.% GNP to the PP/GF composites led to additional improvements in the mechanical properties compared to the composites with the same GF content. Subsequently, with the incorporation of GNP-c-GF, a further increase in the tensile modulus was observed, surpassing the values achieved by the GF-only composites. The tensile modulus of the composite containing 30% glass fiber (GF) was determined to be 5512 MPa, while the composite with 25% GF, supplemented with GNP and GNP-c-GF, exhibited a higher value of 5658 MPa. By using GNP-c-GF, the increase in surface roughness promotes a larger contact area between the fiber and matrix, leading to enhanced interfacial shear bonding through improved mechanical interlocking between the two components [125]. This finding suggests the potential for attaining stronger composites with reduced GF content, highlighting the importance of precise composite formulation. Moreover, a 5% reduction in GF loading can offer significant advantages in terms of weight and density for the composite. Additionally, the incorporation of GNP-c-GF resulted in a considerable reduction in the standard deviation values associated with the mechanical properties of the composites. The assessment of standard deviation is crucial in evaluating the consistency and homogeneity of results, indicating a more uniform distribution of properties throughout the composite. Notably, the GF-only composites exhibited elevated standard deviation values, whereas the addition of GNP-c-GF led to nearly identical tensile modulus results in five consecutive measurements. This observation underscores the achievement of enhanced filler dispersion and improved homogeneity facilitated by the incorporation of GNP-c-GF. Tensile strength is a fundamental mechanical property used to assess the maximum stress capacity of a material under tension, providing crucial insights into its structural integrity and reliability. A strong and well-bonded fiber-matrix interface ensures efficient stress transfer and prevents fiber pull-out or debonding, leading to improved tensile strength. The analysis of tensile strength values depicted in Figure 40b reveals that the composite filled with 30% glass fiber (GF) displayed the highest value of 74 MPa, aligning with

expectations due to its elevated GF content. However, upon closer examination of composites with identical GF content, with the addition of GNP or GNP-c-GF, no discernible pattern of notable increase, decrease, or consistent trend is observed, suggesting that the tensile strength values do not exhibit significant changes. Notably, the standard deviation values of composites containing GNP-c-GF are much lower than those of the other composites. This reduction in standard deviation suggests a higher degree of homogeneity in both the obtained results and the overall behaviour of the composites. Flexural modulus and flexural strength are important mechanical properties that provide insights into the structural behaviour and performance of composite materials under bending loads. The flexural modulus represents the material's resistance to deformation when subjected to a bending force, indicating its stiffness and ability to maintain its shape. The flexural modulus and flexural strength values of the produced composites can be seen in Figures 42c and 42d. Overall, when looking at composites with the same GF content, the addition of GNP and GNP-c-GF has resulted in a gradual increase in flexural modulus values. In particular, the GNP and GNP-c-GF-containing composite with 25% GF loading exhibits a value of 4370 MPa with a low standard deviation, which is very close to the 4370 MPa shown by the 30% GF-filled composite. When examining the tensile strength values, increasing strength values were observed with increasing GF content, and slight increases were obtained with the addition of GNP. This may be attributed to the resistive response of the glass fibers at certain points, as shown in SEM images in Figure 44a and 44c, which will be discussed in related section later. When glass fibers cluster together, they can collectively generate a resistant force against the applied stress at specific locations. After adding GNP-c-GF, slight decreases were observed which suggests that the agglomerated fibers are separated by GNP-c-GF, leading to more homogeneous dispersion within the matrix and the disruption of the cohesive force between fibers.

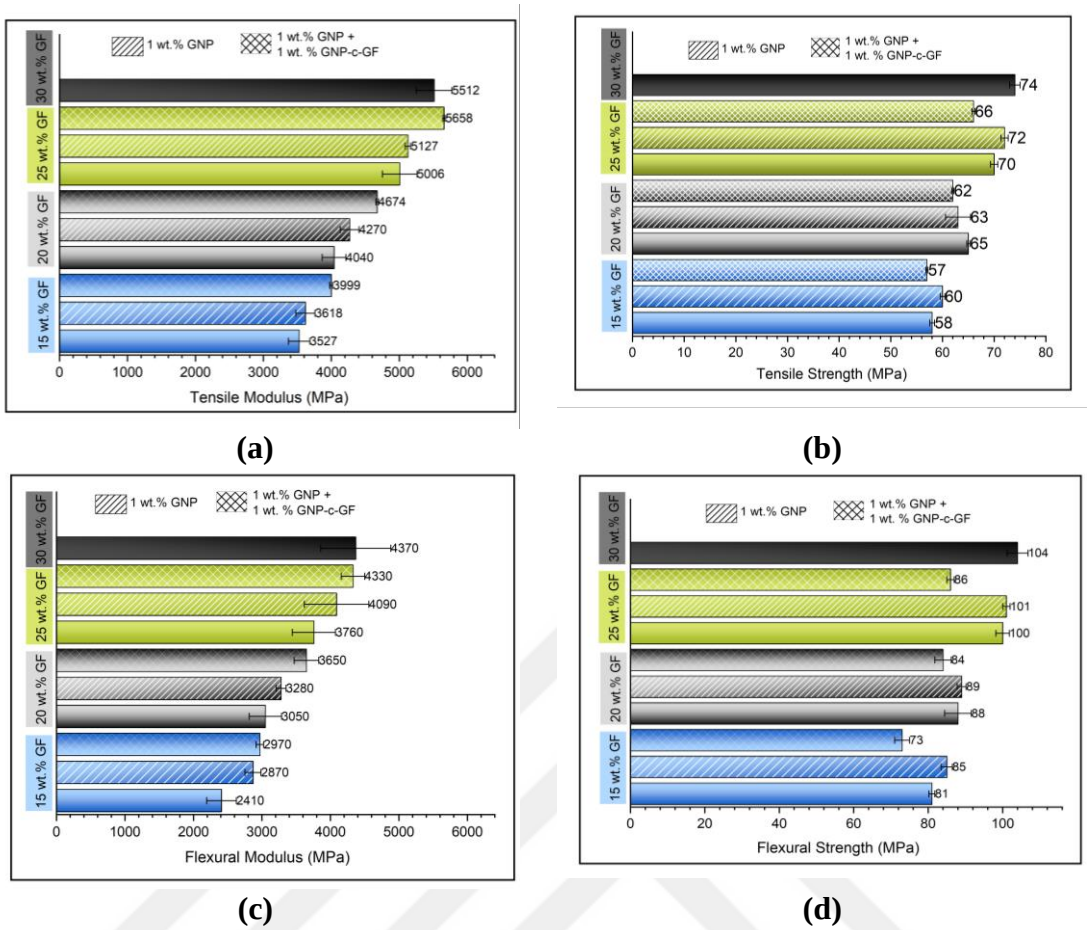

Figure 42. (a) Tensile modulus, (b) tensile strength, (c) flexural modulus, and (d) flexural strength of the GF filled composites.

Melt flow index (MFI) serves as a crucial parameter, offering valuable insights into the viscosity and particle distribution characteristics of the materials. The melt flow index (MFI) values for two types of composites, namely PP/GNP-c-GF and PP/GF/GNP/GNP-c-GF, are depicted in the Figure 43a and Figure 43b, respectively. Examination of the PP/GNP-c-GF composites revealed an increment in MFI values up to a loading ratio of 0.5 wt.%, indicating an enhancement in flow properties. This improvement can be attributed to the oriented alignment of glass fibers (GFs) in the flow direction and the concurrent presence of graphene nanoplatelets (GNPs), which acted as a lubricant within the matrix. However, as the loading ratio reached 1%, a reduction in viscosity was observed due to the formation of an interconnected network structure among the incorporated GNP-c-GF particles. This network structure limited the mobility of the matrix, thereby effectively demonstrating the significant contribution of GNP-c-GF. The interfacial compatibility between the components was investigated by introducing GNP-c-GF into PP/GF/GNP composites. Specifically, the addition of GNP-c-GF to a GNP-reinforced composite with 15% GF loading resulted in a notable 13% increase in MFI,

highlighting the improved interfacial properties. For the composite with 20% GF loading, the observed increase in MFI was reduced to 6%. These findings indicate that the inclusion of GNP-c-GF mitigated the restrictions imposed by rigid GFs, thereby promoting better interfacial compatibility, and exhibiting a lubricating effect within the matrix. Moreover, in the composite with 25% GF loading, the added GNP-c-GF achieved a sufficient level of saturation and facilitated the formation of a network structure among the particles. Consequently, this network structure impeded the flow of the matrix, leading to a 5% reduction in MFI. The decrease in MFI value resulted in an increase in viscosity, reflecting the altered rheological behavior induced by the incorporation of GNP-c-GF. Hence, the experimental results highlight the favourable influence of GNP-c-GF on the melt flow properties, interfacial compatibility, and viscosity of the composites, shedding light on their potential for advanced applications in various fields.

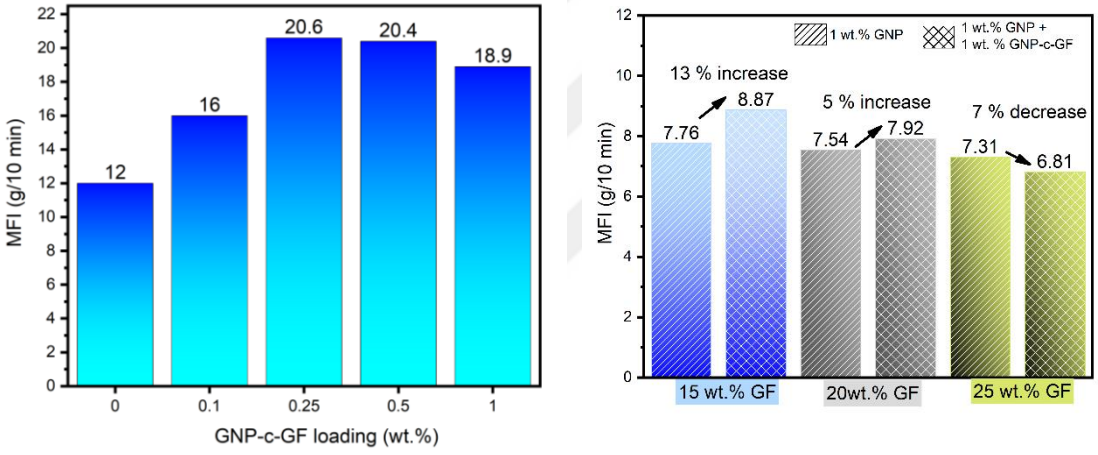

(a) (b)

Figure 43. Melt flow index values of (a) PP/GNP-c-GF composites and (b)PP/GF/GNP and PP/GF/GNP/GNP-c-GF composites

5.1.4.3. Effect of GNP-c-GF on the Morphological Analysis of PP/GF/GNP composites by SEM

SEM is a highly valuable tool in composite research as it enables the examination of the composite's microstructure with exceptional detail and resolution. By analyzing the morphology, distribution, and alignment of the reinforcing fibers or particles in the composite matrix, SEM provides essential insights into the interfacial interactions, bonding, and overall performance of the composite. This information is crucial for understanding how the composite behaves under various conditions and aids in optimizing its design and manufacturing proce**sses.** Figure 44 presents morphological

analysis of the effect of GNP-c-GF on the 20% GF and 1% GNP filled composites. Composites filled with 20% GF have black cavities indicating fiber break points, giving some clues as to the way the fiber breaks from the matrix. For example, the rounds from which the fibers in Figure 44a come out are almost perfectly round (yellow arrows), indicating that the glass fibers break without difficulty as they pull out of the matrix. On the other hand, the round shape of most of the circles in Figure 44b has been distorted and this homogeneity has been disrupted by taking an elliptical structure or forming an angular shape at some points, as indicated by the yellow arrows. This proves that at some points it is more difficult for the fibers to separate from the matrix. With the red arrows, deformed matrix can be seen on the edges of the circles. Contrary to Figure 44a, at the points indicated by the blue arrows in 44b, the bond of the fibers with the matrix is clearly visible due to the polymer matrix adhered to the fiber. Therefore, it can be said that matrix and fiber adhesion become stronger with GNP-c-GF content. In the composite without GNP-c-GF, it is also seen that a few fibers agglomerate at the points indicated by the red circle. Closer images also appear in Figure 44c and Figure 44d. Here, again, there is a gap of 3 fibers that have been agglomerated from the matrix, which is indicated by a red circle. The smooth circles (yellow arrows) of the broken fibers also appear more clearly. In Figure 44d, the deformation of the cavities where the fibers have come out is also shown more closely with yellow arrows. Overall, it is possible to say that increased fiber-matrix compatibility is achieved at some points in the presence of GNP-c-GF in the environment.

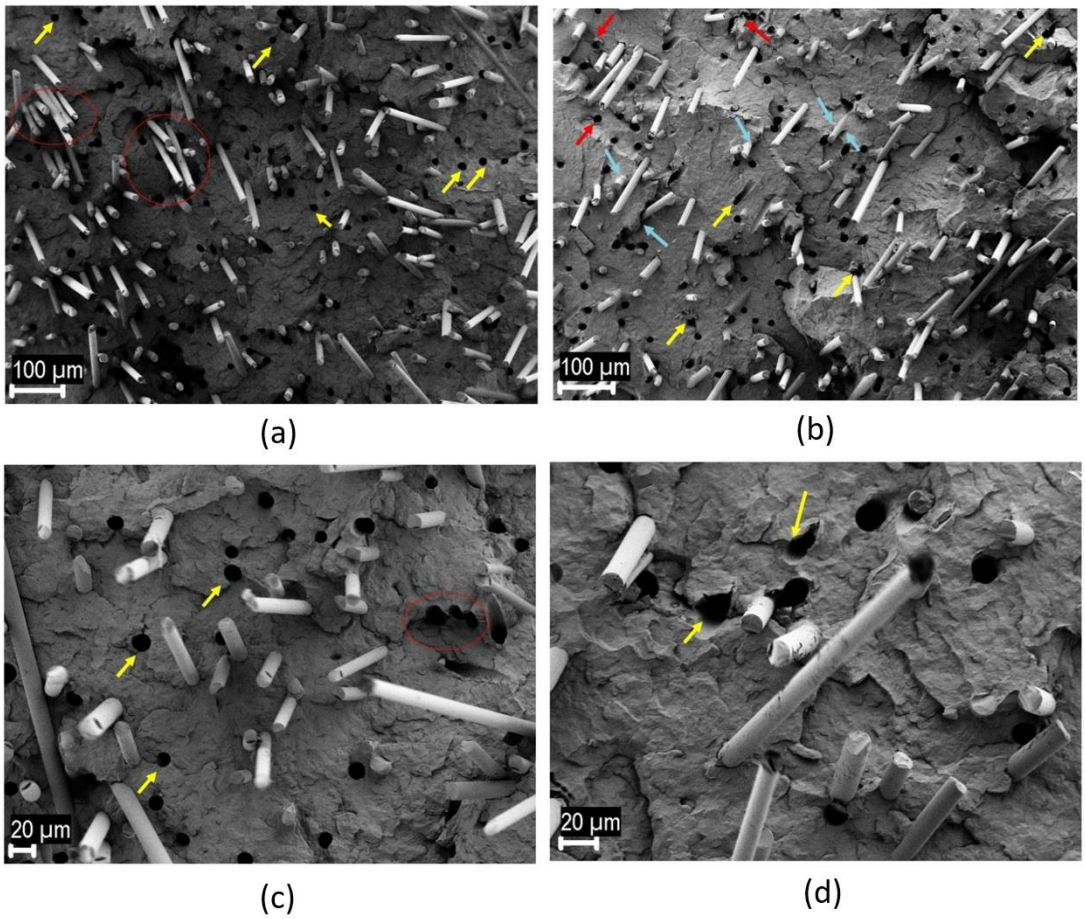

Figure 44. SEM images of (a,c) PP/GF/GNP composites, and (b,d) PP/GF/GNP/GNP-c-GF composites at different magnifications.

5.1.5. Conclusion

Current study utilized a facile and practical coating technique to treat glass fibers (GF) with upcycled graphene nanoplatelets (GNPs) derived from waste tires. The incorporation of unmodified GNPs, followed by an optimization study on dip coating, resulted in the successful production of GNP-coated glass fibers (GNP-c-GF). These GNP-c-GF were effectively integrated into pure polypropylene (PP) and PP/GF/GNP composites, leading to substantial improvements in their mechanical, morphological, and flow properties.

The addition of a small quantity (1%) of GNP and GNP-c-GF into the composites greatly enhanced the interfacial compatibility among GNPs, GFs, and the matrix. Notably, the inclusion of 1% GNP-c-GF in neat PP exhibited a significant 31% increase in tensile modulus compared to pure PP. The introduction of GNP-c-GF also played a crucial role as a compatibilizer, enhancing the homogeneity and dispersion within the composite system. 25 wt.% GF filled PP with the addition of GNP-c-GF and GNP exhibited a better value with 5658 MPa while 30% GF filled PP had a tensile modulus of 5512 MPa.

Furthermore, the addition of GNPs and GNP-c-GF led to increased flexural modulus values in composites with the same GF content. The tensile strength values did not exhibit significant changes with the addition of GNPs or GNP-c-GF. However, the standard deviation values of composites containing GNP-c-GF were significantly lower, indicating improved homogeneity. The melt flow index (MFI) analysis showed that the incorporation of GNP-c-GF enhanced the flow properties of the composites up to a loading ratio of 0.5 wt.%. However, at higher loading ratios, a network structure formed among the GNP-c-GF particles, reducing the viscosity, and limiting the mobility of the matrix. The presence of GNP-c-GF also improved the adhesion between fibres and the matrix, as observed in the morphology analysis. The agglomeration of fibres was reduced, leading to a more homogeneous dispersion within the matrix and disruption of cohesive forces between fibres.

5.2. Production and Optimization Studies of Graphene/Talc/PP Hybrid Composite

In this part of the thesis, a study has been carried out to improve the lightening and mechanical properties of a commercial part with known formulation. 20 wt.% talc filled PP is used in the target part and the mechanical properties of this part are shown in the Table 15. Here, GNP produced from waste tires was integrated into formulations to reduce the amount of talc in this formulation and to lighten the product. At the same time, a research and development study on the production method was presented. Mechanical properties of compound results produced by twin screw extrusion and thermo-kinetic mixer are presented in the Table 16 and Table 17 respectively.

Table 15. Mechanical properties of 20 wt.% talc filled PP

Tensile Modulus (MPa)	Yield Strength (MPa)	Flexural Modulus (MPa)	Flexural Strength (MPa)	Weight (g)
2387	28	1900	40	66

Table 16 summarizes the mechanical properties of the hybrid composites which were manufactured by twin screw extruder. Talc ratio was reduced to 15 wt.%, 10 wt.%, and 5 wt.% and 1 wt.% GNP was incorporated to formulations to compensate mechanical properties and lighten the material. All formulations showed higher value of flexural strength and yield strength. PP/Talc-10/GNP-1 and PP/Talc-15/GNP-1 samples exhibit higher flexural and tensile modulus compared to target value. To keep the inorganic filler

ratio at a minimum, PP/Talc-10/GNP-1 formulation was chosen to replace the target formulation. Additionally, by reducing this inorganic filler, the density of the sample decreased to 0.95 g/cm^3 from 1.05 g/cm^3. That change of density lead to a 10% weight reduction in the plastic part.

Table 16. Mechanical properties of PP/Talc/GNP Hybrid composites by twin screw extruder

Composite Name	Flexural Modulus [MPa]	Flexural Strength [MPa]	Tensile Modulus [MPa]	Yield Strength [MPa]
PP/Talc-5/GNP-1	1590	48.7	2067.98	35.23
PP/Talc-10/GNP-1	2040	52.2	2381.36	35.09
PP/Talc-15/GNP-1	2140	52.1	2712.44	35.24

Table 17 summarizes the mechanical properties of same formulations by applying a different compound method which is high shear rate thermo- kinetic mixer. By applying a high shear rate thermo-kinetic mixer all formulations showed higher value in terms of flexural modulus, flexural strength, tensile modulus, and tensile strength compared to target values. Results proved that manufacturing technique has a great influence on mechanical properties of the hybrid composites. PP/Talc-10/GNP-1 sample showed 55% increase in flexural modulus, 52% increase in flexural strength, and 48% increase in tensile modulus compared to target values in Table 15.

Table 17. Mechanical properties of PP/Talc/GNP Hybrid Composites by thermokinetic mixer

Composite Name	Flexural Modulus [MPa]	Flexural Strength [MPa]	Tensile Modulus [MPa]	Flexural Modulus [MPa]
PP/Talc-5/GNP-1	2542	58.60	3117	41
PP/Talc-10/GNP-1	2948	60.70	3539	41
PP/Talc-15/GNP-1	3423	62.30	3744	41

Table 18 also compares the mechanical properties of PP/Talc-10/GNP-1 composites according to its production type. Even though the results by thermo-kinetic mixer were higher, these formulations were also suitable for twin screw extrusion. Target values were achieved by halving the talc content and adding 1 wt.% of GNP.

Table 18. Comparison of mechanical properties by production methods

	(PP/Talk%20) Target Value	**(PP/Talk %10/GNP 1%) Obtained Value (twin screw extruder)**	**(PP/Talk %10/GNP 1%) Obtained Value (Thermo-kinetic mixer)**
Tensile Modulus	2387 MPa	2381 MPa	3539 MPa
Yield Strength	28 MPa	35.09 MPa	41 MPa
Flexural Modulus	1900 MPa	2040 MPa	2948 MPa
Flexural Strength	40 MPa	52.2 MPa	60.7 MPa

Figure 45 shows the morphology of PP/Talc-10/GNP-1 samples by comparing their production methods. In Figure 45a, the talc layer shows an orientation in a single axis. This is the result of production by extrusion which orient the layers in one direction. However, in Figure 45b, it is seen that the talc layers are oriented on every axis and do not prefer a particular orientation. Talc layers were oriented in all directions and better dispersed in the matrix by mixer and therefore increased the performance of the composite.

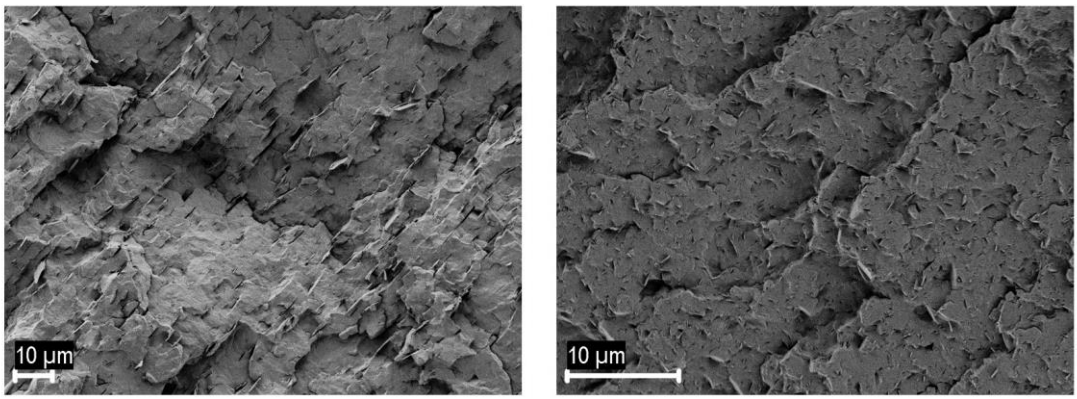

Figure 45. SEM images of the PP/10 wt.% Talc/ 1wt GNP by (a) twin screw extruder, (b) thermo-kinetic mixer

CHAPTER 6. General Conclusion

The research presents groundbreaking findings in the field of graphene-based polymer composites, highlighting the significant impact of utilizing process techniques, synthesis techniques, formulations, and modified materials for various applications, paving the way for sustainable and mechanically superior materials in the future.

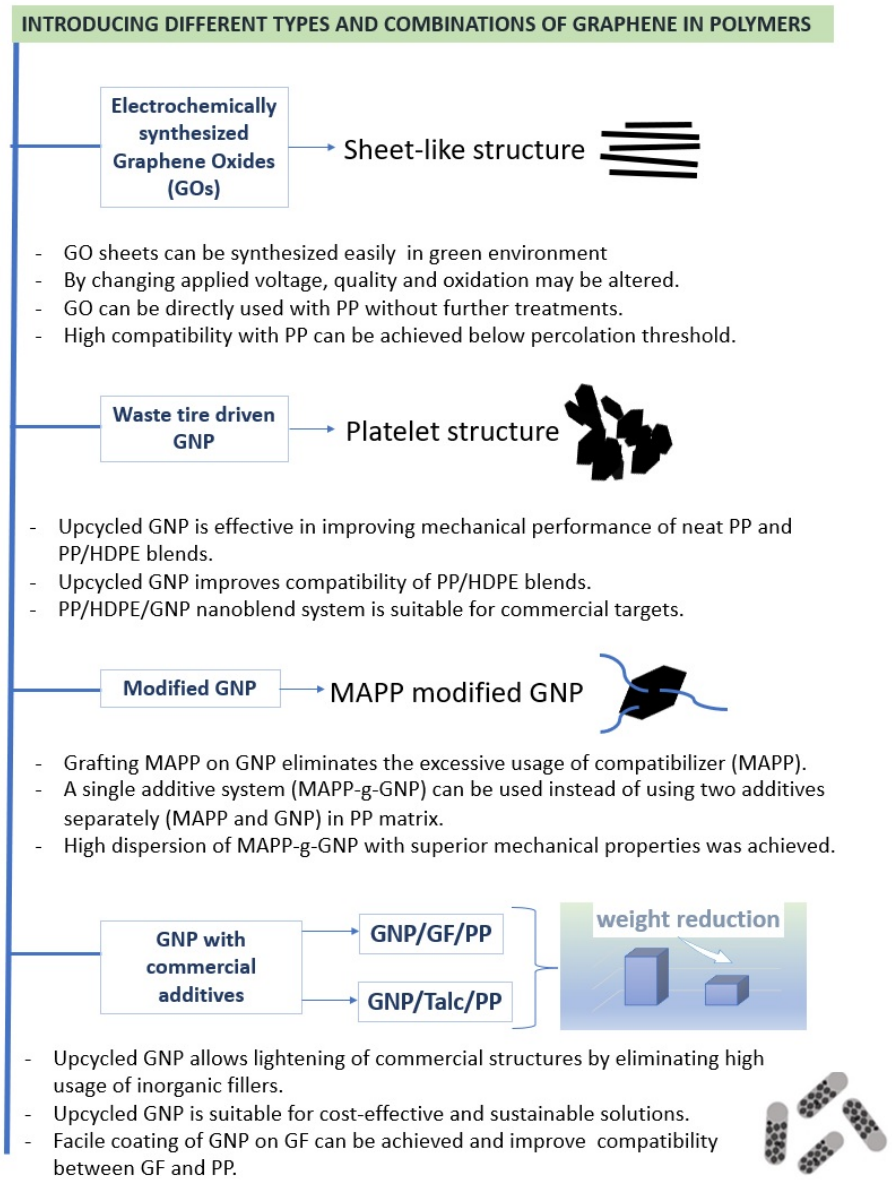

Figure 46. Graphene types, combinations, and key findings employed within the scope of the thesis.

Firstly, the study developed a scalable methodology for incorporating graphene oxide (GO) into polypropylene (PP) using an eco-friendly electrochemical exfoliation method. The incorporation of graphene, with its unique sheet-like structure obtained through electrochemical synthesis, has demonstrated its potential to improve composite mechanics below the percolation threshold. The addition of 1 wt.% GO significantly improved the flexural modulus and strength of PP composites. The rheological characterization showed improved dispersion and viscosity with lower GO loadings. The study demonstrated the potential of electrochemical synthesis for the mass-scale commercialization of graphene materials. Future research could focus on optimizing the electrochemical synthesis process and investigating the long-term stability and performance of PP/GO composites. Further exploration of different solvent systems and upscaling techniques would also be valuable for the composite industry.

Secondly, waste tire-derived graphene nanoplatelets (GNP) were chemically grafted with MAPP (MAPP-g-GNP) and compounded with PP using high shear rates. The effect of MAPP-g-GNP on the processability, viscoelastic response, and mechanical performance of PP composites was investigated. The results showed a high degree of interfacial enhancement through the chemical combination of MAPP with GNP in the PP matrix. The addition of 0.1 wt.% MAPP-g-GNP resulted in a 38% increase in flexural modulus, a 26% increase in flexural strength, and a 26% increase in tensile modulus compared to neat PP. Rheological studies supported the superior performance of MAPP-g-GNP over MAPP alone, as it improved particle dispersion, strengthened the interface, and enhanced the melt strength of neat PP. The study also elucidated the mechanism of interface interactions, highlighting the potential of chemically modified GNP to reduce the excessive use of compatibilizers and decrease the total amount of required GNP while achieving superior mechanical properties. Moving forward, further exploration of the mechanical properties and dispersion behaviour at higher filler concentrations would be valuable. Assessing the performance of the composite at elevated GNP loadings can provide insights into achieving enhanced properties while maintaining good dispersion. Additionally, extending the investigation to other polyolefin matrices, such as polyethylene (PE), would broaden the potential applications of the MAPP-g-GNP composite system. Optimization of compounding process parameters, such as melt temperature, shear rate, and mixing time, could further enhance dispersion and interfacial adhesion, paving the way for industrial-scale production.

Thirdly, the study utilized a high shear rate thermo-kinetic mixer to produce PP/HDPE binary blends and PP/HDPE/GNP ternary nanoblends. Through mechanical, rheological, and morphological analysis, it was observed that the right manufacturing technique and optimized GNP loading allowed for the localization of GNP at the interface of the binary blends, leading to improved mechanical properties. Additionally, the PP/HDPE blend matrix showed promise as an alternative to pure PP, exhibiting higher mechanical performance through the synergistic effects of the blend.

Lastly, the study opens several avenues for future research and development in the field of graphene-coated glass fiber (GNP-c-GF) composites. While the current study utilized a practical dip coating technique for GNP-c-GF production, further optimization, and refinement of the coating process can be explored. Fine-tuning parameters such as coating time, temperature, and concentration could potentially enhance the coating efficiency and ensure uniform dispersion of GNPs on the GF surface. While the current study focused on tensile modulus and flexural strength improvements, future investigations can delve into other mechanical properties, such as impact strength, fatigue resistance, and creep behaviour. Exploring the effects of different GNP-c-GF loadings and fabrication techniques on these properties would contribute to a more comprehensive understanding of the composite's performance. The influence of processing parameters on the dispersion and alignment of GNP-c-GF within the matrix can be explored further. Investigating alternative processing techniques, such as injection moulding or extrusion, and their impact on the composite properties would aid in optimizing the manufacturing process. The successful integration of GNP-c-GF in the current study provides valuable insights and suggests several potential future applications and benefits. GNP-c-GF composites can be explored as lightweight alternatives in various industries such as automotive, aerospace, and construction. Their improved mechanical properties and compatibility could enable the design of lightweight components with enhanced strength and stiffness. The utilization of upcycled GNPs derived from waste tires in the current study aligns with the growing demand for sustainable materials. Further research could explore the environmental impact and life cycle analysis of GNP-c-GF composites, highlighting their potential as eco-friendly alternatives in various industries. Further exploration of the scalability and feasibility of the GNP-c-GF production process is crucial. Investigating the potential for large-scale manufacturing and cost-effectiveness would facilitate the practical implementation of these composites in industrial settings.

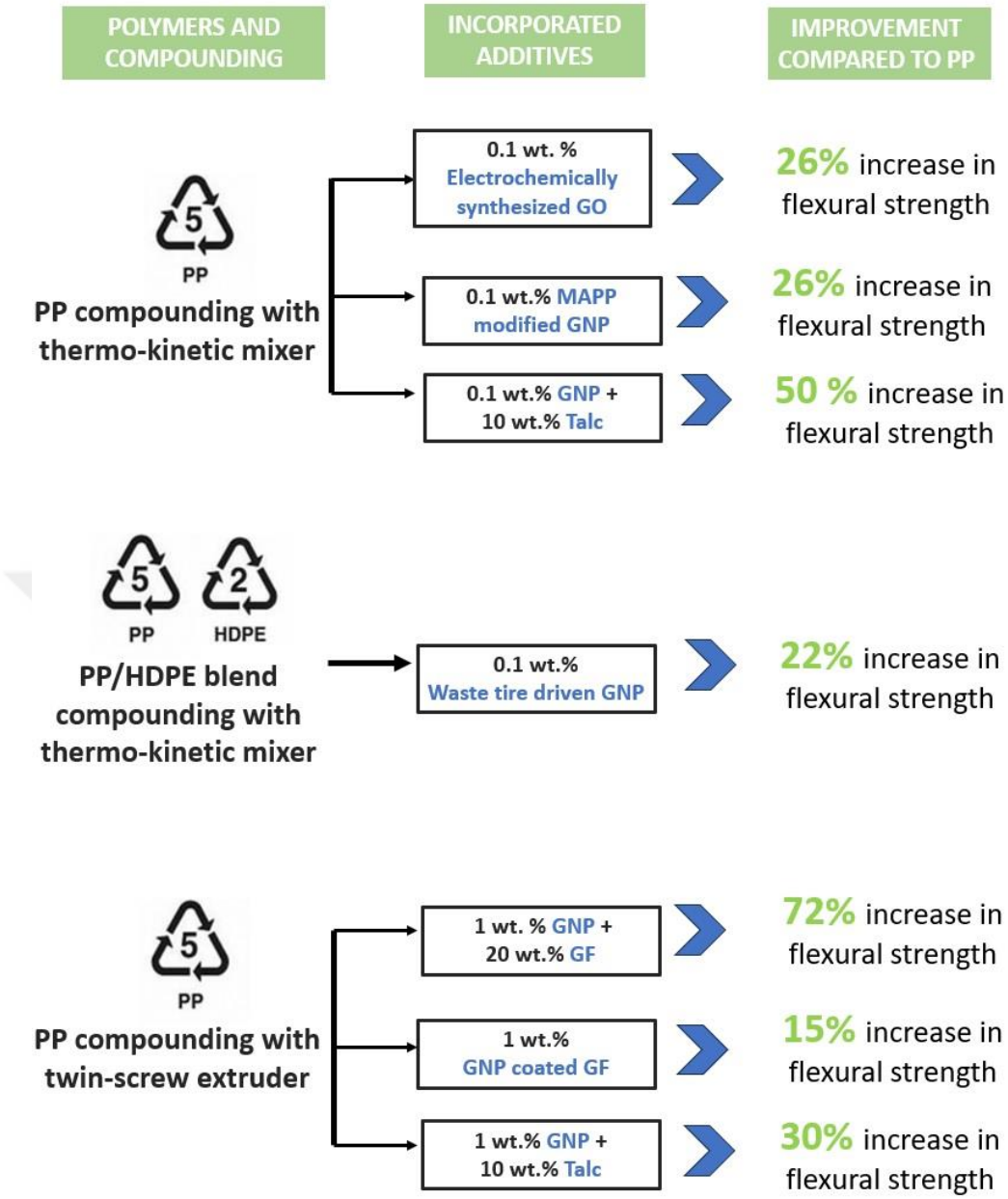

Figure 47. Composites produced within the scope of the thesis and the maximum improvement ratios achieved with the same additive content.

Overall, this study represents a significant stride towards advancing the realm of polymer composites through the strategic integration of diverse graphene-based materials. The synthesis and incorporation of different graphene types have unveiled a spectrum of properties, with GO contributing its unique sheet-like structure acquired through electrochemical synthesis, and GNP introducing a distinct platelet structure. These variations in structure significantly impact mechanical properties, enabling improvements in composite strength while maintaining dispersion below percolation thresholds. The utilization of waste tire-derived GNP demonstrates the potential of harnessing

unconventional sources for sustainable materials, further accentuating the study's commitment to eco-friendly practices.

Moreover, the study underscores the pivotal role of synthesis and modification techniques in tailoring the interactions between graphene and the polymer matrix. The effective grafting of MAPP onto GNP surfaces showcases the power of chemical modification in strengthening interfaces and reducing the reliance on additional compatibilizers. The utilization of high shear rate thermo-kinetic mixing has emerged as a game-changer, allowing for precise localization of GNP at interfaces within binary and ternary nanoblends. This approach highlights the criticality of process techniques in achieving desired composite characteristics.

As the field of polymer composites evolves, this research opens new avenues for future exploration. The promising potential of graphene-coated glass fiber (GNP-c-GF) composites offers a lightweight alternative across industries such as automotive, aerospace, and construction. The current study's focus on mechanical properties sets the stage for future investigations into impact strength, fatigue resistance, and creep behavior. The emergence of new fabrication techniques, such as injection molding and extrusion, holds promise for optimizing manufacturing processes and expanding composite applications.

Ultimately, this research pioneers a transformative path for polymer composite development, showcasing that through careful material selection, strategic synthesis and modification, and innovative processing techniques, the potential of graphene-based materials can be harnessed for enhanced mechanical performance and sustainable applications.

REFERENCES

[1] B. Wang *et al.*, "Graphene-based composites for electrochemical energy storage," *Energy Storage Mater.*, vol. 24, no. August 2019, pp. 22–51, 2020, doi: 10.1016/j.ensm.2019.08.004.

[2] Q. T. H. Shubhra, A. K. M. M. Alam, and M. A. Quaiyyum, "Mechanical properties of polypropylene composites: A review," *Journal of Thermoplastic Composite Materials*, vol. 26, no. 3. pp. 362–391, 2013, doi: 10.1177/0892705711428659.

[3] D. Bikiaris, "Microstructure and properties of polypropylene/carbon nanotube nanocomposites," *Materials*, vol. 3, no. 4. pp. 2884–2946, 2010, doi: 10.3390/ma3042884.

[4] J. Bian, Z. Jun, H. Lan, X. Zhou, W. Qiang, and X. Wei, "Composites : Part A Thermal and mechanical properties of polypropylene nanocomposites reinforced with nano-SiO 2 functionalized graphene oxide," *Compos. Part A*, vol. 97, pp. 120–127, 2017, doi: 10.1016/j.compositesa.2017.01.002.

[5] J. E. An, G. W. Jeon, and Y. G. Jeong, "Preparation and properties of polypropylene nanocomposites reinforced with exfoliated graphene," *Fibers Polym.*, vol. 13, no. 4, pp. 507–514, 2012, doi: 10.1007/s12221-012-0507-z.

[6] P. Song, Z. Cao, Y. Cai, L. Zhao, Z. Fang, and S. Fu, "Fabrication of exfoliated graphene-based polypropylene nanocomposites with enhanced mechanical and thermal properties," *Polymer (Guildf).*, vol. 52, no. 18, pp. 4001–4010, 2011, doi: 10.1016/j.polymer.2011.06.045.

[7] A. P. Bafana *et al.*, "Polypropylene nanocomposites reinforced with low weight percent graphene nanoplatelets," *Compos. Part B Eng.*, vol. 109, pp. 101–107, 2017, doi: 10.1016/j.compositesb.2016.10.048.

[8] N. Song, D. Cao, X. Luo, Q. Wang, P. Ding, and L. Shi, "Highly thermally conductive polypropylene/graphene composites for thermal management," *Compos. Part A Appl. Sci. Manuf.*, vol. 135, no. April, p. 105912, 2020, doi: 10.1016/j.compositesa.2020.105912.

[9] Y. S. Jun, J. G. Um, G. Jiang, G. Lui, and A. Yu, "Ultra-large sized graphene nano-platelets (GnPs) incorporated polypropylene (PP)/GnPs composites engineered by melt compounding and its thermal, mechanical, and electrical properties," *Compos. Part B Eng.*, vol. 133, pp. 218–225, 2018, doi: 10.1016/j.compositesb.2017.09.028.

[10] K. Gaska, G. C. Manika, T. Gkourmpis, D. Tranchida, A. Gitsas, and R. Kádár, "Mechanical behavior of melt-mixed 3D hierarchical graphene/polypropylene nanocomposites," *Polymers (Basel).*, vol. 12, no. 6, pp. 1–18, 2020, doi: 10.3390/polym12061309.

[11] J. S. M. Zanjani, L. H. Poudeh, B. G. Ozunlu, Y. E. Yagci, Y. Menceloglu, and B. Saner Okan, "Development of waste tire-derived graphene reinforced polypropylene nanocomposites with controlled polymer grade, crystallization and mechanical characteristics via melt-mixing," *Polym. Int.*, vol. 69, no. 9, pp. 771–779, 2020, doi: 10.1002/pi.6012.

[12] M. Liebscher, M. O. Blais, P. Pötschke, and G. Heinrich, "A morphological study on the dispersion and selective localization behavior of graphene nanoplatelets in immiscible polymer blends of PC and SAN," *Polymer (Guildf).*, vol. 54, no. 21, pp. 5875–5882, Oct. 2013, doi: 10.1016/j.polymer.2013.08.009.

[13] B. Yuan, C. Bao, L. Song, N. Hong, K. M. Liew, and Y. Hu, "Preparation of functionalized graphene oxide/polypropylene nanocomposite with significantly improved thermal stability and studies on the crystallization behavior and mechanical properties," *Chem. Eng. J.*, vol. 237, pp. 411–420, 2014, doi: 10.1016/j.cej.2013.10.030.

[14] M. G. Lee, S. Lee, J. Cho, S. Bae, and J. Y. Jho, "Effect of the fluorination of graphene nanoflake on the dispersion and mechanical properties of polypropylene nanocomposites," *Nanomaterials*, vol. 10, no. 6, pp. 1–11, 2020, doi: 10.3390/nano10061171.

[15] H. Shin, M. Y. Lim, J. Oh, Y. Lee, and J. C. Lee, "Preparation of bottom-up graphene oxide using citric acid and tannic acid, and its application as a filler for polypropylene nanocomposites," *RSC Adv.*, vol. 11, no. 13, pp. 7663–7671, 2021, doi: 10.1039/d0ra09856f.

[16] S. N. Tripathi, G. S. S. Rao, A. B. Mathur, and R. Jasra, “Polyolefin/graphene nanocomposites: A review,” *RSC Adv.*, vol. 7, no. 38, pp. 23615–23632, 2017, doi: 10.1039/c6ra28392f.

[17] A. T. Smith, A. M. LaChance, S. Zeng, B. Liu, and L. Sun, “Synthesis, properties, and applications of graphene oxide/reduced graphene oxide and their nanocomposites,” *Nano Mater. Sci.*, vol. 1, no. 1, pp. 31–47, 2019, doi 10.1016/j.nanoms.2019.02.004.

[18] J. R. Potts, D. R. Dreyer, C. W. Bielawski, and R. S. Ruoff, “Graphene-based polymer nanocomposites,” *Polymer*, vol. 52, no. 1. Elsevier Ltd, pp. 5–25, 2011, doi: 10.1016/j.polymer.2010.11.042.

[19] C. Dessi, L. G. Amurin, P. A. R. Muñoz, Y. D. C. de Oliveira, G. J. M. Fechine, and R. J. E. Andrade, “Graphene oxide dispersion state in polystyrene-based composites below percolation threshold via linear melt rheology,” *Rheol. Acta*, pp. 209–218, 2021, doi: 10.1007/s00397-021-01263-7.

[20] A. Naz, I. Riaz, R. Jalil, S. Afzal, and A. Qayyum Khan, “Creep strain and recovery analysis of polypropylene composites filled with graphene nanofiller,” *Polymer (Guildf).*, vol. 217, no. January, p. 123423, 2021, doi 10.1016/j.polymer.2021.123423.

[21] S. Cao, W. Ge, Y. Yang, Q. Huang, and X. Wang, “High strength, flexible , and conductive graphene/polypropylene fiber paper fabricated via papermaking process,” *Adv. Compos. Hybrid Mater.*, pp. 104–112, 2022, doi: 10.1007/s42114-021-00374-2.

[22] C. Y. Su, A. Y. Lu, Y. Xu, F. R. Chen, A. N. Khlobystov, and L. J. Li, “High-quality thin graphene films from fast electrochemical exfoliation,” *ACS Nano*, vol. 5, no. 3, pp. 2332–2339, 2011, doi: 10.1021/nn200025p.

[23] J. Phiri, P. Gane, and T. C. Maloney, “General overview of graphene: Production, properties, and application in polymer composites,” *Mater. Sci. Eng. B Solid-State Mater. Adv. Technol.*, vol. 215, pp. 9–28, 2017, doi: 10.1016/j.mseb.2016.10.004.

[24] A. Ambrosi and M. Pumera, “Electrochemically Exfoliated Graphene and Graphene Oxide for Energy Storage and Electrochemistry Applications,” *Chem. - A Eur. J.*, vol. 22, no. 1, pp. 153–159, 2016, doi: 10.1002/chem.201503110.

[25] A. M. Abdelkader, A. J. Cooper, R. A. W. Dryfe, and I. A. Kinloch, "How to get between the sheets: A review of recent works on the electrochemical exfoliation of graphene materials from bulk graphite," *Nanoscale*, vol. 7, no. 16. pp. 6944–6956, 2015, doi 10.1039/c4nr06942k.

[26] P. Yu, S. E. Lowe, G. P. Simon, and Y. L. Zhong, "Electrochemical exfoliation of graphite and production of functional graphene," *Curr. Opin. Colloid Interface Sci.*, vol. 20, no. 5–6, pp. 329–338, 2015, doi: 10.1016/j.cocis.2015.10.007.

[27] C. T. J. Low, F. C. Walsh, M. H. Chakrabarti, M. A. Hashim, and M. A. Hussain, "Electrochemical approaches to the production of graphene flakes and their potential applications," *Carbon N. Y.*, vol. 54, pp. 1–21, 2013, doi: 10.1016/j.carbon.2012.11.030.

[28] T. Palden, B. Onghena, M. Regadío, and K. Binnemans, "Methanesulfonic acid: A sustainable acidic solvent for recovering metals from the jarosite residue of the zinc industry," *Green Chem.*, vol. 21, no. 19, pp. 5394–5404, 2019, doi: 10.1039/c9gc02238d.

[29] T. G. Gopakumar and D. J. Y. S. Page, "Compounding of Nanocomposites by Thermokinetic Mixing," 2004, doi: 10.1002/app.21597.

[30] E. C. Sarac *et al.*, "Performance Comparison of CVD Grown Carbon Nanofiber Based on Single- and Multi-Layer Graphene Oxides in Melt-Compounded PA6.6 Nanocomposites," *Open J. Compos. Mater.*, vol. 09, no. 02, pp. 99–123, 2019, doi: 10.4236/ojcm.2019.92005.

[31] K. Parvez *et al.*, "Exfoliation of graphite into graphene in aqueous solutions of inorganic salts," *J. Am. Chem. Soc.*, vol. 136, no. 16, pp. 6083–6091, 2014, doi: 10.1021/ja5017156.

[32] B. Saner, J. Seyyed, M. Zanjani, I. Letofsky-papst, F. Çakmak, and Y. Z. Menceloglu, "Morphology-controllable synthesis and characterization of carbon nanotube/polypyrrole composites and their hydrogen storage capacities," *Mater. Chem. Phys.*, vol. 167, pp. 171–180, 2015, doi: 10.1016/j.matchemphys.2015.10.027.

[33] G. Yasin *et al.*, "Exploring the Nickel–Graphene Nanocomposite Coatings for Superior Corrosion Resistance: Manipulating the Effect of Deposition Current Density on its Morphology, Mechanical Properties, and Erosion-Corrosion Performance," *Adv. Eng. Mater.*, vol. 20, no. 7, pp. 1–12, 2018, doi: 10.1002/adem.201701166.

[34] I. Menapace, W. Yiming, and E. Masad, "Chemical analysis of surface and bulk of asphalt binders aged with accelerated weathering tester and standard aging methods," *Fuel*, vol. 202, pp. 366–379, 2017, doi: 10.1016/j.fuel.2017.04.042.

[35] W. I. Hayes, P. Joseph, M. Z. Mughal, and P. Papakonstantinou, "Production of reduced graphene oxide via a hydrothermal reduction in an aqueous sulphuric acid suspension and its electrochemical behaviour," *J. Solid State Electrochem.*, vol. 19, no. 2, pp. 361–380, 2015, doi: 10.1007/s10008-014-2560-6.

[36] J. Shen *et al.*, "Fast and facile preparation of graphene oxide and reduced graphene oxide nanoplatelets," *Chem. Mater.*, vol. 21, no. 15, pp. 3514–3520, 2009, doi: 10.1021/cm901247t.

[37] N. Liu, J. Yao, and L. Shi, "A novel method to anchor methanesulfonic acid in silica matrix," *Sci. CHINA Chem.*, vol. 59, no. 3, pp. 370–379, 2016, doi: 10.1007/s11426-015-5506-7.

[38] H. C. Zhiliang Shi, Xiaoke Liu, Yuhui Zhou, "Study of graphene oxide complexed hemicucurbit[6]uril onpolypropylene composites: Crystallization behavior, foaming performance, and mechanical properties," *Polym. Adv. Technol.*, doi 10.1002/pat.57042498© 2022 John Wiley & Sons Ltd.Polym Adv Technol.2022;33:2498–2510.wileyonlinelibrary.com/journal/pat.

[39] S. R. Ahmad, C. Xue, and R. J. Young, "The mechanisms of reinforcement of polypropylene by graphene nanoplatelets," *Materials Science and Engineering B: Solid-State Materials for Advanced Technology*, vol. 216. pp. 2–9, 2017, doi: 10.1016/j.mseb.2016.10.003.

[40] Y. Jun and G. Jiang, "A study on the effects of graphene nano-platelets (GnPs) sheet sizes from a few to hundred microns on the thermal, mechanical , and electrical properties of polypropylene (PP)/ GnPs composites," *Express Polym. Lett.*, no. September, 2018, doi: 10.3144/expresspolymlett.2018.76.

[41] M. Hareesha, B. Yogesha, L. L. Naik, and D. Saravanabavan, “Development on graphene based polymer composite materials and their applications - A recent review,” in *AIP Conference Proceedings*, 2021, vol. 2316, no. February, doi: 10.1063/5.0036854.

[42] a I. G. and M. A. Mohammad Sabzi, ab Long Jiang,*a Fei Liu, “Graphene nanoplatelets as poly(lactic acid) modifier: linear rheological behavior and electrical conductivity,” *J. Mater. Chem. A*, pp. 8253–8261, 2013, doi: 10.1039/c3ta11021d.

[43] Y. Ren, Y. Zhang, H. Fang, T. Ding, J. Li, and S. L. Bai, “Simultaneous enhancement on thermal and mechanical properties of polypropylene composites filled with graphite platelets and graphene sheets,” *Compos. Part A Appl. Sci. Manuf.*, vol. 112, no. February, pp. 57–63, 2018, doi: 10.1016/j.compositesa.2018.05.017.

[44] B. S. Okan, Y. Menceloğlu, B. G. Ozunlu, and Y. E. Yagci, “Graphene from waste tire by recycling technique for cost-effective and light-weight automotive plastic part production,” in *AIP Conference Proceedings*, 2020, vol. 2205, no. January, doi: 10.1063/1.5142961.

[45] R. Doufnoune, T. Baouz, and S. Bouchareb, “Influence of functionalized reduced graphene oxide and compatibilizer on mechanical, thermal and morphological properties of polypropylene/polybutene-1 (PP/PB-1) blends,” *J. Adhes. Sci. Technol. ISSN*, vol. 33, no. 16, pp. 1729–1757, 2019, doi: 10.1080/01694243.2019.1611367.

[46] F. Ashenai Ghasemi, I. Ghasemi, S. Menbari, M. Ayaz, and A. Ashori, “Optimization of mechanical properties of polypropylene/talc/graphene composites using response surface methodology,” *Polym. Test.*, vol. 53, pp. 283–292, 2016, doi: 10.1016/j.polymertesting.2016.06.012.

[47] M. Iman, S. Estaji, S. Rasoul, and H. Ali, “Degradation of polymer nanocomposites filled with graphene oxide and reduced graphene oxide nanoparticles : A review of current status,” *Polym. Degrad. Stab.*, vol. 206, no. August, 2022, doi: https://doi.org/10.1016/j.polymdegradstab.2022.110179.

[48] A. Kumar, K. Sharma, and A. R. Dixit, “A review of the mechanical and thermal properties of graphene and its hybrid polymer nanocomposites for structural applications,” *Journal of Materials Science*, vol. 54, no. 8. pp. 5992–6026, 2019, doi: 10.1007/s10853-018-03244-3.

[49] F. Zhang, K. Yang, G. Liu, Y. Chen, M. Wang, and S. Li, "Recent advances on graphene : Synthesis, properties, and applications," *Compos. Part A*, vol. 160, no. June, p. 107051, 2022, doi https://doi.org/10.1016/j.compositesa.2022.107051.

[50] M. G. Lee, S. Lee, J. Cho, and J. Y. Jho, "Improving Dispersion and Mechanical Properties of Polypropylene/Graphene Nanoplatelet Composites by Mixed Solvent-Assisted Melt Blending," *Macromol. Res.*, vol. 28, no. 12, pp. 1166–1173, 2020, doi: 10.1007/s13233-020-8144-7.

[51] G. Şahin Dündar and B. Saner Okan, "An efficient interface model to develop a scalable methodology of melt processing of polypropylene with graphene oxide produced by an improved and eco-friendly electrochemical exfoliation," *J. Appl. Polym. Sci.*, vol. 140, no. 2, pp. 1–14, 2023, doi: 10.1002/app.53282.

[52] R. Watanabe, A. Sugahara, H. Hagihara, J. Mizukado, and H. Shinzawa, "Insight into interfacial compatibilization of glass-fiber-reinforced polypropylene (PP) using maleic-anhydride modified PP employing infrared spectroscopic imaging," *Compos. Sci. Technol.*, vol. 199, no. July, p. 108379, 2020, doi 10.1016/j.compscitech.2020.108379.

[53] C. Srivabut, T. Ratanawilai, and S. Hiziroglu, "Response surface optimization and statistical analysis of composites made from calcium carbonate filler-added recycled polypropylene and rubberwood fiber," *J. Thermoplast. Compos. Mater.*, vol. 35, no. 3, pp. 391–415, 2022, doi 10.1177/0892705719889988.

[54] N. A. Rahman, A. Hassan, and J. Heidarian, "Effect of compatibilizer on the properties of polypropylene/glass fibre / nanoclay composites," *Polimeros*, vol. 28, no. 2, pp. 103–111, 2018.

[55] M. Doddashamachar, R. Nama, and V. Setty, "Dielectric Properties of Banana Fiber Filled Polypropylene Composites : Effect of Coupling Agent," *Fibers Polym.*, vol. 23, no. 5, pp. 1387–1395, 2022, doi: 10.1007/s12221-022-4395-6.

[56] M. A. Venkatachalaiah, R. Nama, V. Setty, and M. A. Venkatachalaiah, "Effect of Compatibilizer on the Properties of Areca- Fiber Reinforced Polypropylene Composites Effect of Compatibilizer on the Properties of Areca-Fiber Reinforced Polypropylene Composites," *J. Nat. Fibers*, vol. 19, no. 17, pp. 15261–15275, 2022, doi: 10.1080/15440478.2022.2121354.

[57] N. F. Braga, H. M. Zaggo, T. L. A. Montanheiro, and F. R. Passador, “Preparation of maleic anhydride grafted poly(trimethylene terephthalate) (PTT-g-MA) by reactive extrusion processing,” *J. Manuf. Mater. Process.*, vol. 3, no. 2, 2019, doi: 10.3390/jmmp3020037.

[58] Q. B. Ho and M. Kontopoulou, “Compatibilized polypropylene nanocomposites containing expanded graphite and graphene nanoplatelets,” *Polym. Eng. Sci.*, no. October 2020, pp. 1–13, 2021, doi: 10.1002/pen.25647.

[59] O. E. Ezenkwa, “Comparison of mechanical properties and thermal stability of graphene-based materials and halloysite nanotubes reinforced maleated polymer compatibilized polypropylene nanocomposites,” *Polym. Compos.*, vol. 43, no. October 2021, pp. 1852–1863, 2022, doi: 10.1002/pc.26503.

[60] Y. Cao, J. Feng, and P. Wu, “Polypropylene-grafted graphene oxide sheets as multifunctional compatibilizers for polyolefin-based polymer blends,” *J. Mater. Chem.*, vol. 22, no. 30, pp. 14997–15005, 2012, doi: 10.1039/c2jm31477k.

[61] A. Graziano, C. Garcia, S. Jaffer, J. Tjong, and M. Sain, “Novel functional graphene and its thermodynamic interfacial localization in biphasic polyolefin systems for advanced lightweight applications,” *Compos. Sci. Technol.*, vol. 188, p. 107958, Mar. 2020, doi: 10.1016/j.compscitech.2019.107958.

[62] I. Berktas, M. Hezarkhani, L. Haghighi, P. Burcu, and S. Okan, “Recent developments in the synthesis of graphene and graphene ‐ like structures from waste sources by recycling and upcycling technologies : a review,” *Graphene Technol.*, vol. 5, no. 3, pp. 59–73, 2020, doi: 10.1007/s41127-020-00033-1.

[63] F. Zhou *et al.*, “Ultrathin, ethylenediamine-functionalized graphene oxide membranes on hollow fibers for CO2 capture,” *J. Memb. Sci.*, vol. 573, no. November 2018, pp. 184–191, 2019, doi: 10.1016/j.memsci.2018.11.080.

[64] A. Tariq *et al.*, “Reactive extrusion of maleic-anhydride-grafted polypropylene by torque rheometer and its application as compatibilizer,” *Polymers (Basel).*, vol. 13, no. 4, pp. 1–17, 2021, doi: 10.3390/polym13040495.

[65] X. Li, P. Bandyopadhyay, T. T. Nguyen, O. kyung Park, and J. H. Lee, "Fabrication of functionalized graphene oxide/maleic anhydride grafted polypropylene composite film with excellent gas barrier and anticorrosion properties," *J. Memb. Sci.*, vol. 547, no. October 2017, pp. 80–92, 2018, doi: 10.1016/j.memsci.2017.10.031.

[66] S. Wang *et al.*, "Ethylenediamine modified graphene and its chemically responsive supramolecular hydrogels," *Ind. Eng. Chem. Res.*, vol. 53, no. 33, pp. 13205–13209, 2014, doi: 10.1021/ie501448p.

[67] a A. B. M. and R. J. Sandeep N. Tripathi, *a G. S. Srinivasa Rao and Polymeric, "Polyolefin/graphene nanocomposites: a review Sandeep," *RSC Adv.*, pp. 23615–23632, 2017, doi: 10.1039/c6ra28392f.

[68] J. Sanes, C. Sánchez, R. Pamies, M. D. Avilés, and M. D. Bermúdez, "Extrusion of polymer nanocomposites with graphene and graphene derivative nanofillers: An overview of recent developments," *Materials (Basel).*, vol. 13, no. 3, 2020, doi: 10.3390/ma13030549.

[69] S. J. Lee, S. J. Yoon, and I. Jeon, "Graphene/Polymer Nanocomposites: Preparation, Mechanical Properties, and Application," *polymers,MDPI*, vol. 14, p. 4733, 2022, doi: https://doi.org/10.3390/polym14214733.

[70] S. P. Rwei and C. C. Lien, "Synthesis and viscoelastic characterization of sulfonated chitosan solutions," *Colloid Polym. Sci.*, vol. 292, no. 4, pp. 785–795, 2014, doi: 10.1007/s00396-013-3115-6.

[71] A. Farzaneh, A. Rostami, and H. Nazockdast, "Thermoplastic polyurethane/ multiwalled carbon nanotubes nanocomposites: Effect of nanoparticle content, shear, and thermal processing," *Polym. Compos.*, vol. 42, no. 9, pp. 4804–4813, 2021, doi: 10.1002/pc.26190.

[72] J. Wang, F. Song, Y. Ding, and M. Shao, "The incorporation of graphene to enhance mechanical properties of polypropylene self-reinforced polymer composites," *Mater. Des.*, vol. 195, p. 109073, 2020, doi: 10.1016/j.matdes.2020.109073.

[73] K. Król-Morkisz and K. Pielichowska, "13 - Thermal Decomposition of Polymer Nanocomposites With Functionalized Nanoparticles," in *Polymer Composites with Functionalized Nanoparticles*, K. Pielichowski and T. M. Majka, Eds. Elsevier, 2019, pp. 405–435.

[74] H. Sutar, B. Mishra, P. Senapati, R. Murmu, and D. Sahu, “Mechanical, Thermal, and Morphological Properties of Graphene Nanoplatelet-Reinforced Polypropylene Nanocomposites: Effects of Nanofiller Thickness,” *J. Compos. Sci.*, vol. 5, no. 1, p. 24, 2021, doi: 10.3390/jcs5010024.

[75] B. S. Okan, “Fabrication of multilayer graphene oxide-reinforced high density polyethylene nanocomposites with enhanced thermal and mechanical properties via thermokinetic mixing,” vol. 41, no. 3, 2017, doi: 10.3906/kim-1608-53.

[76] X. Sun *et al.*, “Recent Progress in Graphene/Polymer Nanocomposites,” *Adv. Mater.*, vol. 33, no. 6, pp. 1–28, 2021, doi: 10.1002/adma.202001105.

[77] A. Kol, S. Kenig, and N. Naveh, “Silane-Modi fi ed Graphene Oxide as a Compatibilizer and Reinforcing Nanoparticle for Immiscible PP / PA Blends,” *Polym. Eng. Sci.*, 2020, doi: 10.1002/pen.25271.

[78] Z. Tomi and A. D. Marinkovi, *Compatibilization of polymer blends by the addition of graft copolymers*. 2020.

[79] M. Salzano De Luna and G. Filippone, “Effects of nanoparticles on the morphology of immiscible polymer blends - Challenges and opportunities,” *European Polymer Journal*, vol. 79. Elsevier Ltd, pp. 198–218, 2016, doi: 10.1016/j.eurpolymj.2016.02.023.

[80] A. Graziano, O. A. T. Dias, C. Garcia, S. Jaffer, J. Tjong, and M. Sain, “Impact of Reduced Graphene Oxide on structure and properties of polyethylene rich binary systems for performance-based applications,” *Polymer (Guildf).*, vol. 202, no. April, p. 122622, 2020, doi: 10.1016/j.polymer.2020.122622.

[81] A. Graziano, C. Garcia, J. Tjong, W. Yang, and M. Sain, “Functionally tuned nanolayered graphene as reinforcement of polyethylene nanocomposites for lightweight transportation industry,” *Carbon N. Y.*, vol. 169, pp. 99–110, 2020, doi: https://doi.org/10.1016/j.carbon.2020.07.040.

[82] A. R. Ajitha, L. P. Mathew, and S. Thomas, “Compatibilization of polymer blends by micro and nanofillers,” in *Compatibilization of Polymer Blends: Micro and Nano Scale Phase Morphologies, Interphase Characterization, and Properties*, Elsevier, 2019, pp. 179–203.

[83] L. Bai, R. Sharma, X. Cheng, and C. W. Macosko, “Kinetic Control of Graphene Localization in Co-continuous Polymer Blends via Melt Compounding,” *Langmuir*, vol. 34, no. 3, pp. 1073–1083, Jan. 2018, doi: 10.1021/acs.langmuir.7b03085.

[84] F. Abbasi, D. A. Shojaei, and S. M. Bellah, “The compatibilization effect of exfoliated graphene on rheology, morphology, and mechanical and thermal properties of immiscible polypropylene/polystyrene (PP/PS) polymer blends,” *Journal of Thermoplastic Composite Materials*, vol. 32, no. 10. Journal of Thermoplastic Composite Materials, pp. 1378–1392, 2019, doi: 10.1177/0892705718797153.

[85] P. Feng, J. Jia, S. Peng, W. Yang, S. Bin, and C. Shuai, “Graphene oxide-driven interfacial coupling in laser 3D printed PEEK/PVA scaffolds for bone regeneration,” *Virtual Phys. Prototyp.*, vol. 15, no. 2, pp. 211–226, 2020, doi: 10.1080/17452759.2020.1719457.

[86] Y. Shen, T. T. Zhang, J. H. Yang, N. Zhang, T. Huang, and Y. Wang, “Selective localization of reduced graphene oxides at the interface of PLA/EVA blend and its resultant electrical resistivity,” *Polymer Composites*, vol. 38, no. 9. pp. 1982–1991, 2017, doi: 10.1002/pc.23769.

[87] M. Bera, U. Saha, A. Bhardwaj, and P. K. Maji, “Reduced graphene oxide (RGO) - induced compatibilization and reinforcement of poly (vinylidene fl uoride) (PVDF) – thermoplastic polyurethane (TPU) binary polymer blend,” vol. 47010, pp. 1–13, 2019, doi: 10.1002/app.47010.

[88] C. Tu and K. Nagata, “Dependence of Electrical Conductivity on Phase Morphology for Graphene Selectively Located at the Interface of Polypropylene / Polyethylene Composites,” 2022.

[89] Y. Ding, C. Abeykoon, and Y. S. Perera, “The effects of extrusion parameters and blend composition on the mechanical, rheological and thermal properties of LDPE / PS / PMMA ternary polymer blends,” *Adv. Ind. Manuf. Eng.*, vol. 4, no. October 2021, p. 100067, 2022, doi: 10.1016/j.aime.2021.100067.

[90] D. N. Trivedi and N. V Rachchh, “Graphene and its application in thermoplastic polymers as nano-filler- A review,” *Polymer (Guildf).*, vol. 240, no. September 2021, p. 124486, 2022, doi: 10.1016/j.polymer.2021.124486.

[91] B. Cetiner, G. S. Dundar, Y. Yusufoglu, and B. S. Okan, “Sustainable Engineered Design and Scalable Manufacturing of Upcycled Graphene Reinforced Polylactic Acid / Polyurethane Blend Composites Having Shape Memory Behavior,” *Polymers (Basel).*, 2023, doi: https://doi.org/10.3390/polym15051085.

[92] H. Kamalvand and P. Rajaee, “An experimental investigation of the tensile, fracture and microstructural characteristics of ABS / SBS reinforced with HNTs,” no. May, pp. 1–13, 2023, doi: 10.1002/pc.27573.

[93] V. Pandey, H. Chen, M. Maia, and J. Ma, “Extension-dominated improved dispersive mixing in single-screw extrusion . Part 2 : Comparative analysis with twin-screw extruder,” no. July, pp. 1–11, 2020, doi: 10.1002/app.49765.

[94] B. Succinate and B. Blend, “Efficiency of Twin-Screw Extrusion of Biodegradable Poly,” 2021.

[95] L. Techawinyutham, J. Tengsuthiwat, and R. Srisuk, “Recycled LDPE / PETG blends and HDPE / PETG blends : mechanical, thermal , and rheological properties,” *J. Mater. Res. Technol.*, vol. 15, pp. 2445–2458, 2021, doi: 10.1016/j.jmrt.2021.09.052.

[96] M. Ahmadlouydarab, M. Chamkouri, and H. Chamkouri, “Compatibilization of immiscible polymer blends (R ‐ PET / PP) by adding PP ‐ g ‐ MA as compatibilizer : analysis of phase morphology and mechanical properties,” *Polym. Bull.*, pp. 5753–5766, 2020, doi 10.1007/s00289-019-03054-w.

[97] E. Vatansever, D. Arslan, D. S. Sarul, Y. Kahraman, and M. Nofar, “Effects of molecular weight and crystallizability of polylactide on the cellulose nanocrystal dispersion quality in their nanocomposites,” *Int. J. Biol. Macromol.*, vol. 154, pp. 276–290, 2020, doi: 10.1016/j.ijbiomac.2020.03.115.

[98] S. Jose *et al.*, “Phase morphology, crystallization behaviour and mechanical properties of isotactic polypropylene/high-density polyethylene blends,” *Eur. Polym. J.*, vol. 40, no. 9, pp. 2105–2115, 2004, doi: 10.1016/j.eurpolymj.2004.02.026.

[99] F. Valorosi *et al.*, “Graphene and related materials in hierarchical fiber composites : Production techniques and key industrial benefits,” *Compos. Sci. Technol.*, vol. 185, no. July 2019, p. 107848, 2020, doi: 10.1016/j.compscitech.2019.107848.

[100] J. Wang *et al.*, "Shear induced fiber orientation, fiber breakage, and matrix molecular orientation in long glass fiber reinforced polypropylene composites," *Mater. Sci. Eng. A*, vol. 528, no. 7–8, pp. 3169–3176, 2011, doi: 10.1016/j.msea.2010.12.081.

[101] D. G. Papageorgiou, I. A. Kinloch, and R. J. Young, "Hybrid multifunctional graphene/glass-fibre polypropylene composites," *Compos. Sci. Technol.*, vol. 137, pp. 44–51, 2016, doi: 10.1016/j.compscitech.2016.10.018.

[102] D. Pedrazzoli and A. Pegoretti, "Hybridization of short glass fiber polypropylene composites with nanosilica and graphite nanoplatelets," *J. Reinf. Plast. Compos.*, vol. 33, no. 18, pp. 1682–1695, 2014, doi: 10.1177/0731684414542668.

[103] E. Tarani, G. Z. Papageorgiou, D. N. Bikiaris, and K. Chrissafis, "Kinetics of crystallization and thermal degradation of an isotactic polypropylene matrix reinforced with graphene/glass-fiber filler," *Molecules*, vol. 24, no. 10, 2019, doi: 10.3390/ molecules24101984.

[104] N. D. Sansone *et al.*, "Tailoring Multifunctional and Lightweight Hierarchical Hybrid Graphene Nanoplatelet and Glass Fiber Composites," 2022, doi: 10.1021/acsami.2c11 231.

[105] F. A. Ghasemi, M. N. Niyaraki, and I. Ghasemi, "Predicting the tensile strength and elongation at break of PP / graphene / glass fiber / EPDM nanocomposites using response surface methodology," *Mech. Adv. Mater. Struct.*, vol. 28, no. 10, pp. 981–989, 2021, doi: 10.1080/15376494.2019.1614702.

[106] F. Ashenai Ghasemi, A. Ghorbani, and I. Ghasemi, "Mechanical, Thermal and Dynamic Mechanical Properties of PP/GF/xGnP Nanocomposites," *Mech. Compos. Mater.*, vol. 53, no. 1, pp. 131–138, 2017, doi: 10.1007/s11029-017-9647-y.

[107] H. Mahmood, M. Tripathi, N. Pugno, and A. Pegoretti, "Enhancement of interfacial adhesion in glass fiber/epoxy composites by electrophoretic deposition of graphene oxide on glass fibers," *Compos. Sci. Technol.*, vol. 126, pp. 149–157, 2016, doi: 10.1016/j.compscitech.2016.02.016.

[108] W. Liu, Y. Zhu, C. Qian, H. Dai, Y. Fu, and Y. Dong, "Interfacial modification between glass fiber and polypropylene using a novel waterborne amphiphilic sizing agent," *Compos. Part B*, vol. 241, no. November 2021, p. 110029, 2022, doi: 10.1016/j.compositesb.2022.110029.

[109] Y. He, Q. Chen, D. Wu, M. Zhou, T. Wang, and C. Lu, "Effect of multiscale reinforcement by fiber surface treatment with polyvinyl alcohol / graphene oxide / oxidized carbon nanotubes on the mechanical properties of reinforced hybrid fiber composites," *Compos. Sci. Technol.*, vol. 204, no. September 2020, p. 108634, 2021, doi: 10.1016/j.compscitech.2020.108634.

[110] M. Fang, X. Xiong, Y. Hao, T. Zhang, and H. Wang, "Journal of Materials Science & Technology Preparation of highly conductive graphene-coated glass fibers by sol-gel and dip-coating method," *J. Mater. Sci. Technol.*, vol. 35, no. 9, pp. 1989–1995, 2019, doi: 10.1016/j.jmst.2019.05.027.

[111] X. Zeng, C. Wu, and B. T. X. Shen, "Spray-free polypropylene composite reinforced by graphene oxide @ short glass fiber," no. July 2019, pp. 1215–1223, 2020, doi: 10.1002/pc.25447.

[112] R. Naveen, M. Kumar, M. Ramesh, R. Abinaya, and M. S. Prasath, "Materials Today : Proceedings An investigation on effect of ultraviolet (UV) rays on mechanical properties of epoxy laminates," *Mater. Today Proc.*, no. xxxx, 2023, doi: 10.1016/j.matpr.2023.06.257.

[113] F. De Luca, G. Sernicola, M. S. P. Sha, and A. Bismarck, "' Brick-and-Mortar ' Nanostructured Interphase for Glass-Fiber- Reinforced Polymer Composites," 2018, doi: 10.1021/acsami.7b16136.

[114] S. G. Prolongo, A. Ure, R. Moriche, and A. Jim, "Graphene nanoplatelets coated glass fi bre fabrics as strain sensors," vol. 146, pp. 59–64, 2017, doi: 10.1016/j.compscitech. 2017.04.019.

[115] X. Yao, I. A. Kinloch, and M. A. Bissett, "Fabrication and Mechanical Performance of Graphene Nanoplatelet / Glass Fiber Reinforced Polymer Hybrid Composites," *Front. Mater.*, vol. 8, no. November, pp. 1–9, 2021, doi: 10.3389/fmats.2021.773343.

[116] M. Tripathi *et al.*, "Nanoscale friction of graphene oxide over glass- fi bre and polystyrene," *Compos. Part B*, vol. 148, no. March, pp. 272–280, 2018, doi: 10.1016/j.compositesb.2018.04.001.

[117] R. Umer, Y. Li, Y. Dong, H. J. Haroosh, and K. Liao, “The effect of graphene oxide (GO) nanoparticles on the processing of epoxy / glass fiber composites using resin infusion,” *Int. J. Adv. Manuf. Technol.*, pp. 2183–2192, 2015, doi: 10.1007/s00170-015-7427-1.

[118] X. Yang, T. Mei, J. Yang, C. Zhang, M. Lv, and X. Wang, “Synthesis and characterization of alkylamine-functionalized graphene for polyolefin-based nanocomposites,” *Appl. Surf. Sci.*, vol. 305, pp. 725–731, 2014, doi: 10.1016/j.apsusc.2014.03.184.

[119] M. F. Maqsood *et al.*, “Fabrication and characterization of graphene oxide and glass fiber-based hybrid epoxy composites,” no. July, pp. 8072–8083, 2022, doi: 10.1002/pc.26952.

[120] P. Jagadeesh, S. M. Rangappa, and S. Siengchin, “Advanced Industrial and Engineering Polymer Research Advanced characterization techniques for nanostructured materials in biomedical applications,” *Adv. Ind. Eng. Polym. Res.*, no. xxxx, 2023, doi: 10.1016/j.aiepr.2023.03.002.

[121] R. V Lakshmi, P. Bera, S. T. Aruna, and H. C. Barshilia, *Chapter 9 - XPS and SIMS studies of nanoscale polymer-based coatings*. Elsevier Inc., 2023.

[122] A. Kaur and P. Chahal, “Selective Fabrication of SiC / Si Diodes by Excimer Laser under Ambient Conditions,” *IEEE Electron Device Lett.*, no. February, 2016, doi: 10.1109/LED.2015.2508479.

[123] A. A. Dongargaonkar and J. D. Clogston, “Chapter 6,” vol. 1682, 2018, pp. 57–63.

[124] C. Li, Z. Duan, Q. Chen, Z. Chen, and F. Edmond, “The effect of drying condition of glassfibre core material on the thermal conductivity of vacuum insulation panel The effect of drying condition of glassfibre core material on the thermal conductivity of vacuum insulation panel,” *J. Mater.*, vol. 50, no. November 2015, pp. 1030–1037, 2013, doi: 10.1016/j.matdes.2013.03.021.

[125] M. Wilsey, K. Watson, and C. Cox, “Selective hydroxylation of carbon surfaces for long- lasting hydrophilicity by a green chemistry process Selective hydroxylation of carbon surfaces for long- lasting hydrophilicity by a green chemistry process,” 2022.